Investigation on Seismic Performance of Reinforced Concrete Columns Concealing Drainage Pipe

Amir Bahador Nataj

Submitted to the
Institute of Graduate Studies and Research
in partial fulfillment of the requirements for the degree of

Doctor of Philosophy
in
Civil Engineering

Eastern Mediterranean University
September 2018
Gazimağusa, North Cyprus

Approval of the Institute of Graduate Studies and Research

Assoc. Prof. Dr. Ali Hakan Ulusoy
Acting Director

I certify that this thesis satisfies all the requirements as a thesis for the degree of Doctor of Philosophy in Civil Engineering.

Assoc. Prof. Dr. Serhan Şensoy
Chair, Department of Civil Engineering

We certify that we have read this thesis and that in our opinion it is fully adequate in scope and quality as a thesis for the degree of Doctor of Philosophy in Civil Engineering.

Prof. Dr. Ghani Razaqpur
Co-Supervisor

Assoc. Prof. Dr. Serhan Şensoy
Supervisor

Examining Committee

1. Prof. Dr. Süleyman Adanur
2. Prof. Dr. Özgür Eren
3. Prof. Dr. Metin Hüsem
4. Assoc. Prof. Dr. Giray Özay
5. Assoc. Prof. Dr. Serhan Şensoy

ABSTRACT

An investigation is carried out to evaluate under constant axial load and concomitant monotonic and reversed cyclic loading the structural behavior of reinforced concrete columns containing a service pipe within the column core. The study comprises an experimental part involving the design, construction and testing of nine specimens, including two control specimens and seven specimens with a pipe embedded in their cores. All columns have 200×200 mm cross-section and 1500 mm length. Among the ones with pipe, two are highly confined with closely spaced stirrups. The numerical study consists of the Finite Element (FE) modeling of response of the same columns as well as sectional analysis. The commercial software ABAQUS is utilized for the FE simulations.

The results show good agreement between the experimental and the companion numerical responses, both revealing that the column ultimate load carrying capacity, stiffness and ductility are reduced by the presence of service pipes. The extent of reduction depends on the level of axial load, level of confinement and the location of the pipe exit. It is observed that the length of plastic hinge, l_p is highly affected by the presence of pipe, and existing well known equations for calculating the plastic hinge length underestimate the value of l_p. Finally a high degree of stress concentration in the vicinity of the pipe is noticed. The latter, causes local damage in the region around the location of the pipe exit.

To mitigate the negative impact of pipe embedment on column strength and ductility, some tentative design recommendations are made, including the preferred location of

the pipe exit and the details of extra confinement steel that must be provided in the exit region.

Keywords: compressive strength, cracks, failure, Finite Element Analysis, concrete columns

ÖZ

İçinde servis borusu bulunduranbetonarme kolonların yapısal davranışı,sabit eksenel yük altında ve eşzamanlı olarak hem monoton hem deters çevrimli yükleme kullanılarakyapısal davranışı inceleyen bir araştırma yürütülmüştür. Çalışma, iki kontrol örneği ve servis borularının mevcut olduğu yedi numune dahil olmak üzere toplam dokuz örneğin tasarımı, inşası ve testini içermektedir. Ayrıcasonlu elemanlar (SE) modelleriniiçeren sayısal çözümlemede test kapsamında gerçekleştirilmiştir. Tüm kolonlar 200 × 200 mm enine kesite ve 1500 mm uzunluğuna sahiptir. Servis borularının bulunduğu numunelerden ikisinde etriye sıklaştırılması yapılmıştır. Sayısal çalışmaise, ABAQUSsimülasyonyazılımı kullanılarak gerçekleştirilmiştir.Hem deneysel hem de tamamlayıcı sayısal sonuçlar arasında iyi bir uyum olduğu görülmektedir.Elde edilen sonuçlarda,kolonun nihai yük taşıma kapasitesi, rijitliği ve sünekliğiincelenmiş olup,servisborularının varlığıyla genel kapasitesinin azaldığıgörülmüştür. Gerek kapasite,gerekse rijitlik ve sünekliğin azalmasında, eksenel yük seviyesi, sargı donatısı miktarın ve boru çıkışkonumunun önemli rol oynadığı gözlemlenmiştir.Plastik mafsal uzunluğu,lp'nin boru mevcudiyetinden dolayı büyük ölçüde etkilendiği ve plastik mafsaluzunluğunun hesaplanması için literatürde mevcut denklemlerin yeterli olmadığıgözlemlenmiştir. Son olarak, borunun çevresinde yüksek derecede bir gerilmeyoğunlaşması tespit edilmişveboru çıkışının bulunduğu yerin çevresindekibölgede yerel hasara neden olmuştur.

viGenel olarak, boru gömülmesinin kolon mukavemeti ve sünekliği üzerindeki olumsuz etkisini azaltmak için, boru çıkışının tercih edilen yeri ve çıkış

bölgesindeki ilave sargı donatısı detayları da dâhilolmak üzere bazı tasarım önerileri yapılmıştır.

Anahtar Kelimeler: Betonarme kolon testi, çatlak oluşumu, kırılma, Sonlu Elemanlar Analizi, betonarmekolonlardaki borula

To

Melika mostafanejad

ACKNOWLEDGEMENT

Firstly, I would like to express my most humble gratitude to my supervisor Assoc. Prof. Serhan Şensoy for all the support through my study and research, for his motivation, and kindness that I received continuously during my research program, I owe him too much for all the trust that he put in me. And also I would like to state my deepest gratitude toward Prof.Dr. Ghani Razaqpur, my co-supervisor, with his paternal patience, whose guidance helped me in all the time of research. I could not have imagined having accomplished my study without the presence of them.

I am also truly grateful for the opportunity given by the Civil Engineering Department, EMU for the all facilities and opportunities given by them, during my assistantship and my study, which taught me a lot and paved the path of my academic career.

My special and sincere thanks goes to my friend and colleague Ismail Safkan for all his support, brilliant ideas and all days that we have shared hardships together in the lab. I also thank my friend Mohammad Musavi for all the stimulating discussions that helped me a lot during this research.

My humble thanks to my parents, Abas and batool, my in laws Mehdi and ashraf for all the love that I received always from them, through my life, I owe them everything.

Last but not least, my best friend, my soulmate and my wife, **Melika**, thanks for unconditional support and love, round the clock.

TABLE OF CONTENTS

LIST OF TABLES

LIST OF FIGURES

LIST OF SYMBOLS

E_c	Elastic Modulus of Concrete
$f_{cu,28}$	28 d Compressive Strength of Concrete
f_u	Ultimate Strength of Reinforcing Bars
f_y	Yield Strength of Reinforcing Bars
i	Increment Number
l_p	Length of Plastic Hinge
n	Total Number of Increments
P_b	Balanced Load
P_u	Maximum Applied Load
Φ	Bar Diameter
Δ_m	Targeted Maximum Deformation Amplitude
Δ_y	Displacement Corresponding to Yield State
$\Delta_{20\%}$	Displacement Corresponding to 20%S Loss
ε_u	Ultimate Strain of Reinforcing Bars
ε_y	Yield Strain of Reinforcing Bars
μ	Displacement Ductility Factor
ψ	Dilation Angle

Chapter 1

INTRODUCTION

1.1 General

Openings in structural members such as beams, slabs, columns and walls, for passage of mechanical components, have always been a concern to structural engineers. During construction due to practical or architectural reasons, structures may undergo some changes which in turn create deficiencies in their seismic performance. One such change is embedment of service pipes in structural members like beams, slabs and columns. In regions with high amount of rainfall, like Mediterranean countries, Malaysia and some other parts of Asia, in some buildings, PVC drainage pipes are concealed in the core of reinforced concrete columns (see Figure 1.1 and Figure 1.2). In most of these cases, as shown in Figure 1.3 and Figure 1.4, pipe exits are located in the ground floor column with 200-300 mm distance from the foundation level.

There are not many studies on openings in RC members, and the existing ones mainly focus on opening in beams and slabs, while the structural response of RC columns with holes, particularly under reversed cyclic loads, has been inadequately investigated. The very few available studies on columns with openings, consider the response of columns under axial load only, which does not represent a realistic practical situation since columns in their life span experience more than just axial load, especially under seismic excitations. Hence this lack of information on this specific subject motivates the present study on the response of columns with embedded pipes

to simultaneous action of axial and lateral loadings, which is representative of actual loading condition in a typical column in buildings.

Figure 1.1. PVC pipes embedded in columns

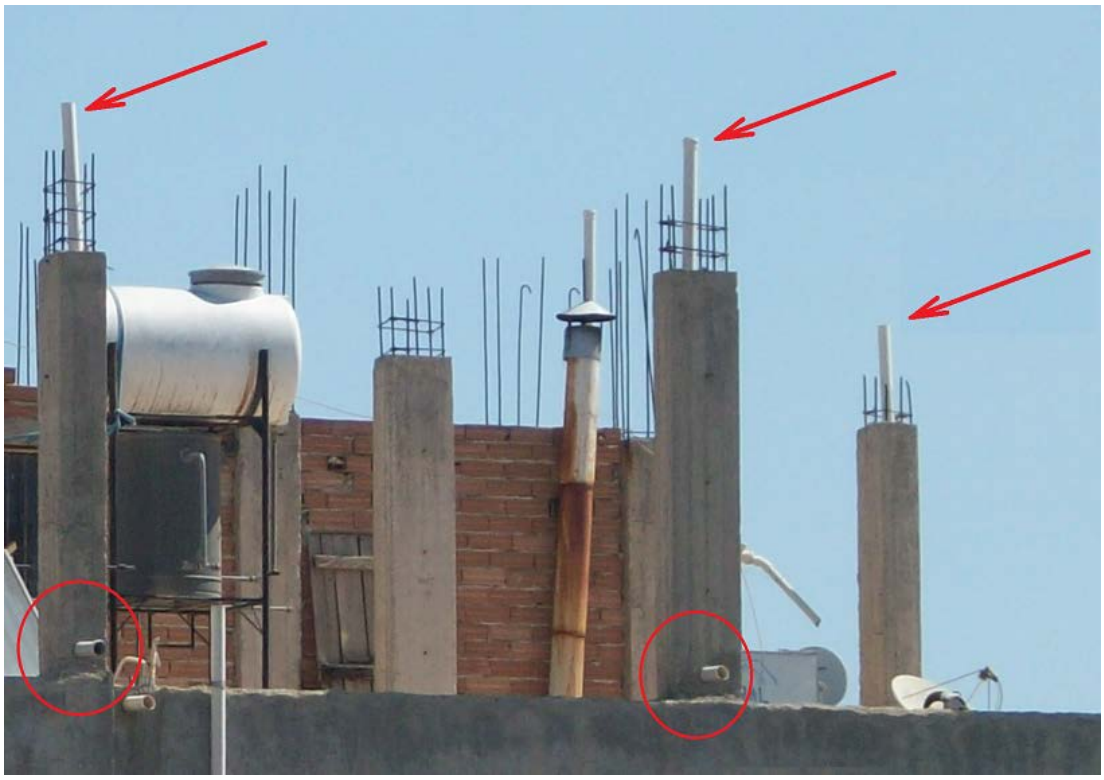

Figure 1.2. Pipe embedded in RC columns

Figure 1.3. Pipe exit at ground floor

Although it can be easily predicted that the presence of these pipes in the column core may alter the column behavior, given that at the pipe exit location the column has asymmetric cross section, nevertheless there are very few studies investigating the shortcomings of this practice and its effect on the behavior of the column under reversal cyclic loading. Furthermore, the sudden change in section properties at the pipe exit, with the exit located in the region where plastic hinge is expected to form, may adversely affect the column energy dissipation characteristic and ductility. Currently, none of the existing design codes addresses this issue, especially for columns located in active seismic regions. For these reasons, a systematic investigation is necessary to ensure practical and safe design of structures containing columns with embedded pipes. The current study is aimed at such an investigation.

1.2 Objectives and scope

The objective of the current thesis is to investigate experimentally and numerically the response of RC columns, with embedded pipes in their core, to simultaneous constant axial load and reversed cyclic lateral load. Specifically, the study aims to investigate:

- Investigating the behavior of RC columns containing service pipes under simultaneous action of axial and reversal lateral loadings to determine the overall column response and the impact of the embedded pipe on the column strength, ductility and safety.
- Gaining greater insight into the plastic hinge formation and characteristics in such columns and its effect on the column nonlinear response and energy dissipation capacity.
- Providing suitable design recommendations for such columns, especially for the more common cases encountered in practice.

The scope of the current study is limited to:

- Since the study is in the first instance aimed at existing buildings in some specific regions of the world, like Mediterranean countries and some parts of Asia, the material properties and specifications are chosen to be representative of the above mentioned conditions. It is worth mentioning that some new building are also employing embedded pipes in columns albeit their materials properties may somewhat differ from those used in the current study.
- Although the presence of drainage pipe in reinforced concrete column may give rise to issues regarding corrosion, this study does not address corrosion and the associated problems endangered by its occurrence.

- The study is limited to rectangular and square columns as these are common shapes used in the target regions and are expected to be more severely affected by the presence of the pipe because intuitively the axisymmetric nature of circular columns may mitigate the adverse effect of a centrally located pipe in the column cross-section.
- In practice, due to the accidental uneven movement of the pipe during construction, it is likely that the pipe will end up being inclined with respect to column axis, a problem which is expected to exacerbate the negative impact of the pipe on the column seismic response and strength. Due to the stochastic nature of this phenomenon, this study does not address the pipe inclination and its effect on column response; consequently, it only considers cases with vertical PVC drain pipes.

1.3 Dissertation outline

The first chapter starts with an introduction to the subject and some general comments about the topic of study. At the end of chapter the objectives and scope of the study is presented together with the outline of the dissertation.

Chapter 2 is focused on literature review related to the finite element analysis of RC structures, followed by review of the state of art on structures with opening. The chapter concludes with studies conducted on plastic hinge properties in reinforced concrete columns.

The chapter 3 presents the experimental part of the study, starting with material properties used, test setup, instrumentation employed in the test and some explanation about the testing procedure. Afterward, some general observations made during the

test and the hysteresis curves of the columns and the mode and location of failure in the columns.

Chapter 4 focuses on the numerical studies conducted regarding embedded pipes in columns, including the FE analysis of the test columns, sectional analysis and the plastic hinge length computed based on FE analysis results. The chapter opens with an introduction to the FE analysis method and the review of some available software packages for structural analysis. It continues with a brief review of concrete constitutive models from early studies till the recent ones. Next the available models in ABAQUS FE software package are discussed and the related parameters relevant to the current study are defined. Similarly, the steel model, modeling procedure, specifications of models, meshing and analysis procedure together with some results are also discussed. Subsequently, the sectional analysis results and the procedure for finding the plastic hinge length are presented and discussed.

In chapter 5, the effect of pipe presence on different properties and aspects of column response is discussed on the basis of the obtained experiment and numerical results. Specifically the effect of pipe on general response of column, effect of transverse reinforcement ratio on response of columns, effect of the location of pipe exit on response of columns, effect of axial load on the response of columns, effect of the exit on the ductility of member, stiffness degradation due to the pipes, effect of pipe on the value of balanced axial load, effect of pipe on the moment-curvature relationship, effect of the exit on stress distribution and effect of pipe on plastic hinge length are discussed.

Finally, in chapter 6, the study's conclusions together with some tentative design recommendations are presented.

Figure 1.4. Drainage pipe is exited from column

Chapter 2

LITERATURE REVIEW

2.1 Background

In this chapter, firstly, study programs regarding to the finite element modeling of reinforced concrete elements are presented. Afterward, studies focused on reinforced concrete members with openings are reviewed and in the end the state of art pertaining to plastic hinge length in reinforced concrete columns is presented.

2.1.1 Previous works on finite element modeling of RC structures

One of the first publications that focused on the FEA of RC structures was done by Ngo and Scordelis (1967). They analyzed simply supported beams and modeled steel and concrete by constant strain triangular elements, in order to define steel and concrete connection and bond-slip they used a special bond link element. Via a linear elastic analysis, principal stresses of concrete, stresses of steel and also bond stresses were obtained.

In their conclusion it was stated that because of composite action of steel and concrete, modeling of RC members is problematic and only at early loading stages, when member is subjected to a small amount of load, perfect bond of concrete-steel can be seen. With increasing intensity of the load, cracks develop and slippage takes place, hence stress distribution in both materials is altered.

Afterward many researchers attempted to model RC structures by FEM and improved the finite element analysis of plain and RC structures. Vecchio (1992) proposed a method for incorporating concrete lateral expansion into nonlinear-elastic finite element analysis algorithms. Based on his study pre-strains are defined for representation of material stiffness matrix and element nodal forces. G. Sankarasubramanian et al., 1996; suggested a failure criteria for concrete including a spiral ultimate strength surface by utilising artificial neural network (ANN).

Although two-dimensional (2D) models were found practical, they could not capture the actual behavior of concrete structures in all cases. This motivated the development of reliable 3D models to simulate the monotonic and cyclic response of concrete under tri-axial states of stress. Balan et al. (2001) generally formulated a 3D material model for nonlinear finite element analysis of concrete structures inspired by the definition of equivalent uniaxial strain, first proposed by Darwin and Pecknold (1977). Their model could simulate monotonic and cyclic loading and also proportional and non-proportional loads. Post-peak crushing in compression and cracking in tension were also represented.

Researchers like Fantilli et al., (2002); Sumarac et al., (2003); Marfia et al., (2004); Phuvoravan and Sotelino, (2005); Junior and Venturini, (2007) also studied this subject and tried to improve the constitutive relationships of concrete structures.

The complexity of mechanical behavior of concrete makes modelling of this material challenging. Kwak and Fillipou, (1997) have stated the difficulties regarding proper prediction of RC elements behavior as below:

1. Nature of reinforced concrete as a building composite material which is comprised of two different materials in terms of behavior.
2. Concrete shows nonlinear behavior even under small amount of loads. Two phenomena, tension-stiffening and bond-slip have contradictory behaviors, the first one enhances the stiffness and the latter diminishes it.

For modeling of concrete, it should be considered that the material is non-homogeneous and exhibits nonlinear stress-strain relationship. Based on Kupfer et al., (1969); Kotsovos and Newman, (1977) under biaxial compressive, concrete compressive strength will be higher than its uniaxial compressive strength while under biaxial compression-tension it will be lower. By nature, concrete contains many microcracks which are induced mostly by thermal stresses, shrinkage and segregation. Later after load applications, these cracks will further develop and join, which are responsible for the nonlinear behavior of the material.

Due to its composite structure, concrete matrix has porosity as Panoskaltsis and Lubliner, (1994); Ollivier et al., (1995) have shown that the porosity is non-homogenous, especially around the inclusions formed by the aggregates, the porosity is intensified this region is referred to as the “transition zone”. The mechanical behavior of concrete is directly damaged by the effect of this zone.

Based on Hsieh et al, (1982); size and type of aggregate is also affecting the mechanical behavior of concrete under various types of loadings.

Figure 1.5 depicts non-linear stress-strain behavior of concrete under uniaxial compression as shown by Hsieh et al, (1982). Long before him Kotsovos and Newman,

(1977) stated that concrete compression behavior can be reasoned by forming and developing of micro cracks of concrete. Under different states of loading the concrete behavior may be defined by following stages as illustrated in figure 1.5.

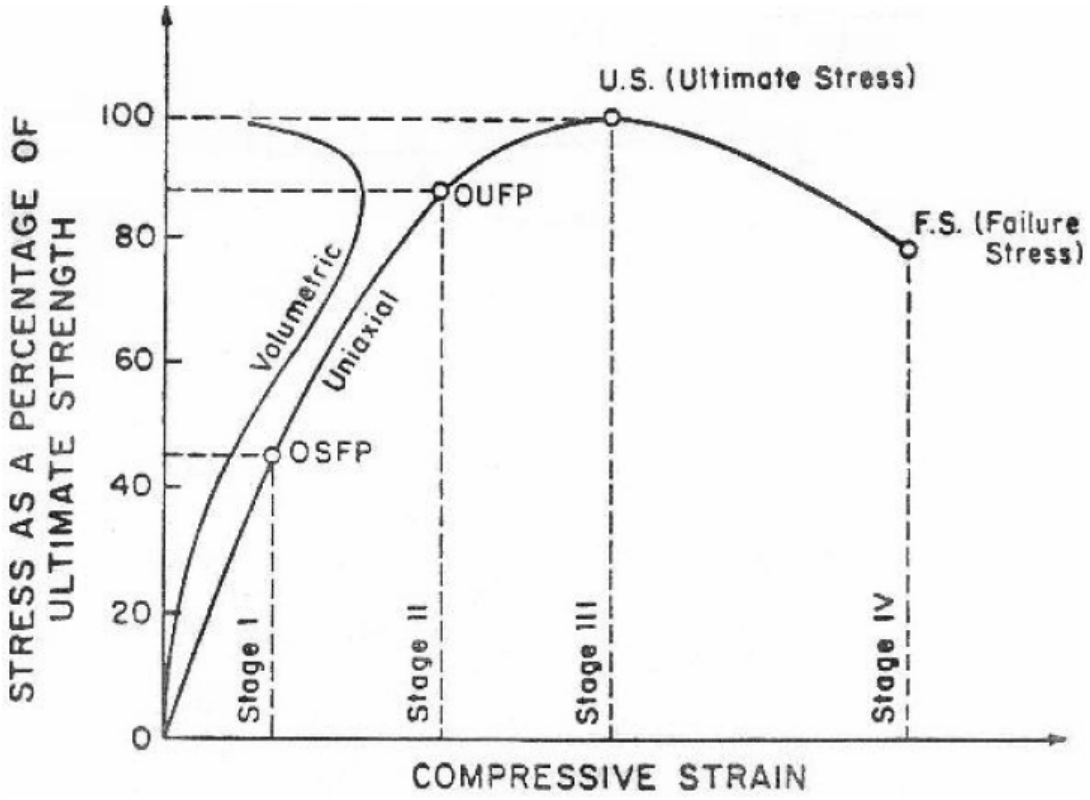

Figure 2.1. Uniaxial compression stress-strain relation of concrete, (Hsieh et al, 1982).

1. It takes place in 30 to 60 percent of ultimate strength of concrete where some micro cracks are created but not developed so the relationship between stress and strain is more or less linear.
2. This stage usually occurs in the range of 70-90 percent of ultimate strength, cracks propagate and stress-strain plot shows nonlinear behavior. A decrease can be seen in stiffness and some permanent deformations are induced in the concrete.

3. At this stage strength goes up to the 100 percent of ultimate strength. Microcracks are connected to each other and failure of concrete has progressive rate here.
4. After reaching to the peak or maximum stress, cracks further develop and propagate until global failure takes place.

A proper and reliable concrete model should contain the above mentioned stages to fully simulate the behavior of concrete.

However, when it comes to tension circumstances are totally different, based on Peterson's, (1981) proposed uniaxial tensile stress-strain curve as illustrated in figure 1.6 behavior is elastic until approximately 60-70 percent of the ultimate tensile strength. For stresses more than this limit, the aggregate to matrix interface microcracks initiate to develop, unlike compression state, there is not any resistance to confine cracks so they propagate quickly and concrete shows brittle behavior in tension.

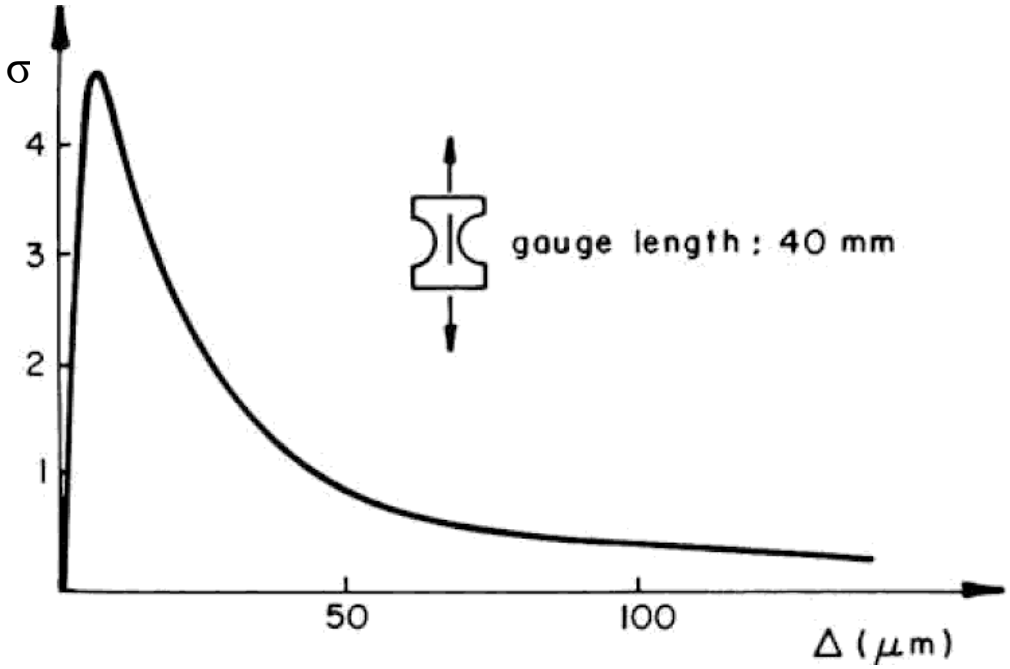

Figure 2.2. Uniaxial tensile stress-elongation curve (Peterson, 1981)

Based on current state of art, the nonlinearity in concrete is attributed to two main reasons: plastic flow and propagated micro cracks and micro voids which the latter one devastates the bond in material particles that results in some un-coverable deformation, so naturally the elastic properties of concrete are altered.

On the one hand, in some studies like Chen and Chen, (1975); William and Warnke, (1975); Bazant, (1978); Dragon and Mroz, (1979); Schreyer, (1983); Chen and Buyukozturk, (1985); Onate et al., (1988); Voyiadjis and Abu-Lebdeh, (1994);Karabinis and Kiousis, (1994); Este and Willam, (1994); Menetrey and Willam, (1995); Grassl et al., (2002) researchers tried to model concrete's behavior merely based on plasticity theories but based on Krajcinovic, (1985); Simo and Ju, (1987a,1987b); Ju et al., (1989); Voyiadjis and Kattan, (1989), (1999), (2006) the softening behavior of concrete cannot be defined and addressed by just plasticity and material stiffness degradation as a results of microcracks is neglected in such models. On the other hand, some researchers like Loland, (1980); Ortiz and Popov, (1982);

Krajcinovic, (1983, 1985); Resende and Martin, (1984); Simo and Ju, (1987a,b); Mazars and Pijaudier-Cabot, (1989) and Lubarda et al., (1994), by only applying continuum damage theories to simulate the nonlinearity in materials behavior but they also were not capable of considering some aspects like irreversible deformation, in-elastic volumetric xpansion in compression, and the crack opening or closure effect in concrete.

Since each of these methods are proven to be imperfect it can be concluded that a constitutive model of concrete should include both plasticity and damage simultaneously and equally.

Some other researchers tried to model these aforementioned phenomena by damage mechanics. The pioneers in this way were Oritz, (1985); Lubliner et al. (1989), they managed to combine plasticity and damage theories via definition of plasticity and damage surfaces, thereafter many publications on this subject appeared and it was tried to employ the plasticity and damage theories in concrete modeling.

Chen and Chen, 1975; Yazdani and Schreyer, 1990; Abu Lebdeh and Voyiadjis, 1993; Voyiadjis and Abu-Lebdeh, 1994; Luccioni et. al., 1996; Lee and Fenves, 1998, 2001; Faria et. al., 1998; Hansen et. al., 2001; Nechnech et. al., 2002; Gatuingt and Pijaudier-Cabot, 2002; Kratzig and Polling, 2004; Salari et. al., 2004; Shen et. al., 2004; Jankowiak and Lodygowski, 2004; Luccioni and Rougier, 2005, Rabczuk et. al., 2005; Wu et. al., 2006; Grassl and Jirasek, 2006; Nguyen and Korsunsky, 2006; Shao et. al., 2006; Jason et. al., 2006; Contrafatto and Cuomo, 2006; Nguyen and Houlsby, 2007; Mohamad-Hussein and Shao, 2007; Ananiev and Ožbolt, 2007; Voyiadjis et. al., 2008a,b; Yu et. al., 2008 can be mentioned out of many.

2.1.2 Previous works on RC members with opening

Most previous studies (e.g. Mansur, 1998, Ashouf et al., 1999, Simpson, 2003, Tayel et al., 2004 and Wang et al., 2008) were carried on mechanical effects of service pipes passing through reinforced concrete beams and slabs. Mansur et al. (1984) proposed an approach for finding the failure load of RC beams with larger sizes of opening. Their method is applicable for simple beams under a point load at a solid section with a specified distance from the ending support. Tan and Mansur (1996) later improved on previously given recommendations and suggested a step by step method for designing RC beams containing large openings which could aid the designer in selecting right sizes and locations for the web openings. Mansur and Tan (1999) stated that the classifying of openings is subjective to the beams' response. An opening may be counted as relatively "small" whenever the beam manages to represent the beam type behavior and correlated beam principles are applicable. And whenever the beam stops to behave like its typical behavior, the opening should be labeled as "large". Li et al., (2015) and Qian et al., 2016 carried series of experimental and numerical studies on the effect of openings on RC walls and proposed an improved strut and tie model for predicting the ultimate strength of a wall with opening.

Studies on openings are also carried out both experimentally and by finite element modeling. Mohamed et al., (2014) tried to illustrate the behavior of RC deep beams with web openings by using Finite Element Method. The 2D finite element models included simply supported and continuous deep beams subjected to 3-points and 4-points loads. In the end, based on location and depth of the openings the results were categorized. Another study by E. M. Lotfy 2013 investigated the concrete columns with transverse holes, subjected to axial force. The study aimed to examine square and circular cross sections for openings, also different sizes of openings have been studied.

Both experimental and numerical analyses were carried out. It was suggested that some specific locations and sizes of openings can be considered as “safe”. However, the effect of lateral forces was not taken into account. Concealed service pipes in columns have been studied by Bakhteri et al., 2005. However, this study is limited to members subjected to axial loading. The cast columns have been tested by subjecting to axial load and failure loads were recorded. It has been concluded that the strength capacity of columns with pipes can be reduced significantly. It is evident that to date very little research programs have been conducted on the behavior of columns containing embedded pipes.

2.1.3 Previous works on plastic hinge length of RC structures

Plastic hinges are formed in some regions of structural elements which are subjected to moments bigger than their yield moment capacity. Structural engineers are interested in plastic hinges due to their important role in the plastic energy dissipation by the member during earthquake events. In the literature there is no specific study on the effect of service pipes passing through the column on the location and length of plastic hinges.

For the past several decades plastic hinges, their locations and their behaviors have been popular research topics. Based on the moment-curvature diagram, when at a section, the moment reaches to its nominal moment capacity, plastic rotation takes place without any significant change in the moment and the member starts to behave as if there was a hinge at that section. For this reason, they are formed in the location of maximum moment in reinforced concrete columns. To enhance the ductility of columns, extra confinement must be provided in plastic hinge regions, thus proper prediction of the location and length of plastic hinges are essential. Many researchers

have attempted to develop some expressions to calculate the location and length of plastic hinges for RC columns.

The earliest study was conducted by Baker 1956. In their suggested formula as presented below, amount of longitudinal bars and level of axial load were not taken into account.

$$l_p = k_1 k_2 k_3 \left(\frac{z}{d}\right)^{0.25} d \quad (2.1)$$

Where k_1, k_2, and k_3 depend on rebars, axial force on the column and class of concrete. Z represents the distance from contra-flexure point and the critical section and d stands for effective depth of column. k_1, k_2, and k_3 can be obtained as follows:

$$k_1 = \begin{cases} 0.7 & , \ mild\ steel \\ 0.9 & , \ cold - worked\ steel \end{cases} \quad (2.2)$$

$$k_2 = 1 + 0.5 \frac{p}{p_u} \quad (2.3)$$

$$k_3 = \begin{cases} 0.6 \ , & C_u = 42\ Mpa \\ 0.9 \ , & C_u = 14\ Mpa \end{cases} \quad (2.4)$$

Where P is the existing axial load on the column, P_u is pure axial load capacity of column and C_u is the class of concrete obtained from cube test. It should be pointed out that the above formula is somewhat conservative.

In 1968 Committee 428 of ACI (ACI-ASCE 1968) proposed a set of equations giving an upper and lower values for estimation of l_p as follows:

$$\text{min of}: \left(R_\varepsilon \left(\frac{d}{4} + 0.03\, z\, R_m\right) \ and \ R_\varepsilon\, d \right) < l_p < R_\varepsilon \left(\frac{d}{2} + 0.10\, z\, R_m\right) \quad (2.5)$$

In which;

$$R_\varepsilon = \frac{0.004 - \varepsilon_{cue}}{\varepsilon_{cuo} - \varepsilon_{cue}} \quad (2.6)$$

$$z = \frac{4\,M_m}{4V_z + \sqrt{w\,M_m\,R_m}} \quad (2.7)$$

$$R_m = \frac{M_m - M_e}{M_u - M_e} \quad (2.8)$$

Where:

d = distance between extreme compression fiber to the centroid of tension reinforcement

w = uniformly distributed load at a section of maximum moment

V_z = shear adjacent to a concentrated load or reaction at a section of maximum moment

M_m = maximum moment in a length of member

M_e = elastic limit resisting moment

P_u = ultimate axial load capacity

ε_{cue} = elastic component of ε_{cu}, calculated or assumed in the range of 0.001 to 0.002

ε_{cu} = maximum compressive strain in concrete at M_u and P_u

ε_{cuo} = basic maximum compressive strain in concrete, a value in the range of 0.003 to 0.004

It is notable that, as presented above, the suggested equations by ACI do not take the effect of longitudinal and transverse steel into consideration.

Later Park and Priestley conducted series of tests on real size columns in 1981 and 1987 and suggested that the height of column should be also taken in to account, they presented an expression which normally yields a value of *0.4h* for l_p for typical RC columns in which *h* is the whole depth of the column cross section. The cross section of their samples were square, rectangle, circle and square hollow sections. In their study axial force varied from $0.2f_c^{`}A_g$ to $0.6f_c^{`}A_g$. In the end, the ratio of axial load,

yield stress of steel and steel ratio were mentioned to have little influence over the plastic hinge length.

Mander 1983 did an investigation on some experimental results and proposed a formula for l_p as shown below.

$$l_{py} = 32\sqrt{d_b} \qquad (mm) \tag{2.9}$$

$$l_p = l_{py} + 0.06\,L \tag{2.10}$$

Where d_b represents the longitudinal bars diameter, l_{py} is yield penetration of rebars and L is the total height of the column. He stated that the plastic deformation comes from spread of plasticity within the member and yield penetration of longitudinal bars beyond the limits of plastic hinge. He also emphasized that the actual length of member that requires detailed confinement should be taken as about *3.0* l_p.

Sakai and Sheikh 1989 performed a vast literature review and concluded that the plastic hinge length is very sensitive to aspect ratio which is shear span to depth of section, transverse steel and axial force.

Tanaka and Park 1990 investigated the case experimentally and indicated that plastic hinge length may vary from $0.4h$ to $0.75h$ They highlighted that increasing the axial load increases the value of l_p. It is notable that the maximum height of their columns was 1800 mm.

Bayrak and Sheikh 1997 reported the length of plastic hinge to be *1.0 h*. It should be mentioned that their test specimens were subjected to high levels of axial load and they used high strength concrete. In their result, the l_p was stated to be insensitive to the ratio of steel and amount of axial load.

Sheikh and Khoury 1993 carried out some tests on concrete column cast by normal and high-strength concrete subjected to relatively high level of axial forces and deduced that longitudinal steel ratio, transverse steel, axial force and class of concrete have no effect on the occurrence of plastic hinges.

Bae 2005 and Bae and Bayrak 2008 studied the effect of many variables, such as shear span to depth ratio, axial force and transverse steel, on the length of plastic hinge l_p and proposed a method for determining plastic hinge region. In their method by obtaining compressive strain of concrete in critical sections and using strain profile, strains in longitudinal bars located in compression face can be calculated. Then based on strains in bars length of region in which the yield strain of steel is exceeded can be obtained. In the end the effect of stub confinement was also embedded in their proposed expression. In their study the effect of axial load, ratio of steel and dimensions of cross section were found to affect the plastic hinge length. Equation 1.7 presents the proposed formula by them:

$$\frac{l_p}{h} = \left[0.3\left(\frac{p}{p_0}\right) + 3\left(\frac{A_s}{A_g}\right) - 0.1\right]\left(\frac{L}{h}\right) + 0.25 \geq 0.25 \qquad (2.11)$$

Where h is the total depth of section, P is the present axial load, P_0 is the axial load capacity, A_s is longitudinal bars area, A_g is the area of gross section and L is the total height of columnn.

2.2 Summary

Since previous studies on RC columns containing embedded pipes have primarily focused on their response to monotonic axial loads, the aim of the work reported in this study is to investigate, for the first time, their seismic response to concurrent axial and reversed cyclic lateral loads.

Also considering the studies regarding to the plastic hinge properties, it can be said that although many research programs have been conducted over the years, except for Priestley and Park (1987), who investigated hollow cross sections plastic hinge properties in bridge columns, there is no study on the effect of irregularity of column cross sections on l_p.

In the present study it is intended to find an answer to the following two questions:

1. How acutely the strength and ductility of a column may be affected by the presence of an axially embedded PVC pipe in the column core while subjected to combined axial and reversed cyclic lateral load?
2. How applicable are the existing equations for calculating the plastic hinge length and damage locations to columns with irregular cross-section along its length, such as the cross-section in the current test columns where the pipe exits?

The main emphasis of this thesis is to answer the above two questions.

Chapter 3

EXPERIMENTAL PROGRAMME

3.1 Test specimen details

A total of nine specimens with two subassemblies- the column and the footing, as shown in figure 3.1 were constructed in the structure lab of EMU Civil Engineering Department. The key parameters of the experiment were the level of axial load, spacing of stirrups, the presence of pipe and location of pipe exit. All columns had 200 × 200 mm square cross section with four φ12 mm longitudinal rebars which made 1.1% steel ratio intended to represent a typical existing reinforced concrete column of a building in Mediterranean region and with 200 × 350 mm rectangular footings reinforced with 6 φ14 mm rebars as planar reinforcement and φ8 mm rebars spaced at 50 mm with 135° hooks as transverse reinforcement. The column transverse reinforcement was also φ8 mm with 135° hooks spaced at 200 mm based on the minimum transverse reinforcement spacing given by Turkish Standard TS 500 (TS 2000). On the other hand, in the case of confined columns, spacing was decreased to 80 mm in order to meet the requirements of TEC 2007. Table 3.1 shows additional details of the specimens.

All pipes embedded in the columns in this investigation were circular, had 50.8 mm (2 inches) diameter, and occupied approximately 5% of the gross sectional area of the column. Figure 3.1 and figure 3.2 also show the exact location and details of the

reinforcing bars, including the concrete cover provided in both the column and their footing.

Table 3.1. Design parameters of specimens

Specimen	Confinement	Details	Axial load (kN)
C-1	Φ8/200mm	exit at 100 mm from footing	450
C-2	Φ8/200mm	exit at 100 mm from footing	100
C-3	Φ8/200mm	exit at 150 mm from footing	100
C-4	Φ8/200mm	exit at 200 mm from footing	450
C-5	Φ8/200mm	exit at side at 100 mm from footing	0
C-6	Φ8/80mm	exit at 100 mm from footing	100
C-7	Φ8/80mm	exit at 100 mm from footing	450
C-8	Φ8/200mm	No pipe	450
C-9	Φ8/200mm	No pipe	100

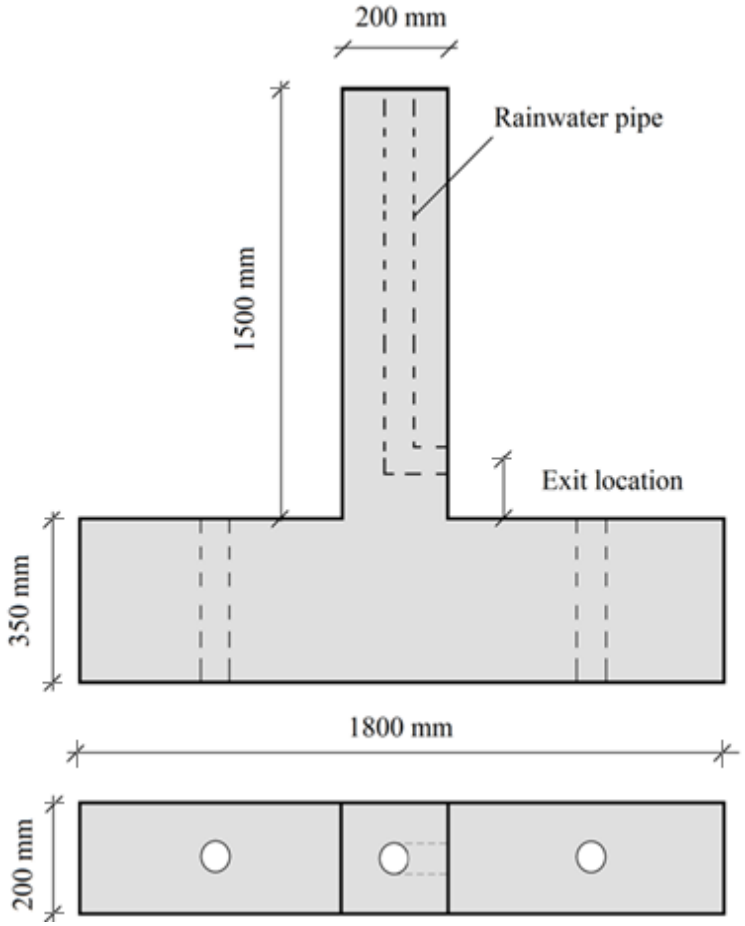

Figure 3.1. Side view and plan view of specimens with service-pipe

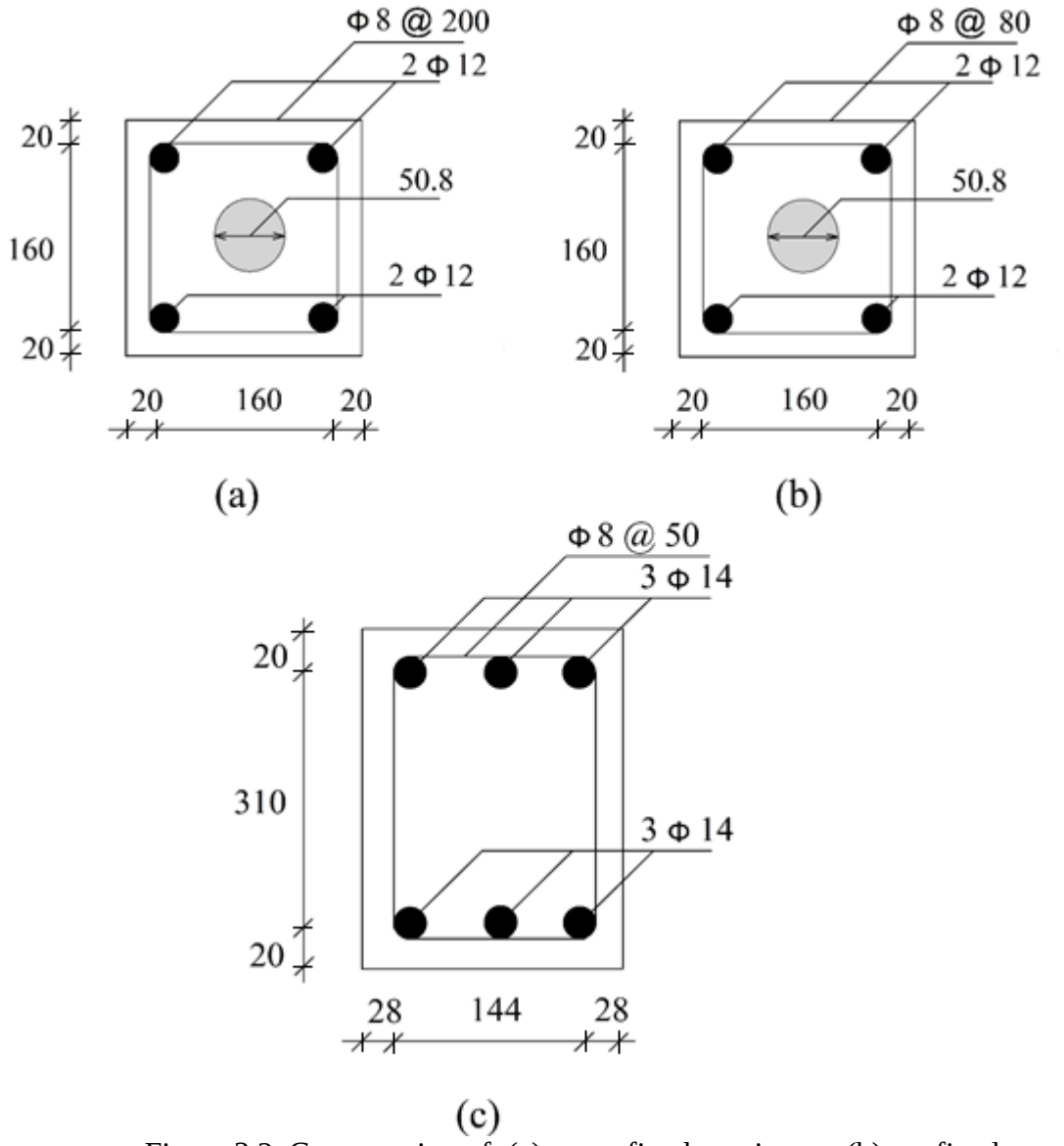

Figure 3.2. Cross section of: (a) unconfined specimens; (b) confined specimens; (c) footing

3.2 Material properties

Ready-mix concrete C16 with 10 mm maximum aggregate size and slump of 180 mm was used for all the test specimens. To avoid a cold joint between the column and the footing each specimen was cast in its entirety in one go. The measured 28-day compressive strength of the concrete obtained based on ASTM C39/C39M from three 150 x 300 mm standard cylinders was found to be 16.8 MPa, 17.3 MPa and 17.5 MPa, respectively, giving an average strength of 17.2 MPa. Note that relatively low concrete

strength was used to simulate the concrete strength normally found in existing buildings in the Middle East. The values of $f_{cu,28}$ and E_c are presented in table 3.2. The nominal yield strength of both the longitudinal and transverse reinforcing bars was 420 MPa but their actual yield strengths obtained from test on three coupons, as reported in Table 3.3, were higher. In addition to the yield strength, f_y, the table also gives the ultimate strength and strain, f_u, and ε_u, respectively, of each bar.

Table 3.2. Material properties of concrete

Material	$f_{cu,28}$**:(MPa)**	E_c**:(MPa)**
Sample 1	17.3	20.0×10^4
Sample 2	16.8	19.9×10^4
Sample 3	17.5	20.2×10^4

Table 3.3. Material properties of steel

	f_y **: MPa**	f_u **: MPa**	ϵ_y	ϵ_u
Longitudinal	451	508	0.0022	0.17
Transverse	460	519	0.0023	0.18

3.3 Test set up, loading procedure and instrumentation

Details of test setup and instruments are shown in figure 3.3 and figure 3.4. To avoid cold joint at the column to footing connection, the two components were cast in one go as shown in figure 3.5. The footing beam was fixed to the rigid laboratory floor via two steel blocks in order to reduce the bending span of footings (Figure 3.6). Lateral and axial loads were applied to the free end of the column. Two hydraulic actuators with maximum capacity of 1000 kN were used as depicted in figure 3.8, to apply constant axial load and cyclic lateral displacement to each specimen according to the

displacement history given in figure 3.4. The displacement incrementation followed the algorithm: $a1=0.048\ \Delta_m$, $a_i+1=1.4a_i$, where Δ_m is the targeted maximum deformation amplitude in the test. Note, each amplitude was repeated over two successive cycles.

In order to monitor the specimen lateral displacement, four linear variable displacement transducers (LVDT) were mounted on each specimen as shown in Figure 3.4, One LVDT was placed near the free end of the column, two at the lower end of the column close to foundation level and another near the top of the footing, the latter LVDT was intended to record possible slippage of the footing and any reading of other LVDTs mounted on the column was considered by deducting from the readings of other LVDT's from the reading of the LVDT near the footing. The column could only move along the imposed displacement as its out of plane movements were restricted.

A preliminary sectional analysis was conducted for columns cross sections and according to the obtained results the value of axial loads were selected as follows: Specimens C-2, C-3, C-6 and C-9 were tested under constant 100 kN axial load, intended to be less than the computed balanced axial load of each column while specimens C-1, C-4, C-7 and C-8 were subjected to constant 450 kN axial load which exceeded the column balanced axial load in these specimens. Specimen C-5 was tested under lateral load only. During testing, some fluctuation in the axial load level occurred but it was always maintained within 10% of its intended value.

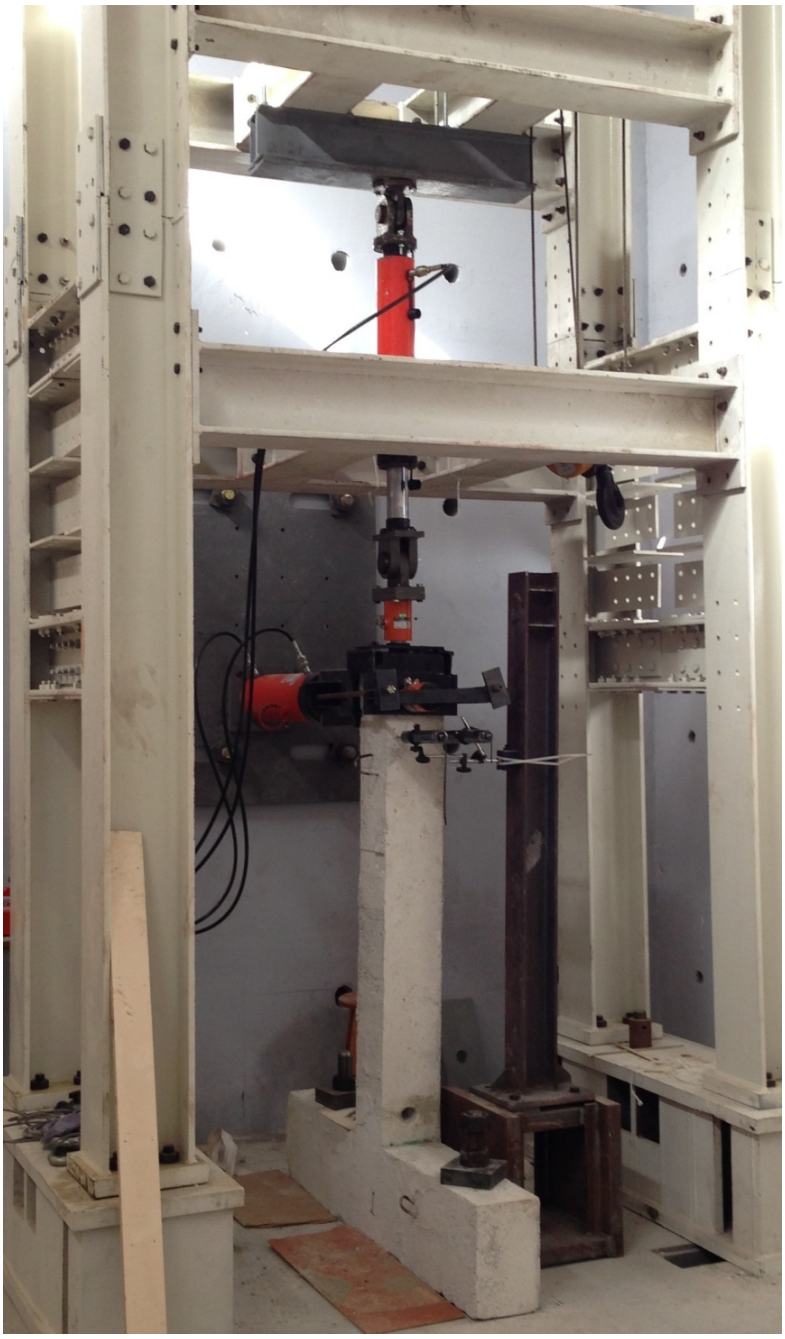

Figure 3.3. Test assembly

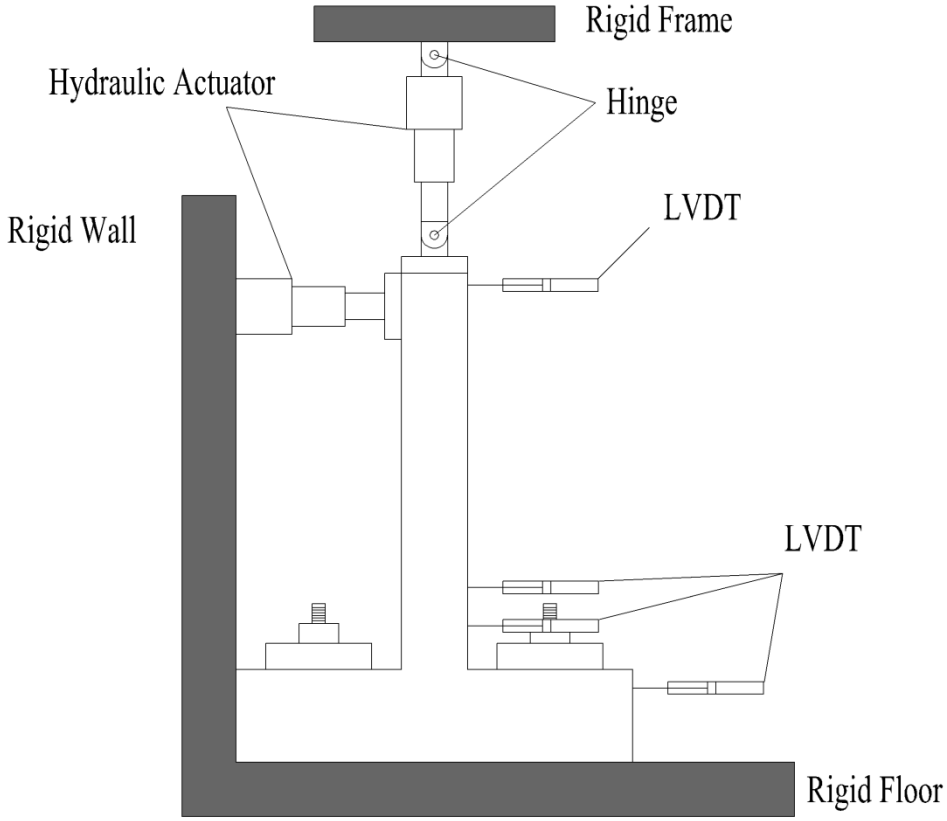

Figure 3.4. Test setup

Figure 3.5. Prepared formworks before reinforcement placement

Figure 3.6. Footing to rigid floor connection

Figure 3.7. Details of hydraulic jacks and load cells placement

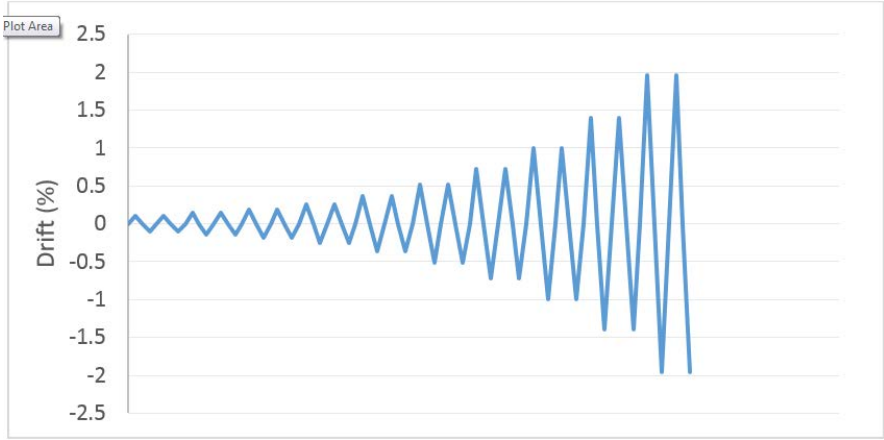

Figure 3.8. Loading history

Figure 3.9. Placement of reinforcements and PVC pipes in formwork

3.4 Experimental results

In this section the load-displacement responses of columns are presented together with some photos showing the damage state of some specimens after the test. The additional plots accompanied by detailed discussions will be presented in Chapter 5.

Figure 3.9 to figure 3.13 demonstrate the cyclic responses of columns, note that the negative cycles correspond to the loading condition that subjects the pipe exit side of the section in compression. Figure 3.14 to figure 3.16 depict some local damages around the exit location captured during the test.

3.5 General observations from the experiment

The test started with applying the targeted axial load first and then the lateral displacement. After applying the axial load, the bolts were re-tightened to minimize any movement of the footing. To avoid dynamic effects, the rate of loading was kept low. The fluctuation of axial load was under watchful eyes and the load was continually adjusted.

In this study strain gauges were applied to the column surface, but the gauges readings showed erratic trend and in some cases the sign of the strains kept changing continuously. Also the values of strains were not rational. This was due to the detachment of gauges from the surface of the concrete.

It is worth mentioning that at early stages of the loading process when specimens were in their elastic state, excluding some minor tension cracks, no specific crack was observed on the surface of the concrete, however with increasing drift to 0.4%, in specimen C-1 at the location of pipe exit, some local damage due to tension and crushing of concrete was detected as depicted in figure 3.16. The same behavior was observed in specimen C-4 at 0.5% drift. Gradually, with increasing the imposed displacement, more or less all specimens experienced some damages. At 2% drift specimen C-1 had the worst performance since it experienced sever spalling and

crushing of concrete. Specimens C-6 and C-7 showed rather good response to the imposed force and displacements.

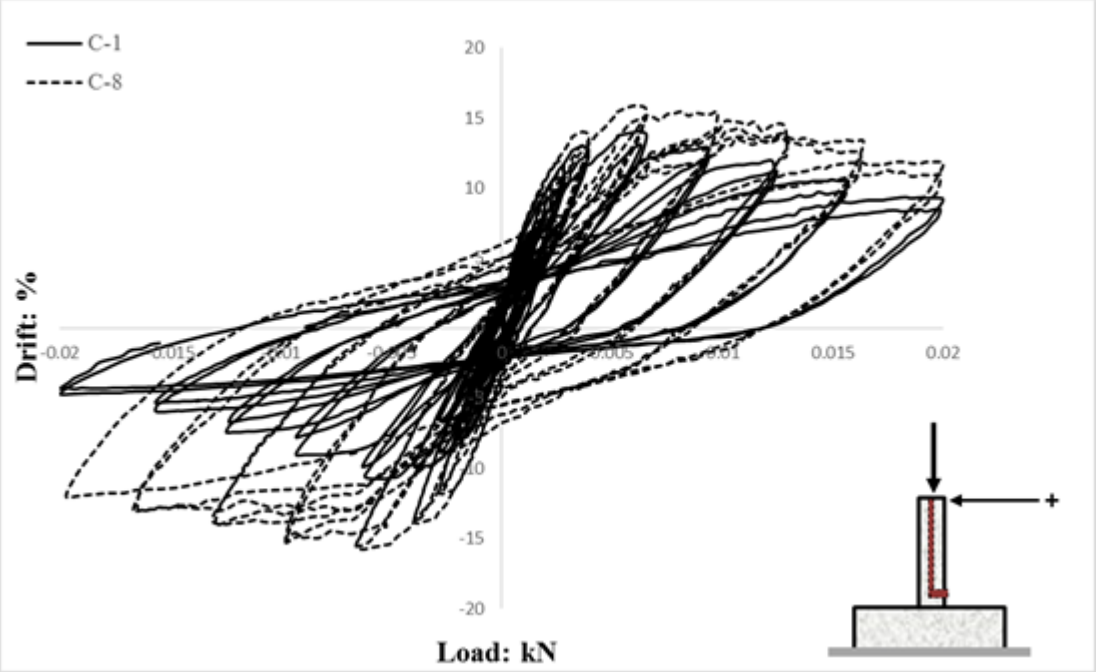

Figure 3.10. Lateral force–displacement responses of columns C-1 and C-8, tested under high axial load

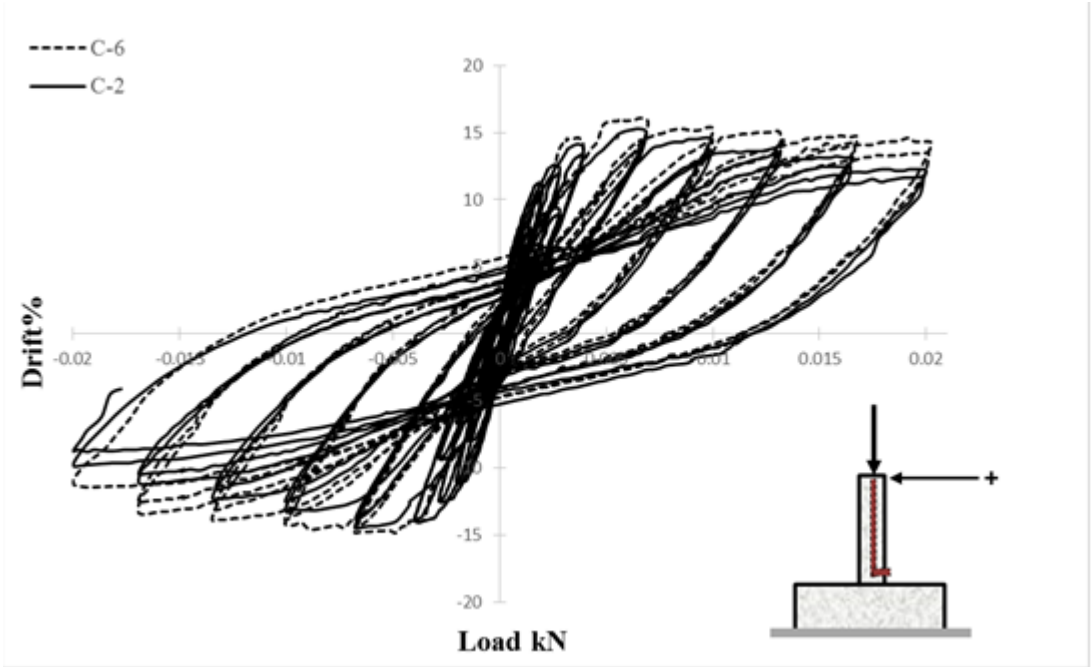

Figure 3.11. Lateral force–displacement responses of columns C-2 and C-6, tested under low axial load

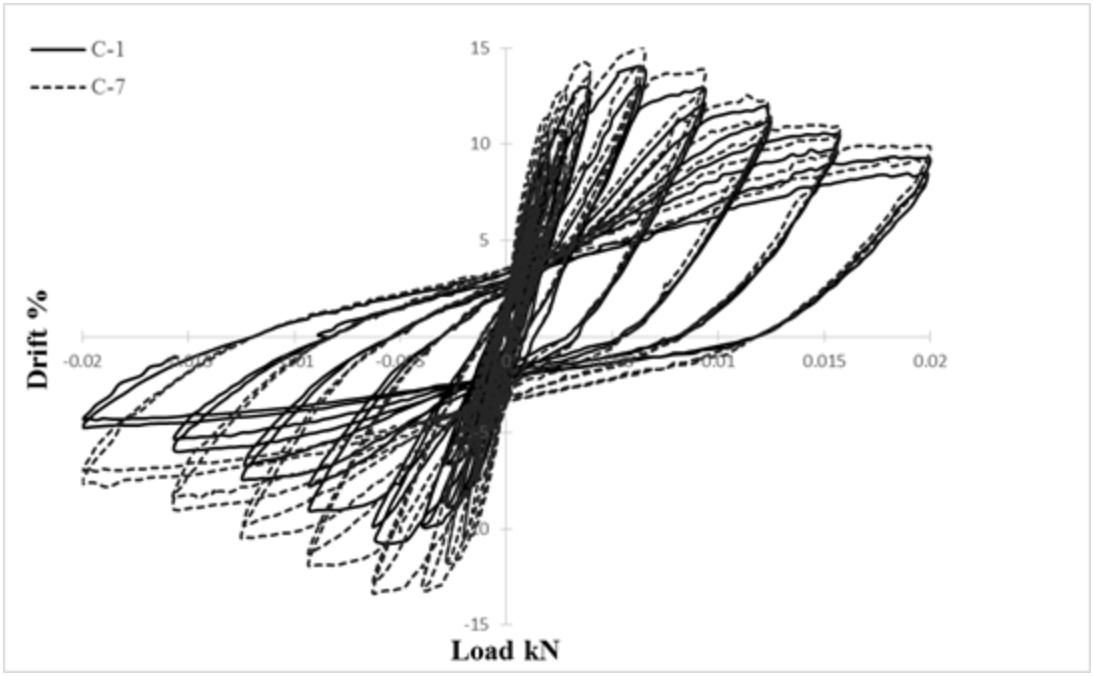

Figure 3.12. Lateral force–displacement responses of columns C-1 and C-7, tested under high axial load

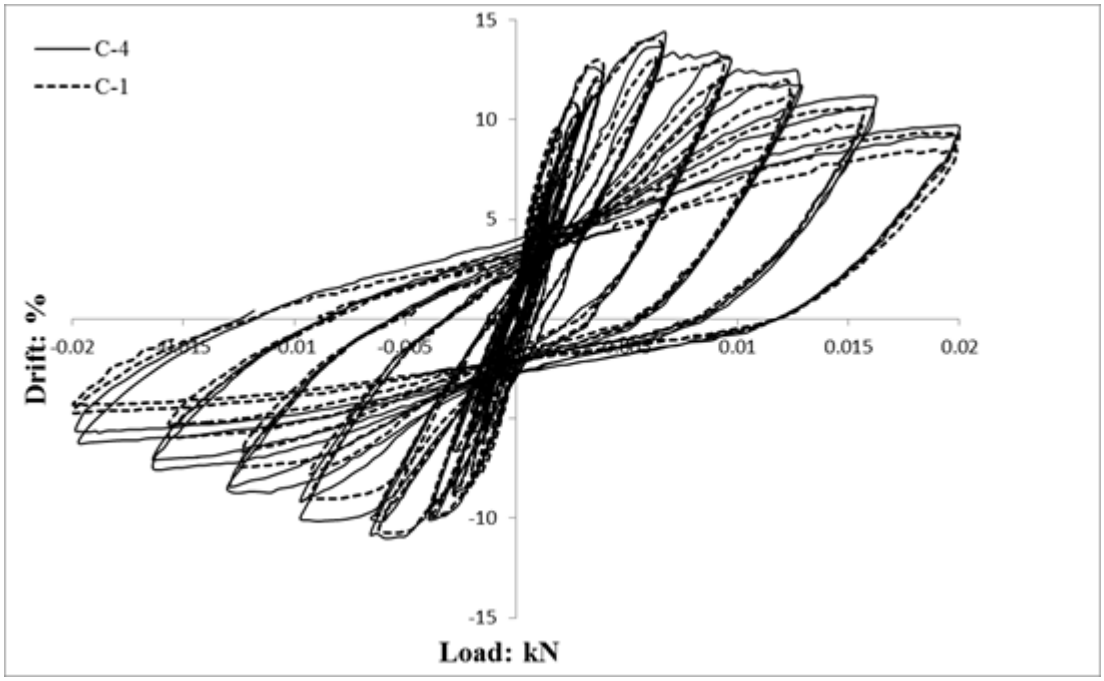

Figure 3.13. Lateral force–displacement responses of columns C-1 and C-4, tested under high axial load

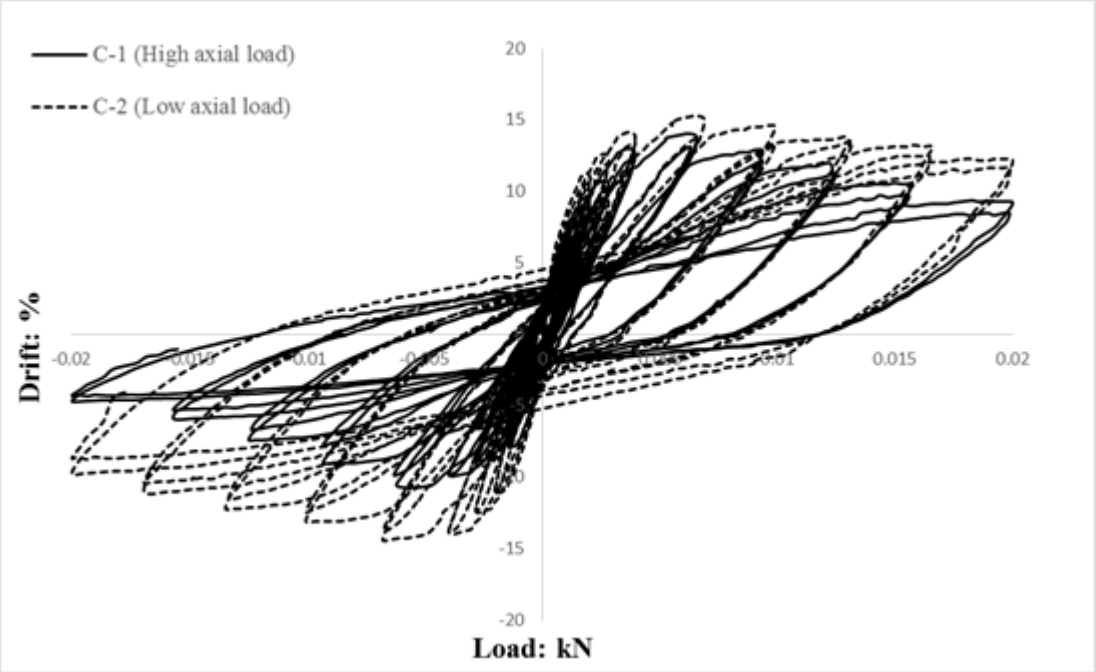

Figure 3.14. Lateral force–displacement responses of columns C-1 and C-2

Figure 3.15. Severe damage at exit location in specimen C-4

Figure 3.16. Spalling of concrete at exit location

Figure 3.17. Tension crack above the exit location observed in early stages of loading

Chapter 4

NUMERICAL ANALYSIS

4.1 Finite Element Analysis

Today, thanks to the superfast computers the tedious and time consuming computations of Finite Element Method can be performed in a relatively short time. This has caused FEM to become popular in different fields of engineering like fluid mechanics, thermal computations, electromagnetics and structural analysis. The method simulates the behavior of the whole structure by dividing it into sub-structures (element). In other words, a large model is broken to small parts with much simpler geometries and easy to analyze. Hence, the method offers intrinsic generality, less operational time, yet acceptable accuracy. It is also notable that in the case of structures with irregularity in geometry or complex boundary conditions the method shows high capability.

The abovementioned features have persuaded researchers to prefer FEM over other numerical methods such as the boundary element and finite difference methods. The popularity of FEM has encouraged companies to invest in developing sophisticated commercial programs to satisfy the user demands.

In a general form FEM analysis can be expressed in five main steps as below:

1. Subdividing the problem domain or structural model into some small sub-regions called element. The elements common junctions are called nodes.

2. Approximating the field variable(s) over each element by use of trial functions, expressed as the product of variable nodal values and interpolation functions, called shape functions.
3. Writing the total potential energy in terms of the trial functions, called functional, or the residual error, both expressed in terms of the unknown coefficients of the trial functions.
4. Minimizing the functional or residual error with respects to each of the coefficients of the trial function. This results in a set of simultaneous algebraic equations whose unknowns are the nodal values of the field variable(s).
5. Solving the resulting simultaneous equations after the imposition of the prescribed boundary and/or initial conditions.
6. Computing the field variable values at other points within each element as function of its nodal values.

An element with its surrounding nodes is called a mesh. An element might be 1D, 2D or 3D and depending on that, it may have different shapes and geometry. Due to the large number of nodal unknowns, this method can be practically implemented only by using the computational speed and data storage capacity of a computer.

As stated earlier many companies have developed finite element analysis software as the method has gained widespread popularity in science and engineering research and practice. Today, there are many commercial software packages available in the market with different capabilities. ANSYS, ABAQUS, COMSOL, ADINA, MECWAY, MIDASNFX, LS-DYNA and NASTRAN are the most prominent ones.

In the present study for the purpose of understanding the nonlinear behavior of columns under different levels of axial load, commercial software, ABAQUS was selected as the FEA solver and has been used to model the mentioned columns. Following the experimental procedure, push over analysis in the presence of axial load was carried out in FE model with different levels of axial forces and different locations of exit. The reasons for selecting this package are as follows:

1. Friendly user interface.
2. The best capability for defining general contact.
3. Extra features for defining non-linear materials like composite materials, rubber and soil.
4. Its models for reinforced concrete are shown to be reliable and accurate.
5. Possibility of defining models with large and complex shapes.
6. Sophisticated fracture and failure algorithms
7. Reputable technical support for users.

4.1.1 Concrete model

Modelling of concrete as a material is always a complicated task since the behavior of material in compression and tension are totally different. A model for concrete cannot be flawless without representing the actual behavior, both in compression and tension. When in compression, both elastic and inelastic states, considering strain softening regime, must be present in model. Also in tension state, tension softening, tension stiffening and the bond between concrete and rebars should be reflected in the model. The concrete models which are embedded in ABAQUS are basically capable of simulating the abovementioned behaviors.

The available models in ABAQUS are Concrete Smeared Cracking (CSC) and Concrete Damage Plasticity (CDP). Each its own advantages and depending on the

condition of model either model may be selected. In the case of static monotonic loading, the CSC is appropriate with enough accuracy and it can be utilized in such cases. However, when the structure is subjected to cyclic loading, the CSC may not reflect the actual behavior of concrete, in such cases the CDP model is preferred since it is mainly created for modeling of reinforced concrete elements subjected to cyclic and/or dynamic loading, like seismic excitations. This model utilizes the theories of isotropic damaged elasticity and isotropic tensile and compressive plasticity simultaneously to simulate the in-elastic nature of concrete. CDP has made it possible to define compression strain hardening with sensitivity to the rate of strain. Also, in the case of cyclic loading, the recovery in stiffness within each cycle plays a vital role in the behavior of structure. The embedded parameter of stiffness recovery in CDP model gives a more realistic behavior to the concrete. The concrete damage plasticity model CDP was proposed by Lee and Han (1998). This model is capable of simulating the behavior of concrete when subjected to any arbitrary loading condition. Also the degradation of the elastic stiffness caused by plastic straining in tension and compression is embedded in this model. Two major failure mechanisms in CDP are tensile cracking and compressive crushing of the concrete material. CDP model also simulate interaction of embedded steel bars in the concrete via tension stiffening. Another important parameter which is allowed to be defined by user is stiffness recovery effects during cyclic load reversals.

Based on the above mentioned definitions the reason that the present study uses the latter model (CDP) to model the behavior of concrete is explained. Figure 4.1 shows the modified stress-strain curve used in CDP.

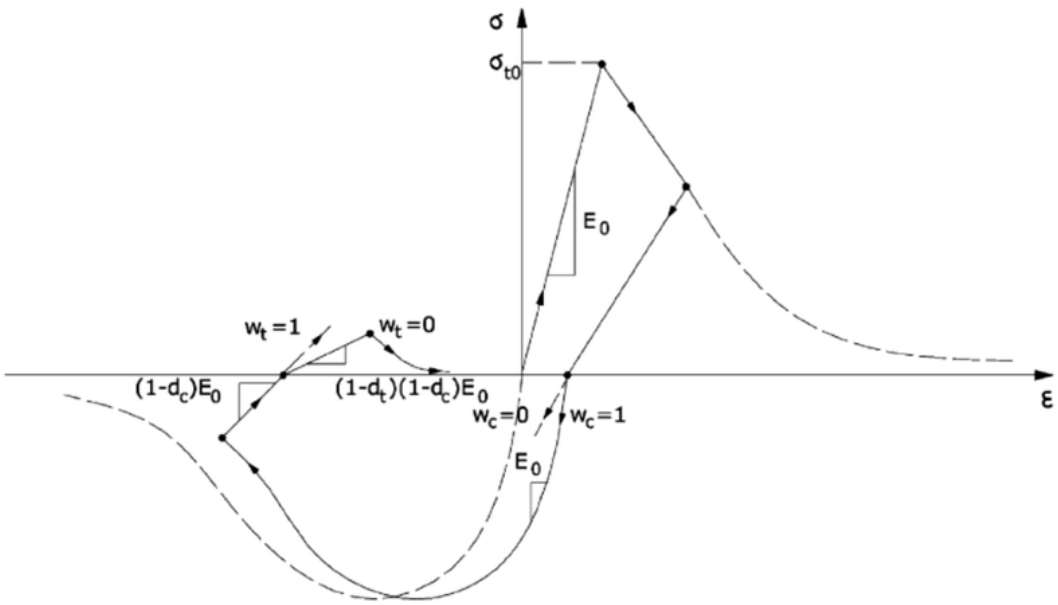

Figure 4.1. Modified stress-strain curve used in CDP

Parameters given in figure 4.1 are defined as:

E_0 = concrete modulus of elasticity

d_c = compression damage factor ($0 < d_c < 1$)

d_t = tension damage factor ($0 < d_t < 1$)

w_c = compression recovery factor ($0 \leq w_c \leq 1$)

w_t = compression recovery factor ($0 \leq w_t \leq 1$)

ε = strain

σ = stress

The dash lines in figure 4.1 represents basic tension and compression. It should be mentioned that the damage and recovery factors should be only defined in the case of cyclic reversals.

The other Concrete Damage Plasticity parameters that should be defined are enlisted as follows:

- Dilation angle $\psi = 30.5°$

- Viscosity parameter μ = 0.001
- The ratio of the second stress invariant on the tensile meridian k_c = 0.666
- Flow potential eccentricity m = 0.1
- Initial biaxial/uniaxial ratio σ_{c0}/σ_{b0} = 1.16

The dilation angle represents an amount of plastic volumetric strain developed during plastic shearing and is assumed constant during plastic yielding. Figure 4.2 demonstrates its definition.

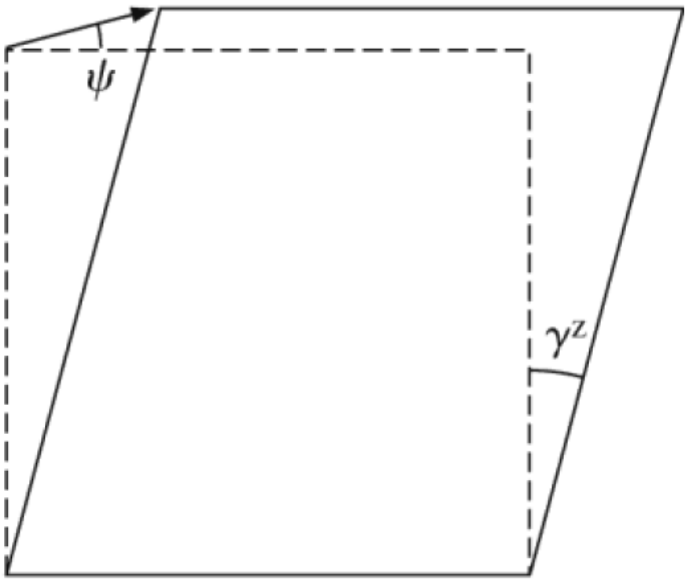

Figure 4.2. Definition of dilation angle

Viscosity parameter is the parameter allowing to suppress numerical instabilities due to convergence problems.

k_c is the ratio of the second stress invariant on the tensile meridian, at initial yield for any given value of the pressure invariant p such that the maximum principal stress is negative, $\sigma_{max}<0$. It must satisfy the condition $0.5 < k_c \leq 1$.

The Flow potential eccentricity is a small positive number that describes the rate at which the hyperbolic flow potential approaches its asymptote.

σ_{c0}/σ_{b0} is the ratio of initial equi-biaxial compressive yield stress to initial uniaxial compressive yield stress.

As presented in the previous chapter the concrete used in experiment was low strength concrete and the properties for tension and compression σ-ε curves are given in table 4.1 to table 4.4 and figure 4.3 to figure 4.6.

Table 4.1. Concrete compression hardening

Stress (MPa)	**Crushing strain (-)**
0	8.24
0.000295073	12.865921
0.000486857	14.99154075
0.000810658	16.50199346
0.001285099	16.9992674
0.002539397	14.5045296
0.003718662	12.42711259
0.008032707	4.318979474

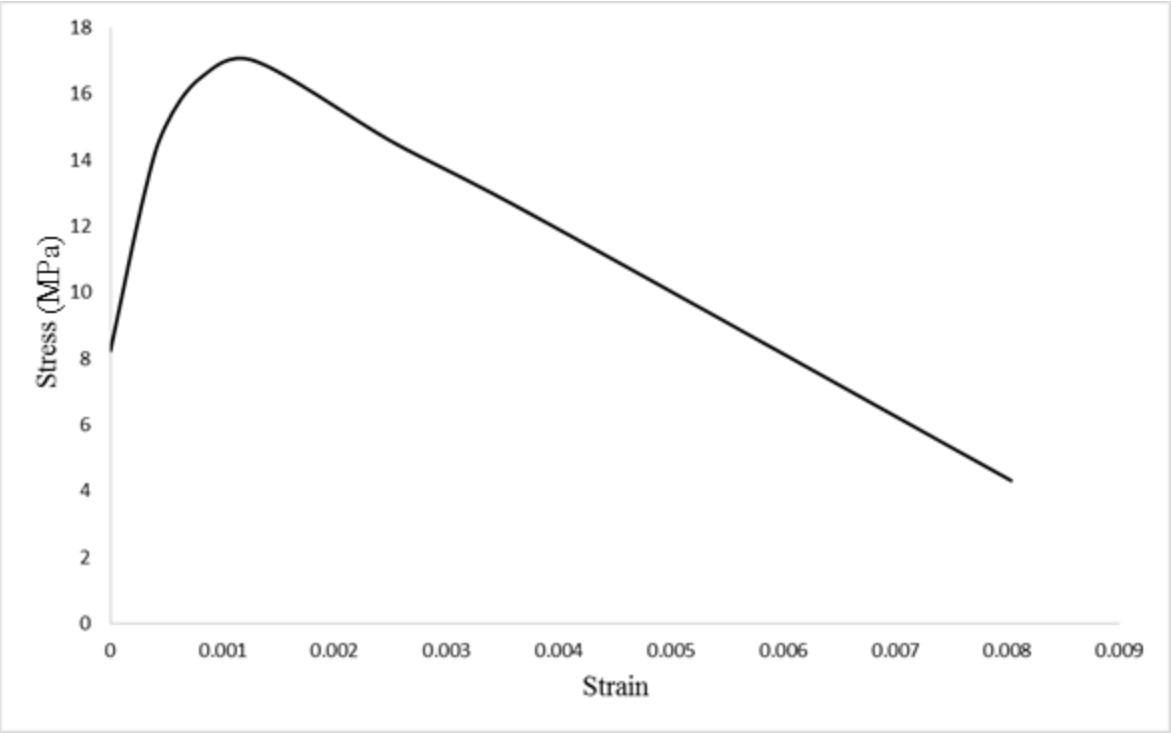

Figure 4.3. Concrete compression hardening

Table 4.2. Concrete compression damage

Damage C (-)	**Crushing strain (-)**
0	0
0	0.001088604
0	0.001185932
0	0.001285099
0.012302	0.001395715
0.269508	0.003939895
0.49745	0.005599143
0.665849	0.007037158

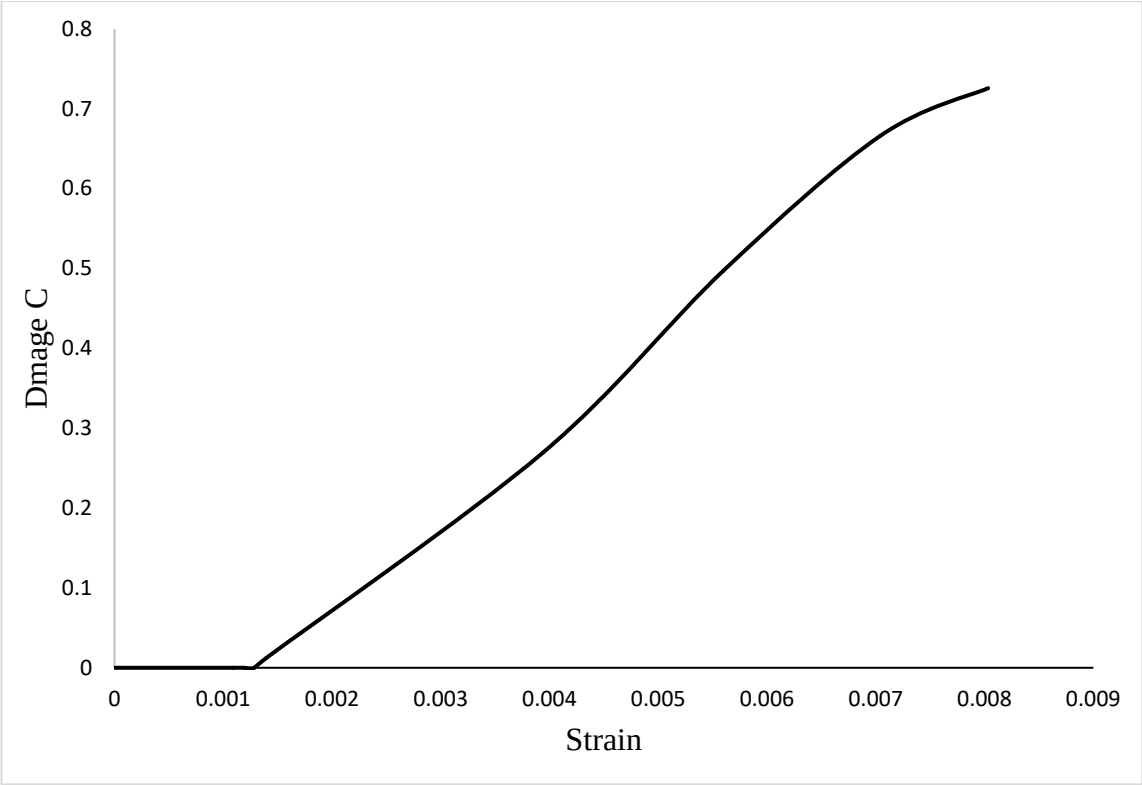

Figure 4.4. Concrete compression damage

Table 4.3. Concrete tension stiffening

Stress (MPa)	**Cracking strain (-)**
0	1.199358
3.33E-05	1.7052
0.00016	1.121886
0.00028	0.517664
0.000685	0.135752

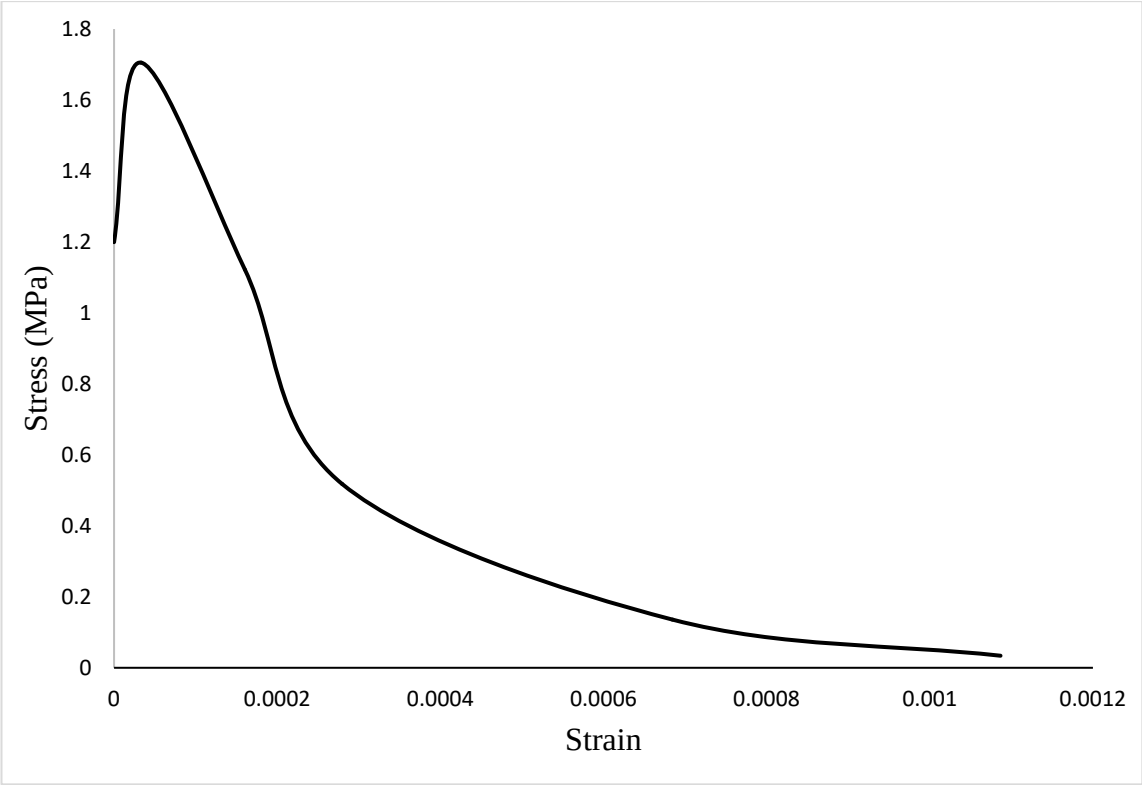

Figure 4.5. Concrete tension stiffening

Table 4.4. Concrete tension damage

Damage C (-)	**Cracking strain (-)**
0	0
0	3.33E-05
0.34208	0.00016
0.69642	0.00028
0.920389	0.000685
0.980093	0.001087

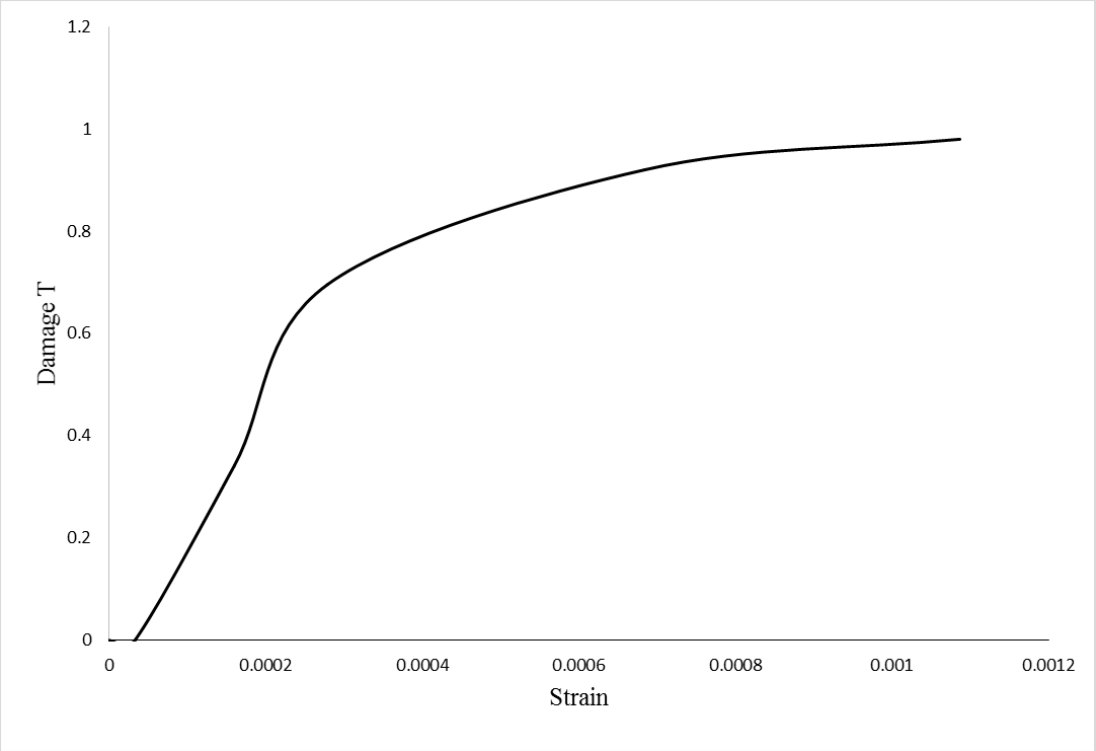

Figure 4.6. Concrete tension damage

4.1.2 Steel model

The steel material was defined for rebars with plastic properties given in Table 4.5. The type of the element which was selected for bars was beam which is capable of demonstrating both longitudinal force and shear force contribution of rebars in concrete. The other option for introducing rebars in concrete is using truss element which is basically capable of resisting just longitudinal force. In the case of embedded rebars in concrete, although beam element behaves closer to the actual behavior of rebars, truss element might be also suitable for rebars with good approximation and is widely used in ABAQUS.

To simulate the load transfer the cracks in concrete based on Hu et al., 2010 tension stiffening can be introduced and employed. The specifications of steel material used in the study are presented in table 4.5 and figure 4.7.

Table 4.5. Steel plastic behavior

Stress (MPa)	Strain (microstrain)
0	451
0.008	452
0.02	490
0.04	510
0.06	526
0.08	539
0.1	527
0.17	508

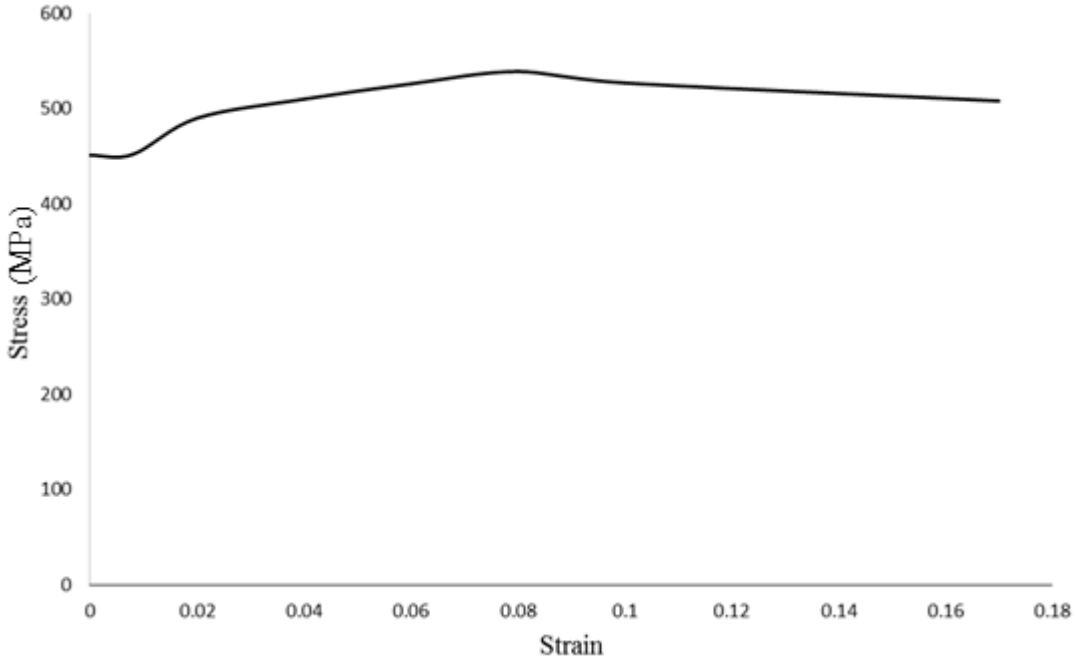

Figure 4.7. Steel plastic behavior

As mentioned earlier, transferring the forces within the cracks to rebars may be introduced by tension stiffening in concrete model (Concrete Damage Plasticity) based on Hu et al., 2010. The Poisson ratio of steel was defined 0.3 and by utilizing the

embedment option they were connected to elements of concrete while the host feature was assigned to the concrete element.

4.1.3 Modeling and meshes

A cantilever column with dimensions of 200 × 200 × 1500 mm, with a 50.8 mm diameter hole (5% of the gross section area) passing through the length with its exit placed at 100, 150 and 200 mm above support level are modeled as tabulated in Table 4.6. Figure 4.8 shows the cross section of columns with pipe and models are shown in figure 4.9 and figure 4.10.

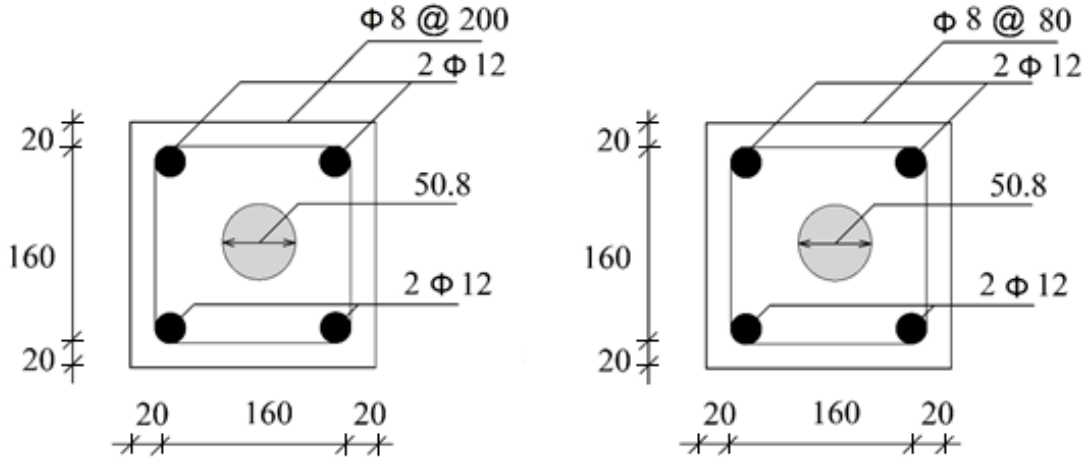

Figure 4.8. Cross section of poorly confined columns and highly confined columns

Table 4.6. Specifications of models

Name	Size: mm	Confining reinforcement	Pipe exit location	Axial load: kN
M - 1	200×200	Ø 8 @ 200 mm	100 mm from footing	100
M - 2	200×200	Ø 8 @ 80 mm	100 mm from footing	100
M - 3	200×200	Ø 8 @ 200 mm	100 mm from footing	500
M - 4	200×200	Ø 8 @ 80 mm	100 mm from footing	500
M - 5	200×200	Ø 8 @ 200 mm	150 mm from footing	100

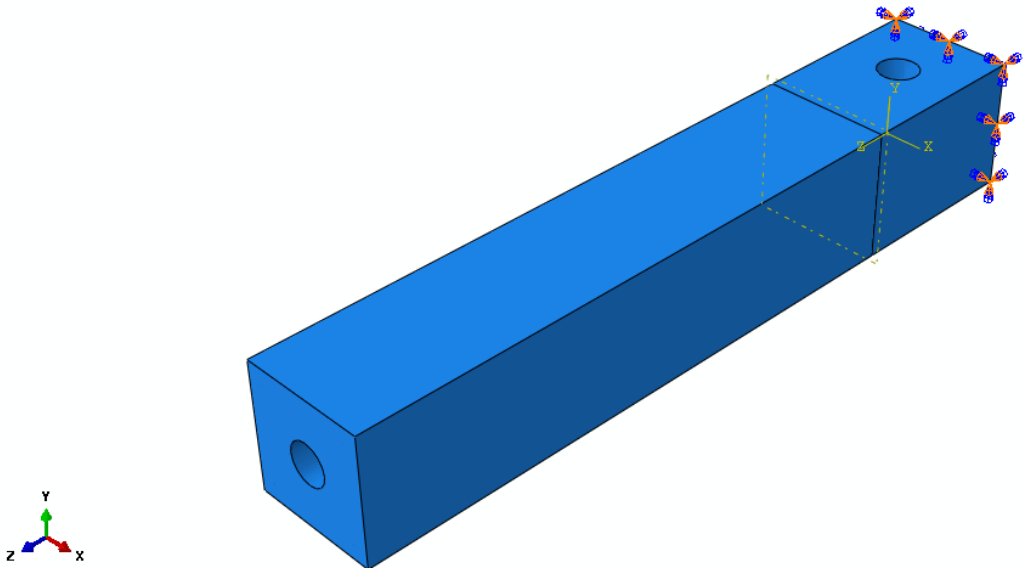

Figure 4.9. modeled columns with pipe

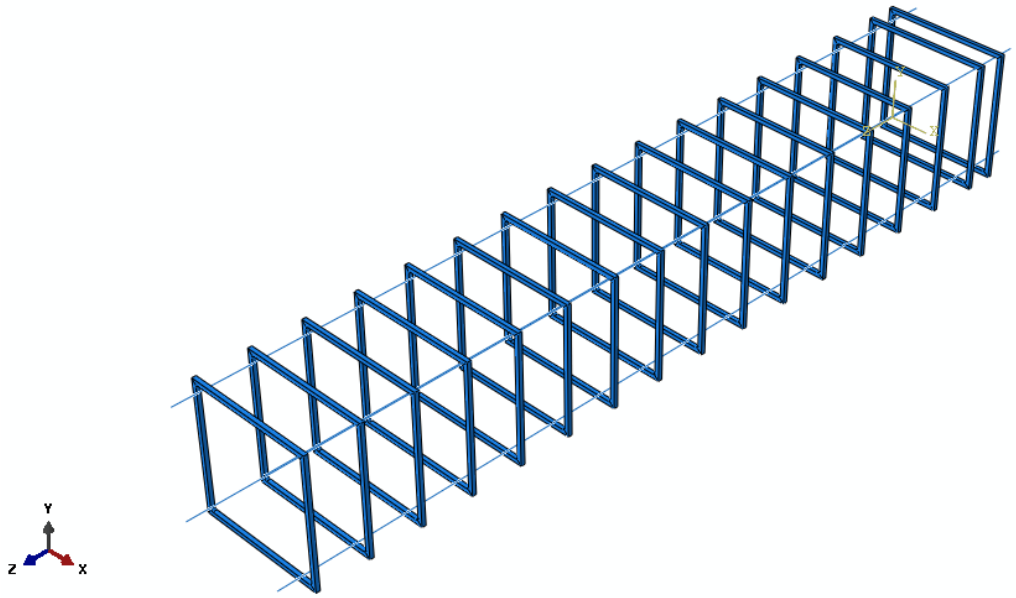

Figure 4.10. Longitudinal and stirrups before embedding in the concrete

4.1.4 Meshing

To achieve a good accuracy in finite element models, it is essential to have proper and refined meshes according to the demand of the model. Although the size of the meshes directly affect the accuracy of the analysis, but fine and small meshes make the calculations expensive both in terms of time and disk space. It should be noted that a good model should employ appropriate and optimum mesh sizes which is not too fine necessarily. Since in the present study, in addition to the global behavior of the element (column), the authors were interested in some local effects such as stress concentration and local damage, especially in the location of maximum moment (support region), it was decided to use finer mesh in the latter regions and coarser meshes in other regions of the column to make the calculations affordable. To make it possible to have different mesh sizes, a section was created at 350 mm distance from the support face to divide the column into two parts. In the part in the vicinity of the support, a finer mesh was applied, and the rest was idealized by a coarser mesh. Figure 4.11 depicts the modelled column after meshing.

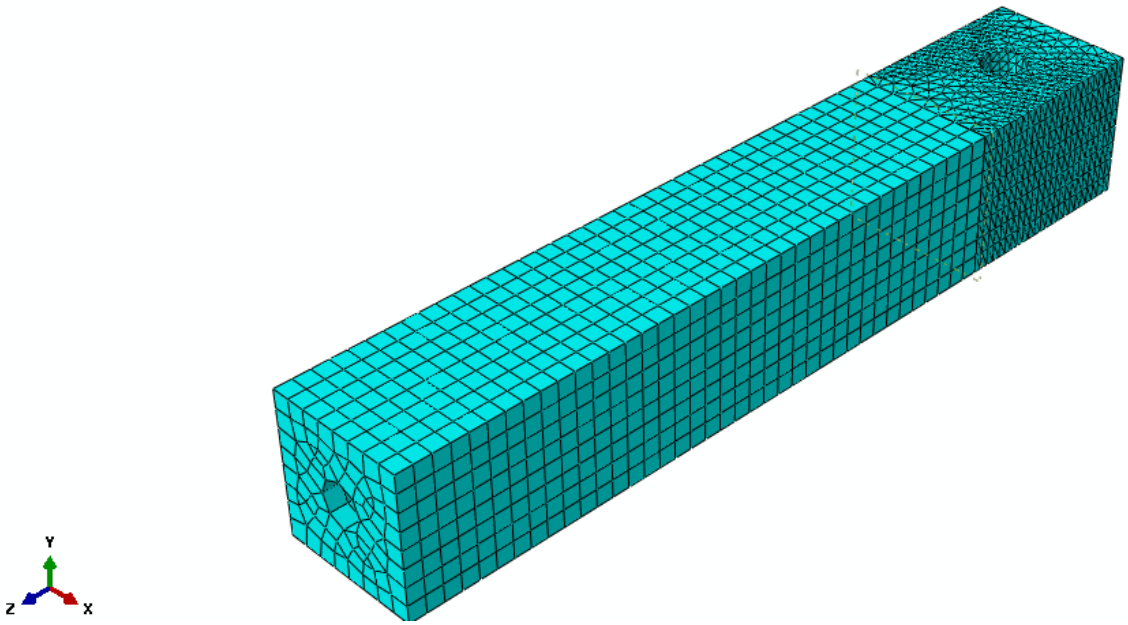

Figure 4.11. The state of the model after meshing

The type of mesh element for concrete were an eight node linear brick C3D8R and C3D10M and for steel was 2D truss T3D2, the regions around the exit were meshed finer as it can be seen in figure 4.11.

4.1.5 Analysis

Like in the experiment, a constant axial force was applied during the analysis process together with an imposed lateral displacement and push over analysis was conducted in FE model. For each model under different levels of axial forces and different locations of exit the load-displacement curves were plotted. Figure 4.12 and 4.13 show the force-displacement curve of M-1 and M-2 in forward and reverse load cycles, i.e. when the exit is in compression and tension, respectively.

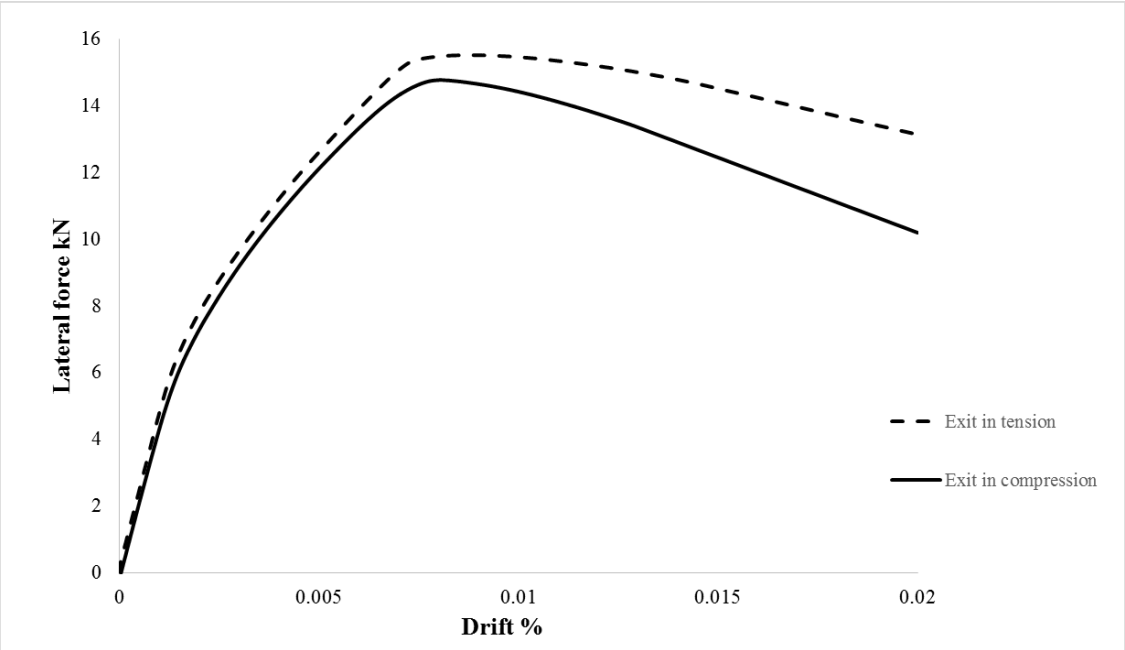

Figure 4.12. Force-Displacement plot of M-1

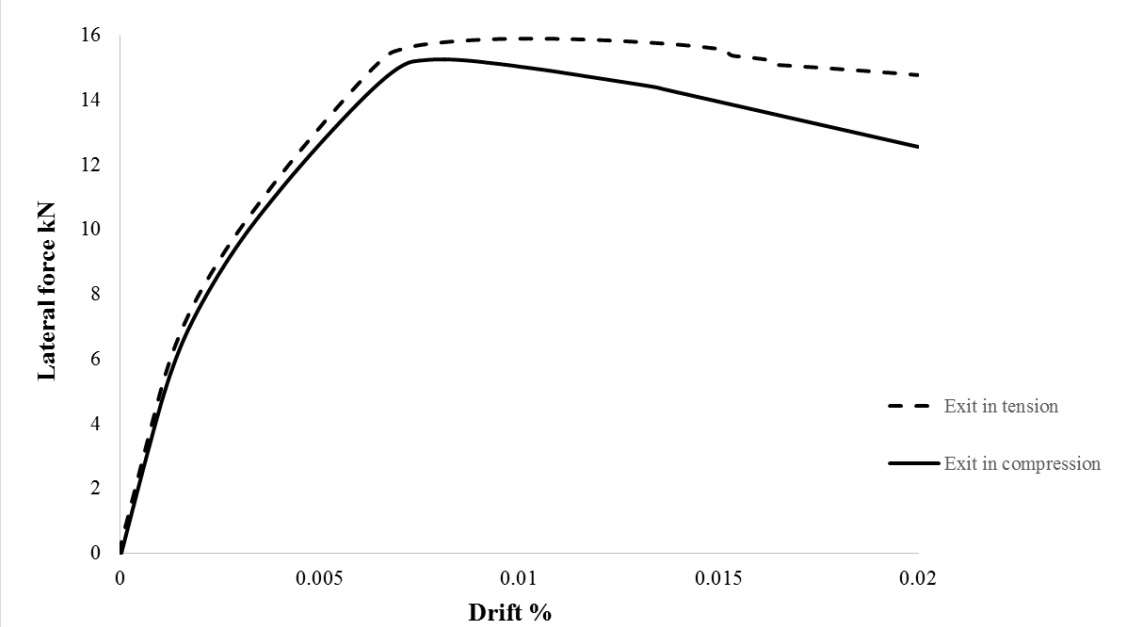

Figure 4.13. Force-Displacement plot of M-2

Also, in order to depict the effect of the level of axial load on the performance of columns with embedded pipe, the force-displacement curves of models M-1 and M-3 when the exit is in compression, are plotted together in Figure 4.14.

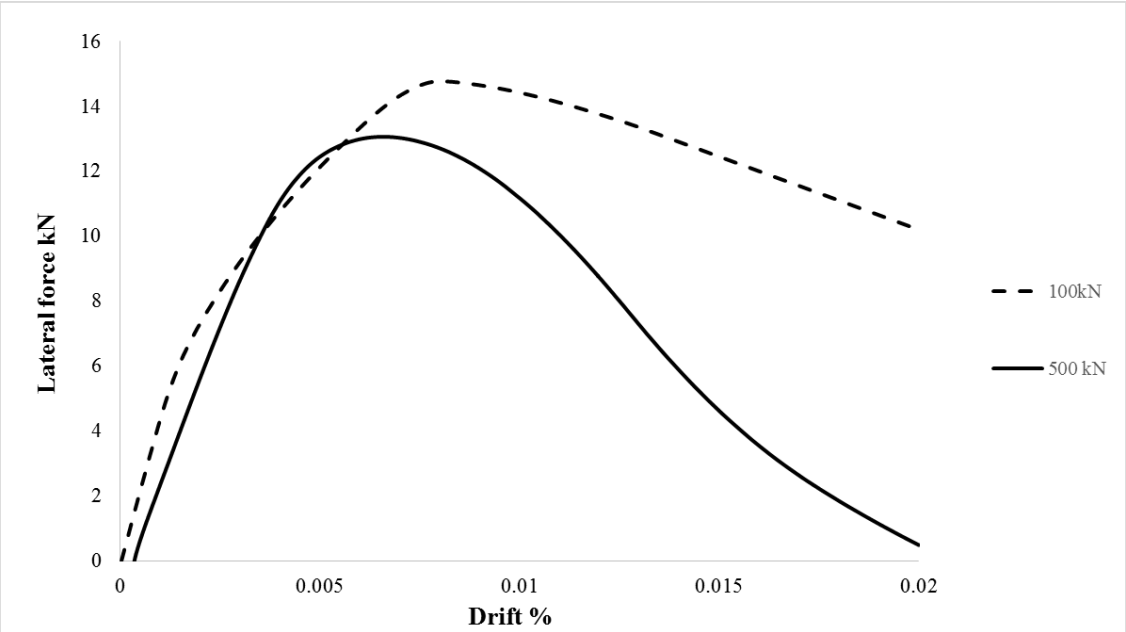

Figure 4.14. Force-Displacement plots of M-1 and M-3

As shown in experiment, the state of confinement was proven to be crucial in the response of the columns with embedded pipe, the FEM analysis also supported this fact. Figure 4.15 shows the effect of confinement on the response of such columns by comparing models M-3 and M-4 under 500 kN with their exit in compression.

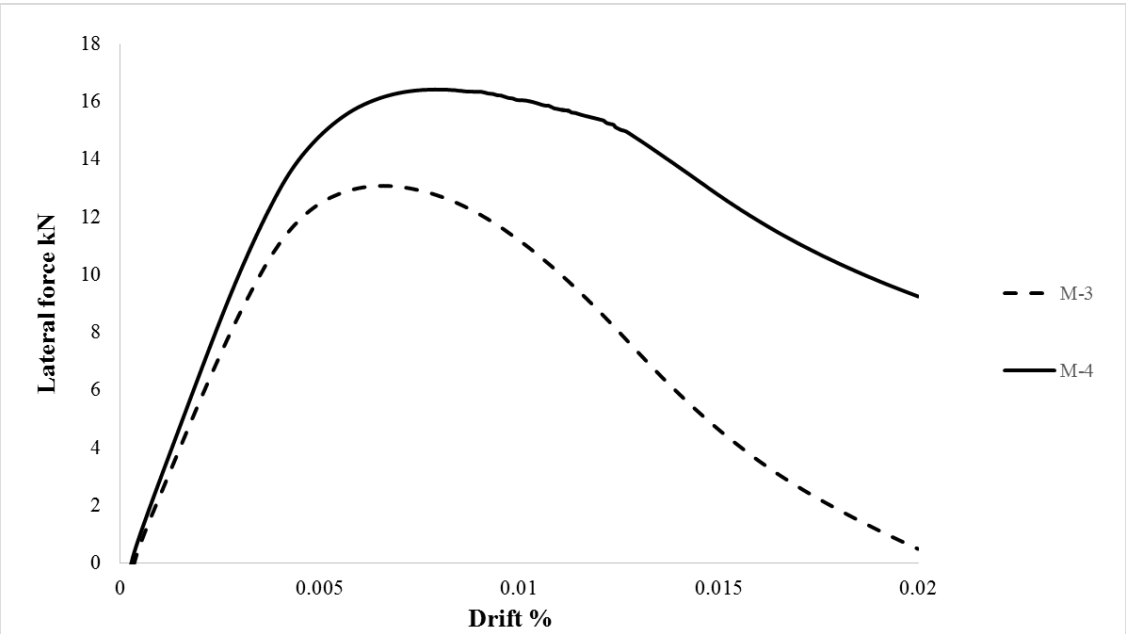

Figure 4.15. Force-Displacement plots of M-3 and M-4 under 500 kN

4.1.6 Stress concentration

Another important parameter which can aid us to study the behavior of columns concealing pipes, is investigating the stress contours obtained from finite element analysis. Figure 4.16 shows the stress contours obtained at % 2 drift of model M-1. As it could be predicted, presence of pipe exit renders the cross section irregular and disturbs the stress flow. This disturbance causes stress concentration around the hole. With increasing the imposed displacement, stress flow increases around the hole and stress concentration causes stress in some regions exceeding their ultimate capacity while in other parts stresses are still far below the ultimate capacity. Figure 4.17 shows close-up state of stresses in the vicinity of pipe exit in model M-3.

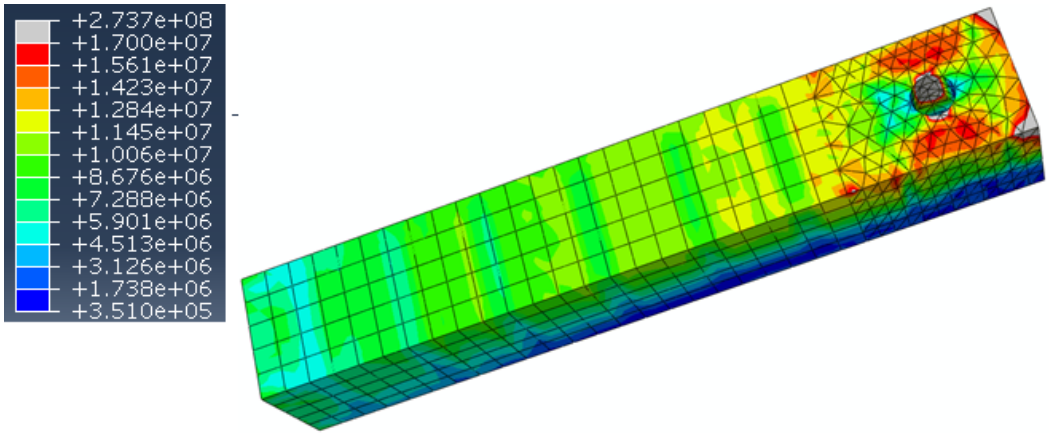

Figure 4.16. Stress contours of M-1

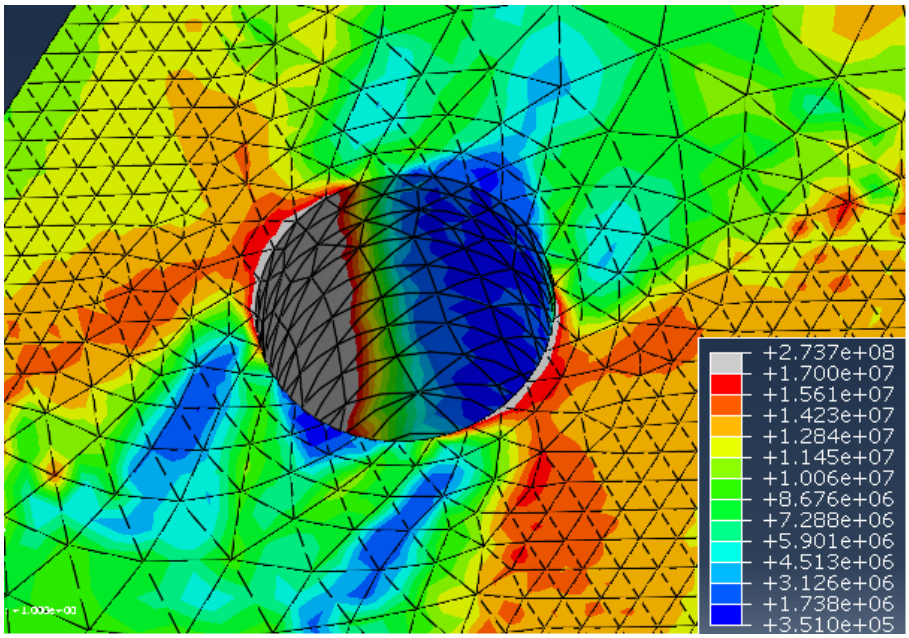

Figure 4.17. Stress concentration around the exit hole in M-3

As it is evident in figure 4.17, two types of stresses are developed around the exit; first, compressive stresses at sides of column which is magnified due to the concentration of stresses and second, tensile stresses at the top and bottom of the exit again caused by sudden changes in section and diversion of force flow to the compression zone. These two types of stresses were observed at very early stages of the imposed displacement and indicates that the stress concentration factor value might be significant.

In order to quantify the extent of the amplification, stress concentration factor k_t which is the maximum stress in a section divided by nominal stress, is calculated for the models with given specifications in Table 4.7. Based on stress analysis, Figure 4.18 shows the changes in k_t when the r/(b-2r) ratio changes, where is the hole diameter and b the width of concrete.

Table 4.7. Column sections used for calculation of k_t

Section size	Pipe size: mm
200×200	50.8
250×250	50.8
200×200	76.2
250×250	76.2

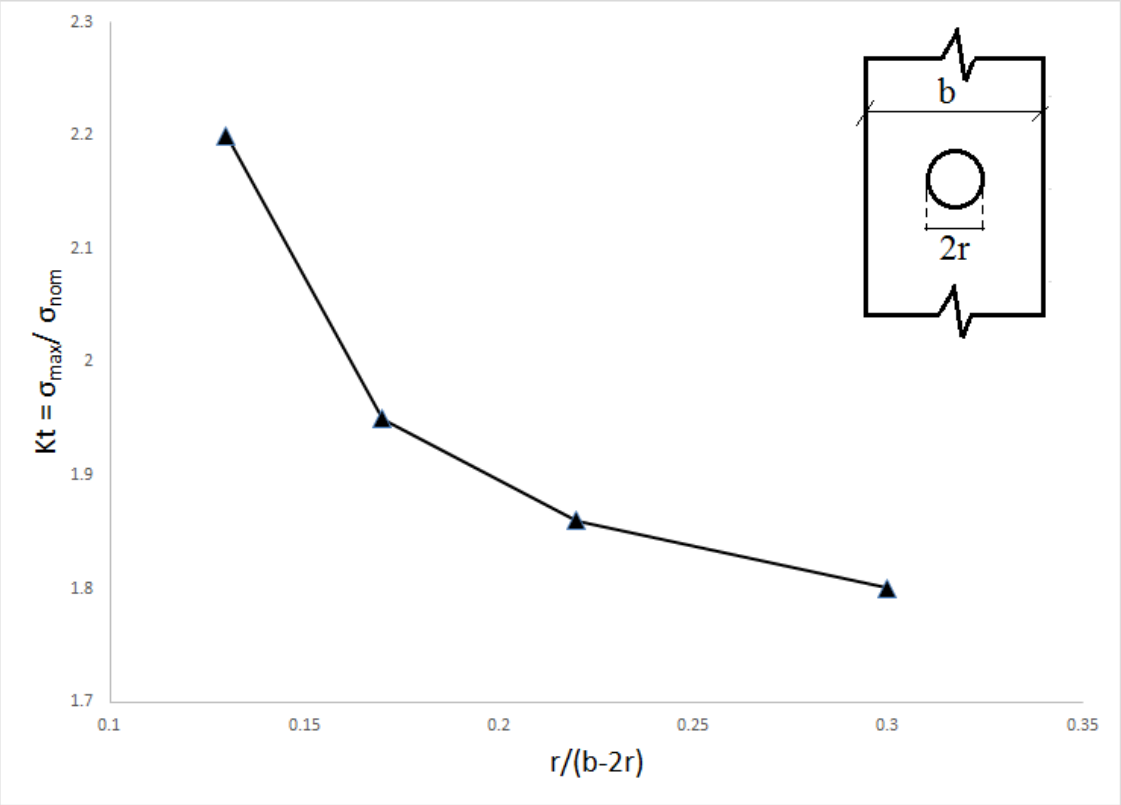

Figure 4.18. Calculated stress concentration factor k_t

4.1.7 Calibration

To validate the finite element model, the FE results were contrasted with test results. The patterns of cracks, load-displacement data and strain gauge readings were used to verify the analysis results against experimental data.

Comparing the strain gauge readings with analysis results showed great differences in strains, which can be attributed to insufficient bonding of strain gauges to the surface of concrete, in some of the cases the gauges were detached at early stages of test, hence the readings were not reliable.

However, The FE model could predict the locations of the cracked and crushed parts of concrete fairly accurately, as it is evident in figure 4.19. At the location of exit, due to tension and compression stresses developed around the pipe, concrete is cracked and crushed, respectively, which is accurately indicated by the FE model. In this figure, it can be seen that these locations in the test specimen perfectly coincide with FE models results.

A comparison between load-displacement results from the experiment and FE analysis indicates excellent match with maximum difference of 5%. Figure 4.20 shows the push over curve of specimen C-3 in experiment and the same column M-5 in FE analysis subjected to low axial load. As its evident both curves are showing similar trends. Overall, it can be said that the numerical results and experimental results show relatively good agreement and finite element models can simulate the actual behavior of the tested columns.

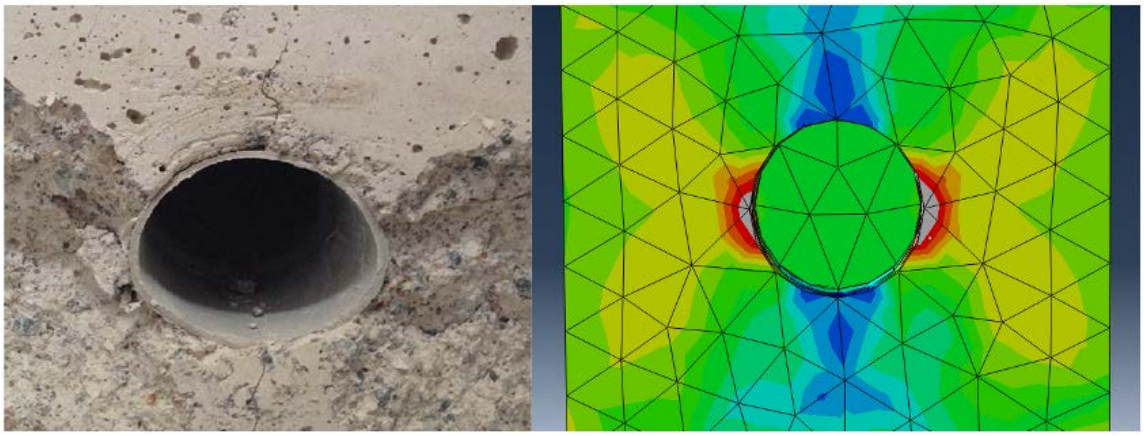

Figure 4.19. Stress state in test vs. FE model

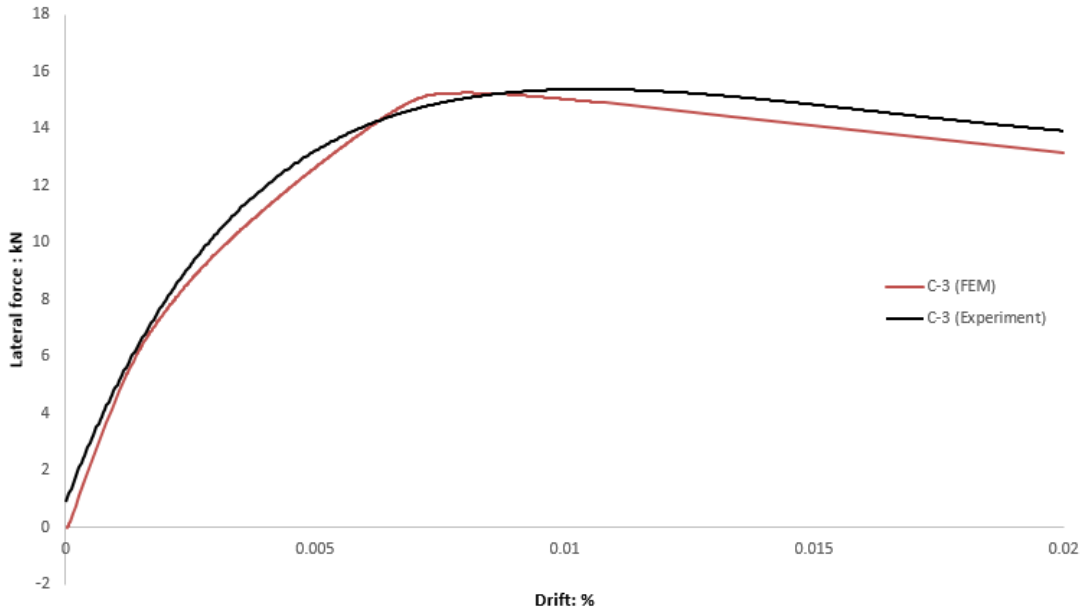

Figure 4.20. Push over curve of C-3 vs. M-5

4.2 Moment-curvature relationship and section analysis

Via interaction diagram it is possible to evaluate the combined effect of column axial load and moment on its ultimate load carrying capacity, however, for the states beyond the yielding of reinforcement and at large drifts values a moment curvature analysis can be more useful. In fact, moment curvature analysis can describe the plastic response of a RC column and based on that, the ductility of member can be studied. A moment curvature diagram represents the variation of the resisting moment of a section

with respect to its curvature. In order to obtain the moment resistance at a specific curvature, the longitudinal strain in the extreme fiber of the concrete should be specified. In addition, is essential to assume that the distribution of strain along the height of the cross section is linear. With the abovementioned assumption, it is possible to locate the neutral axis (N.A.) based on the equilibrium of longitudinal forces. Once the N.A. is located, the moment produced by the compression and tension blocks can be computed. Curvature is the strain gradient which is represented by the angle between the line perpendicular to the axis of bending and the longitudinal strain profile of the cross section.

Moment-curvature diagrams are very useful for showing ductility of reinforced concrete members, especially when the section reaches its plastic state, and provide the energy dissipation potential of member. Needless to say, for seismic design it is crucial to specify the ductility of sections.

It is worth mentioning that in general, ductility can be classified as material ductility, section ductility, member ductility and structural ductility. Ductility in material is the biggest one since all layers are equally under stress, ductility of section (in flexure) is less than material due to the unequal stress state of layers and the fact that layers close to neutral axis do not fully participate in energy absorption, the member ductility is less than section because as soon as a specific section reaches its yield limit the whole rotation takes place at that specific point and the other sections stay elastic without rotation and finally the ductility in structure is a sophisticated parameter which depends on many factors and normally is even less than member ductility due to the fact that not all members are equally stressed and not all members develop plastic hinge at the collapse point.

In view of the foregoing discussion, it can be said that the section ductility directly depends on the geometry of section. In the present study a section analysis is carried out for elements with pipe, at the location of exit (Figure 4.21) and for solid sections, and the results are compared. Two sizes of cross sections are selected to investigate the differences in moment curvature relationship of columns with pipe.

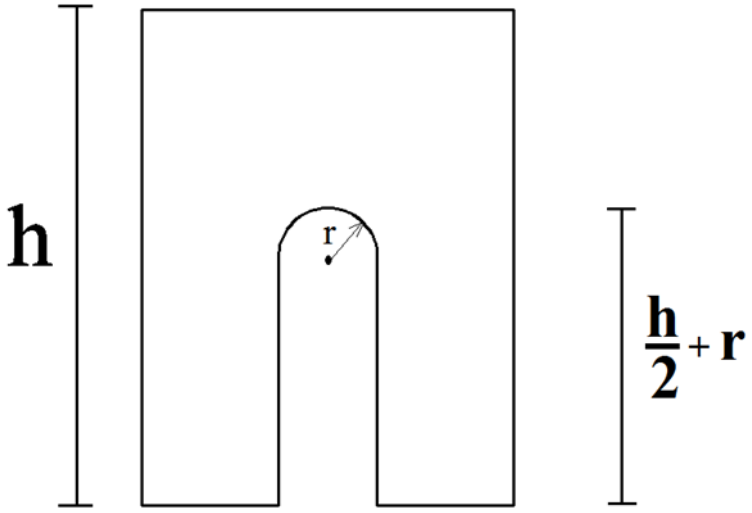

Figure 4.21. Cross-section of column in the location of exit

For each size of cross-section two models were prepared in SAP 2000 v19.1.1, one solid section as control specimen and one as shown in figure 4.21 representing cross-section of columns concealing service pipe in the location of pipe exit. In each model, via fiber model, the sectional analysis was conducted. Models were subjected to different levels of axial forces and the moment-curvature of sections at each level was obtained. In addition to that, for each model, interaction diagram was obtained and the value of balanced axial load was extracted from interaction diagram. Properties of each cross section is tabulated in Table 4.8. It should be mentioned that properties of materials in the models were the same as in the experiments.

Table 4.8. Sections specifications for section analysis

Specimen	Section: mm	Pipe Size: mm	Reinforcement
S-1	200×200	50.8	4 Ø 12
S-2	200×200	-	4 Ø 12
S-3	300×300	50.8	4 Ø 18
S-4	300×300	-	4 Ø 18

Unlike beams, in columns, because of the presence of axial load, the moment-curvature curve for a section is not unique; however, based on interaction diagram for any given combination of axial force and moment, causing column failure, the moment-curvature relation can be plotted and used for investigating the ductility of the member. The prepared models were subjected to two levels of axial load, one below the balanced value of axial load and the other above the balanced value.

Figure 4.22 and figure 4.23 show the interaction diagrams of sections S-1 and S-2 obtained based on the section properties.

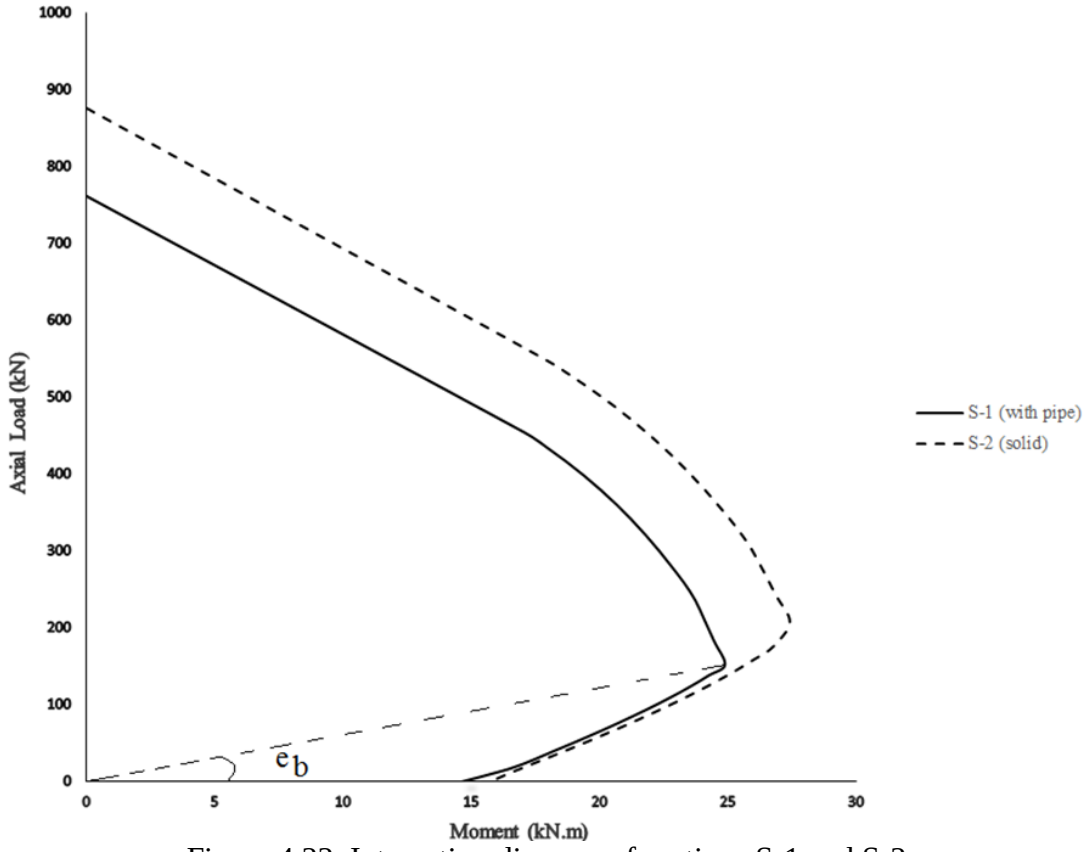

Figure 4.22. Interaction diagram of sections S-1 and S-2

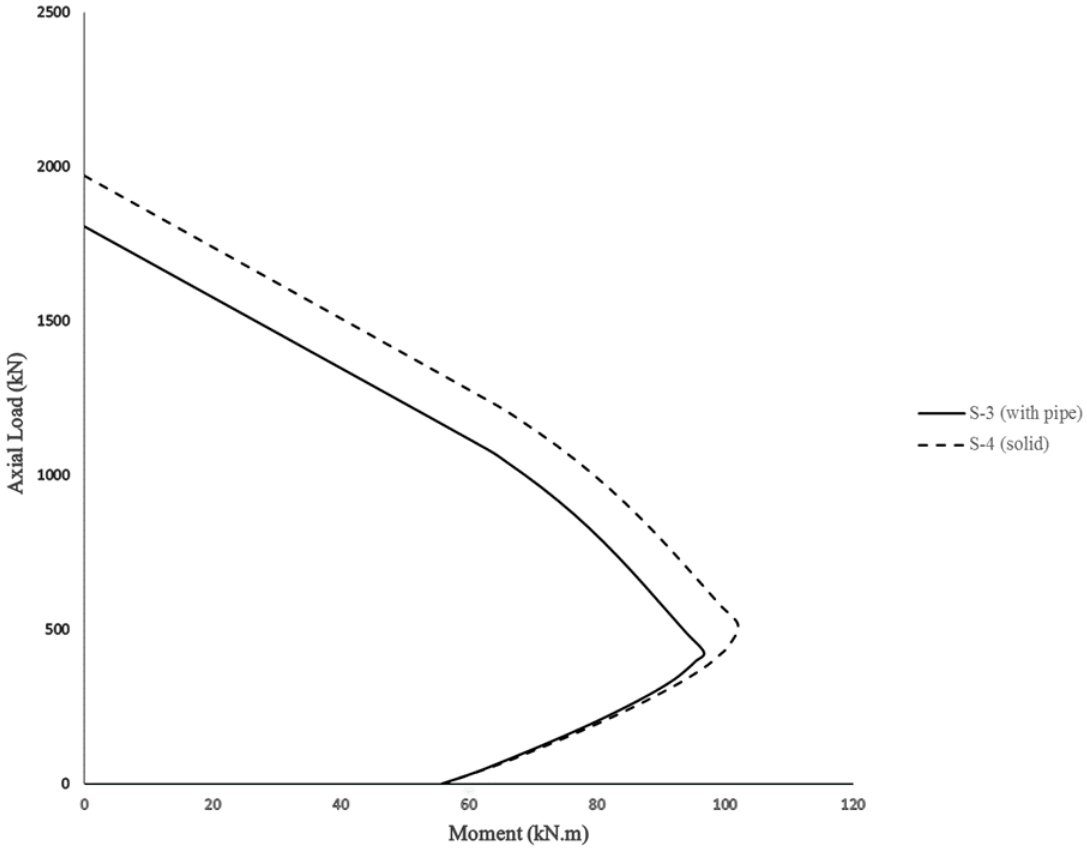

Figure 4.23 Interaction diagram of sections S-3 and S-4

In order to facilitate the comparison, the values of balanced axial load, N_b, for all four sections are tabulated in table 4.9.

Table 4.9. Balanced axial load of each section

Specimen	**N_b (kN)**
S-1	152
S-2	207
S-3	425
S-4	514

As stated above, based on the values of N_b it was decided to subject sections S-1 and S-2 to 100 kN and 300 kN, one below N_b and one above N_b. Considering the location of pipe exit and based on observations made during experiment, the behavior of section

when subjected to reversal cyclic loading is not symmetrical, i.e. when the exit is in compression, the section may exhibit a different behavior in comparison with the case that the section is in tension. In order to verify this, for section S-1 the moment curvature of both directions were obtained and plotted in the same graph as shown in figure 4.24.

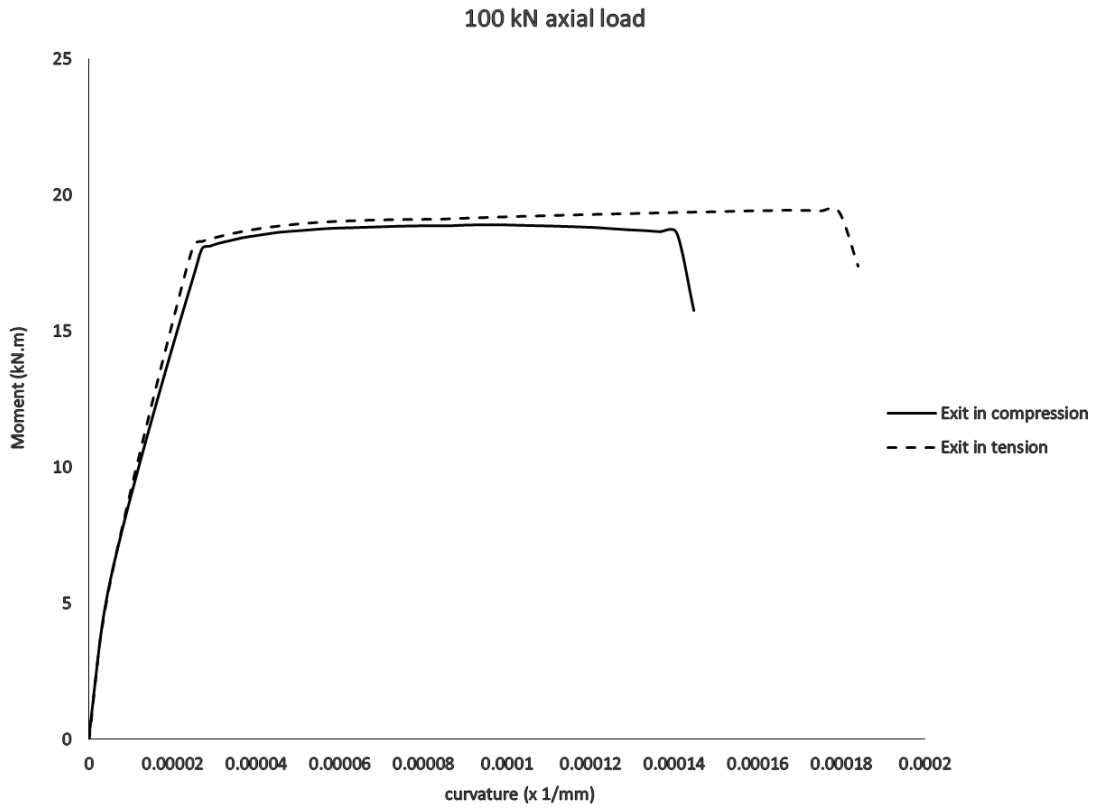

Figure 4.24. Moment-Curvature diagram of sections S-1 in both directions

Figure 4.25 and figure 4.26 show the moment curvature curves of S-1 and S-2 under two different levels of axial load, one below balanced value and one above balanced value.

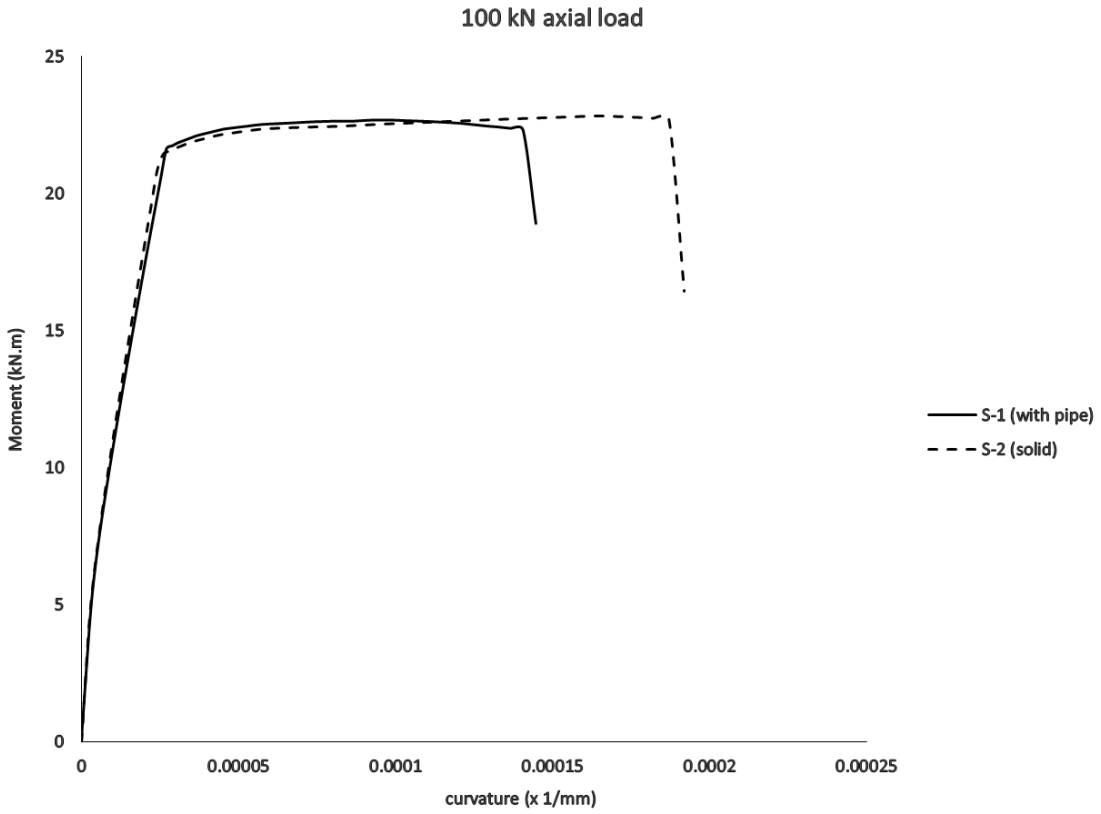

Figure 4.25. Moment-Curvature diagrams of sections S-1 and S-2 under low axial load

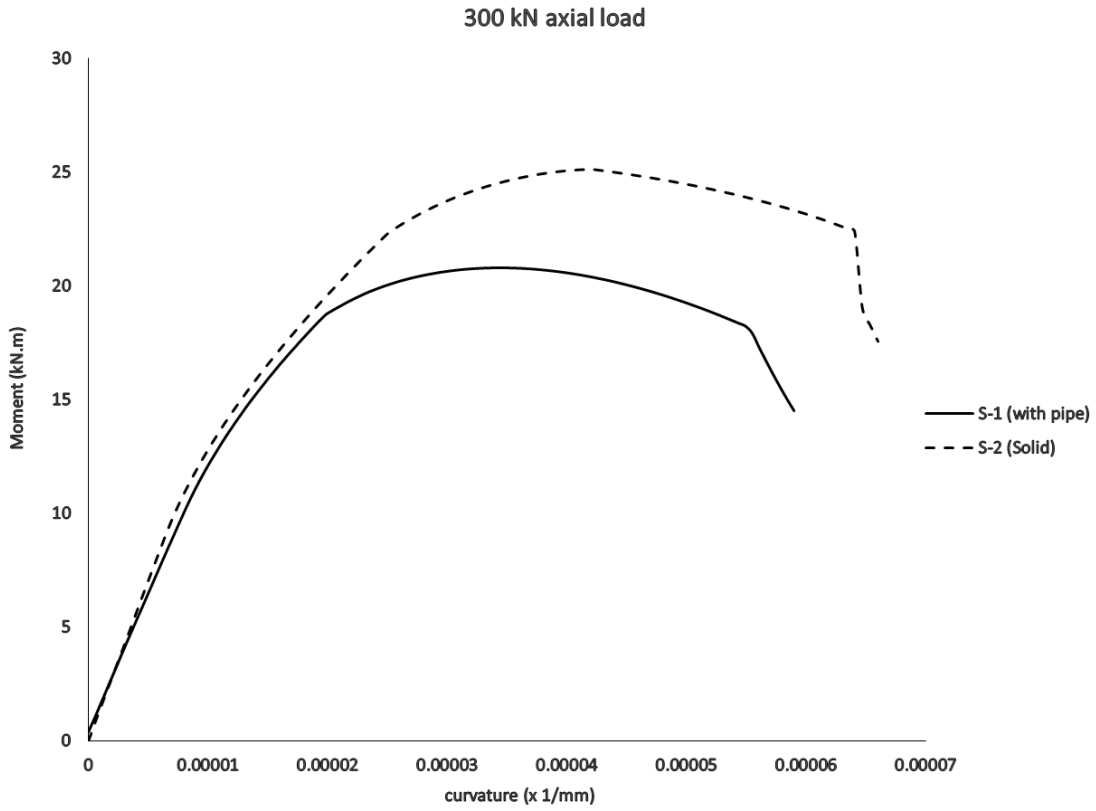

Figure 4.26. Moment-Curvature diagrams of sections S-1 and S-2 under high axial load

For sections S-3 and S-4, since the magnitude of balanced axial load was much higher as demonstrated in table 4.9, they were subjected to 300 kN and 600 kN axial loads and moment curvature graph are depicted in figure 4.27 and 4.28.

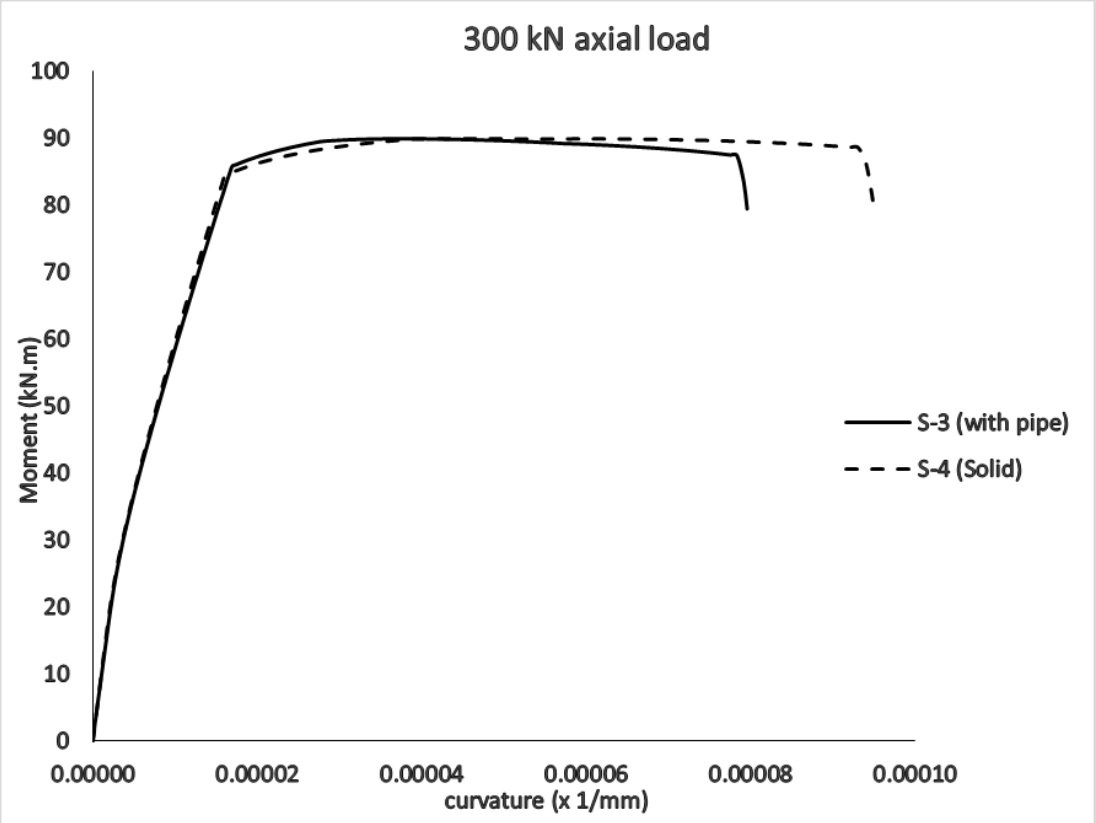

Figure 4.27. Moment-Curvature diagrams of sections S-3 and S-4 under low axial load

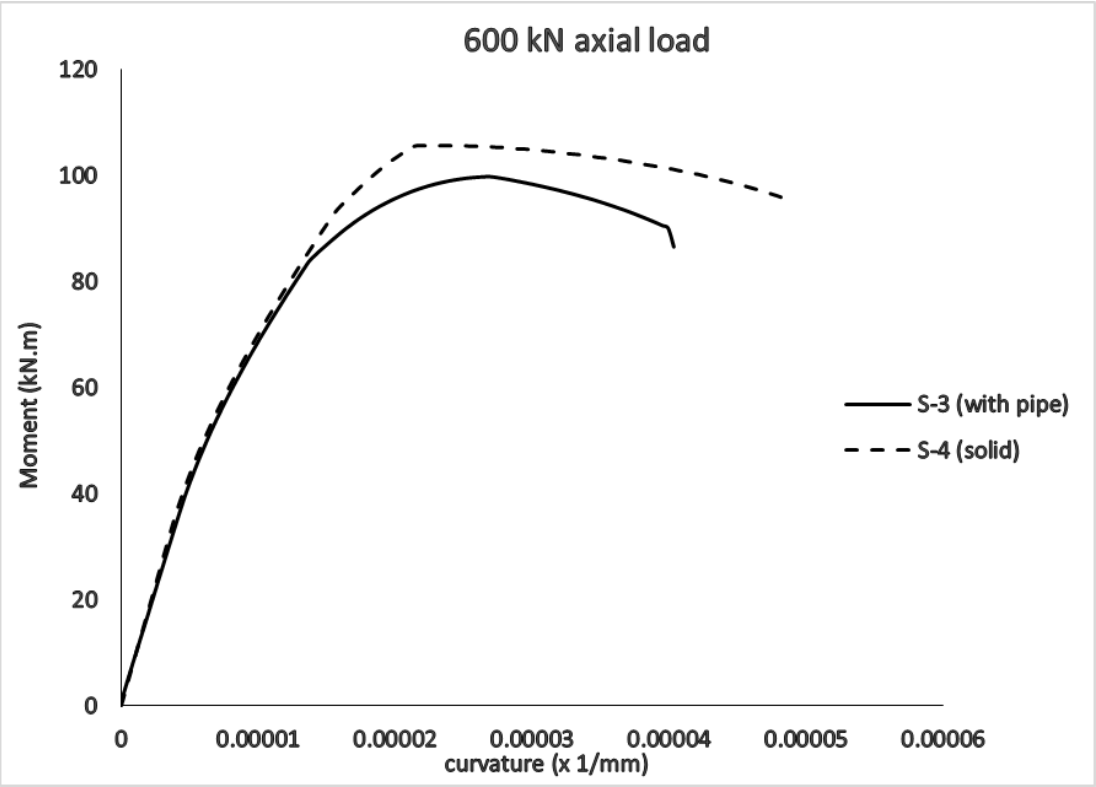

Figure 4.28. Moment-Curvature diagrams of sections S-3 and S-4 under high axial load

The latter figures clearly show that the presence of the hole in the column reduces its strength and ductility.

4.3 Plastic hinge length

To study the effect of irregular cross section of columns on the location and length of the plastic hinge, four different columns with exits positioned in different elevations were modeled in ABAQUS as tabulated in Table 4.10. It is notable that all columns had the same geometric, material specifications and reinforcing bars. As it was reported before by many researchers like Park and Priestley 1982, Sheikh and Khoury 1993 and Bayrak and Sheikh 1998 because of stub confinement phenomenon, the plastic hinge does not form in the first 0.25h distance from the face of support, hence starting from 100 mm to 300 mm distance from the face of support, exits were placed

and different levels of axial load was applied. The criteria for obtaining plastic hinge length was based on curvature localization zone.

Table 4.10. Properties of models used for plastic hinge length

Section	Size	Axial load	Exit distance from support: mm
Ph-1	200×200	0.2 p_0	100
Ph-2	200×200	0.52 p_0	100
Ph-3	200×200	0.2 p_0	150
Ph-4	200×200	0.52 p_0	150
Ph-5	200×200	0.2 p_0	200
Ph-6	200×200	0.52 p_0	200
Ph-7	200×200	0.2 p_0	300
Ph-8	200×200	0.52 p_0	300

For computing curvature at a specific point, Cauchy strains (column axial strain) values at two points in a plane section parallel to support face was obtained from Finite Element model and strain profile was constructed accordingly. The methodology is illustrated in figure 4.29.

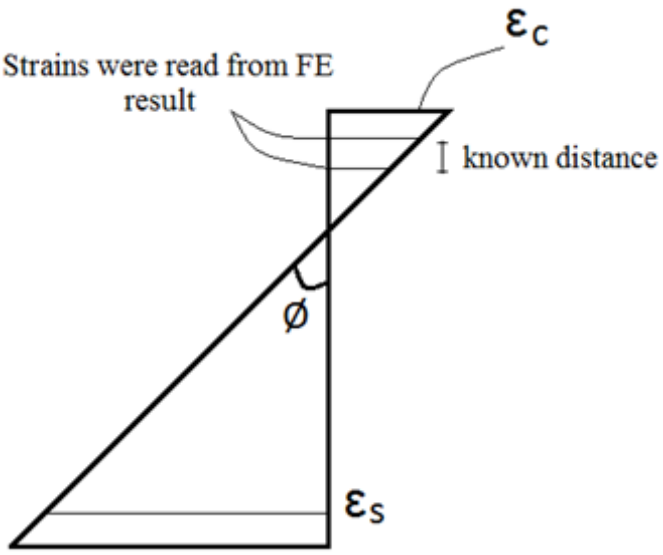

Figure 4.29. Obtaining curvature, ϕ, from strain profile constructed from FEM readings

All four columns have been subjected to two levels of axial loads, 0.2 P_0 and 0.52 P_0. The latter one is the maximum axial force specified by ACI 318-05 (0.65 × 0.8 P_0 = 0.52 P_0 for tie reinforcement), also the analysis was set to be terminated when the lateral load strength reaches to 80% of its highest strength. First, the constant axial load is applied and then the displacement is imposed. Figure 4.30 to figure 4.37 show the curvature profiles of each column under two levels of axial load. The dashline represents the curvature at yield which is obtained from section analysis.

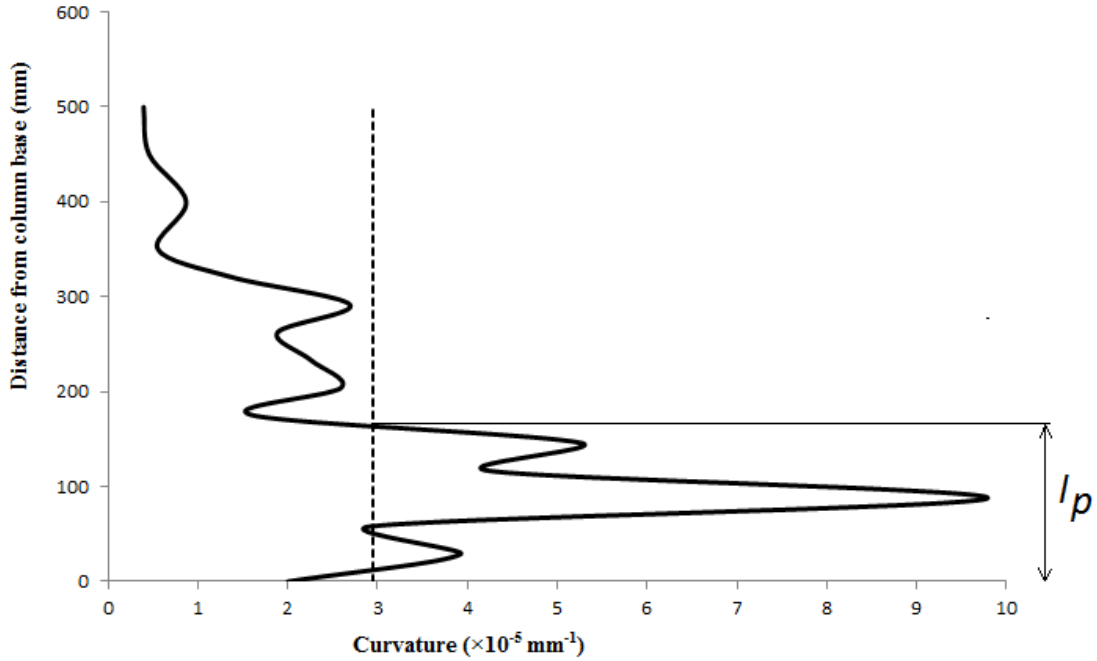

Figure 4.30. Curvature profile of Ph-1

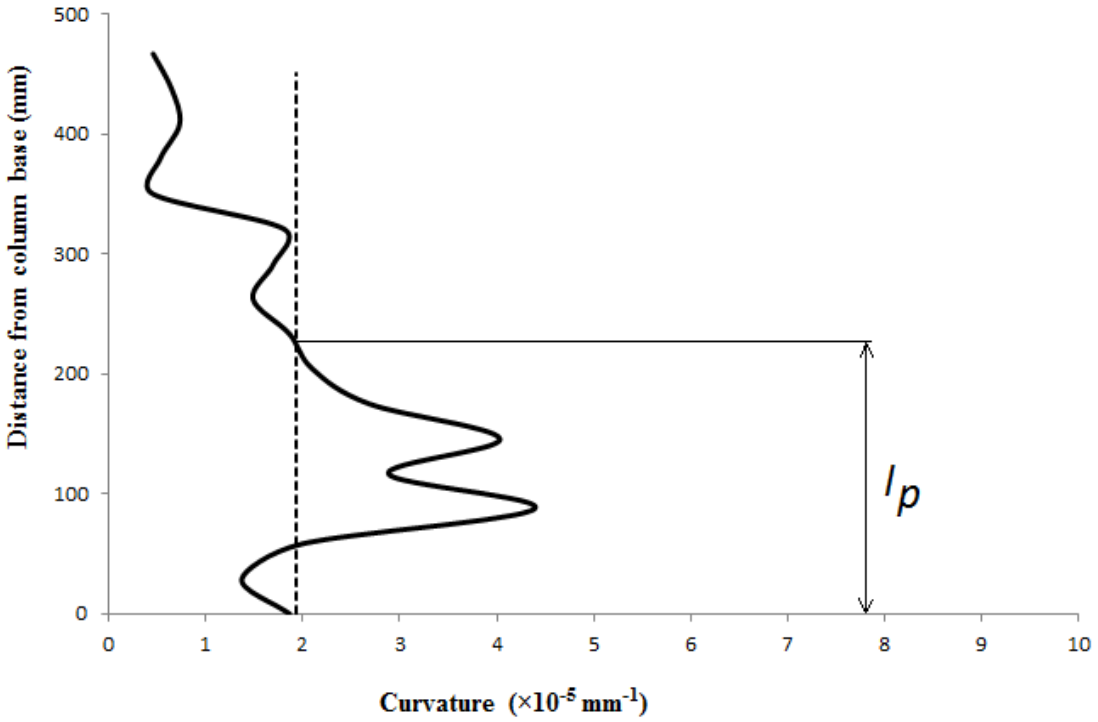

Figure 4.31. Curvature profile of Ph-2

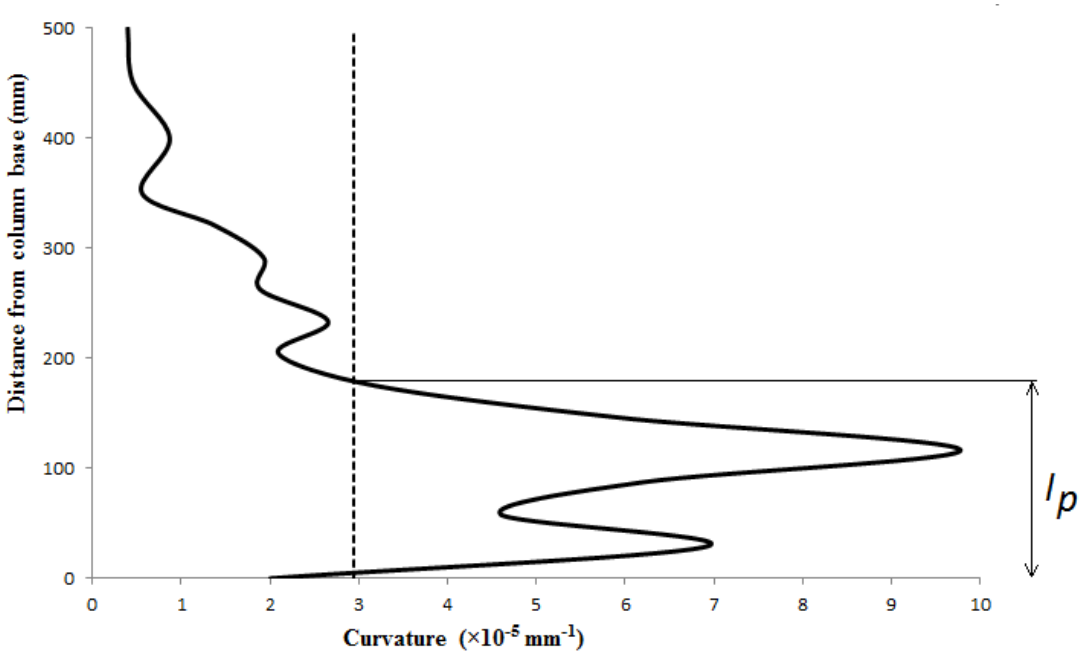

Figure 4.32. Curvature profile of Ph-3

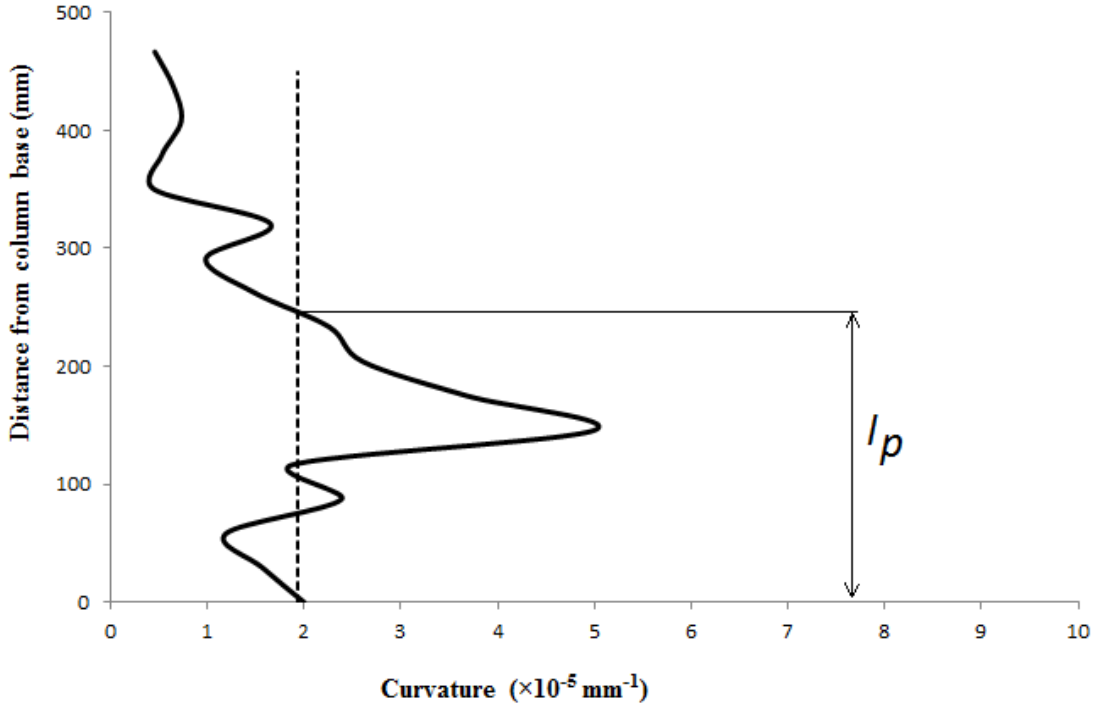

Figure 4.33. Curvature profile of Ph-4

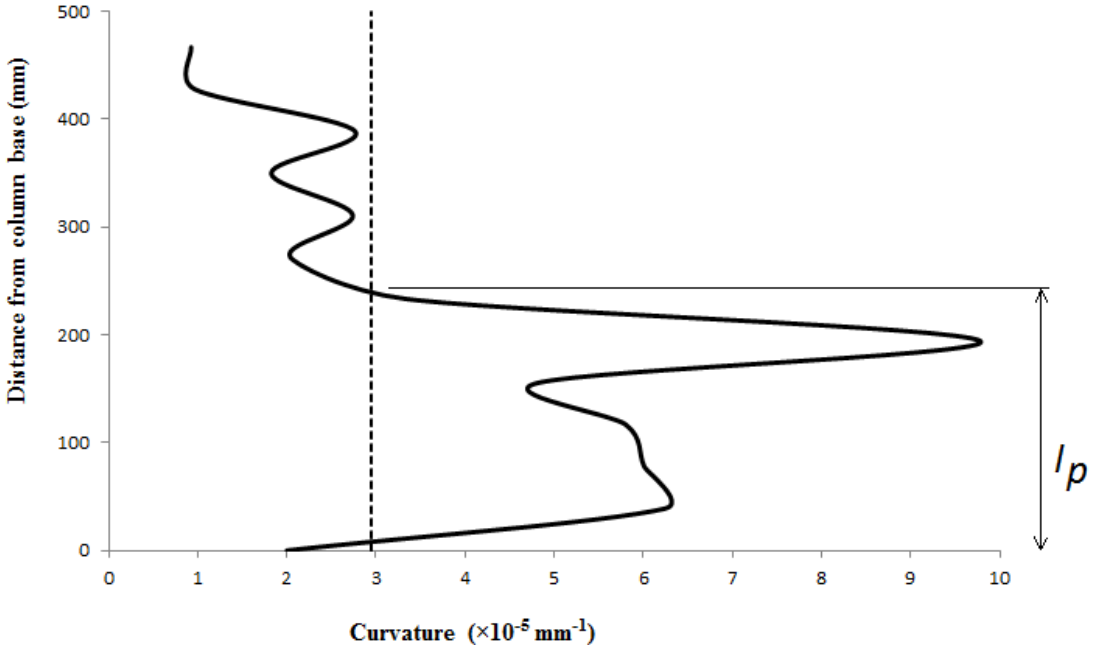

Figure 4.34. Curvature profile of Ph-5

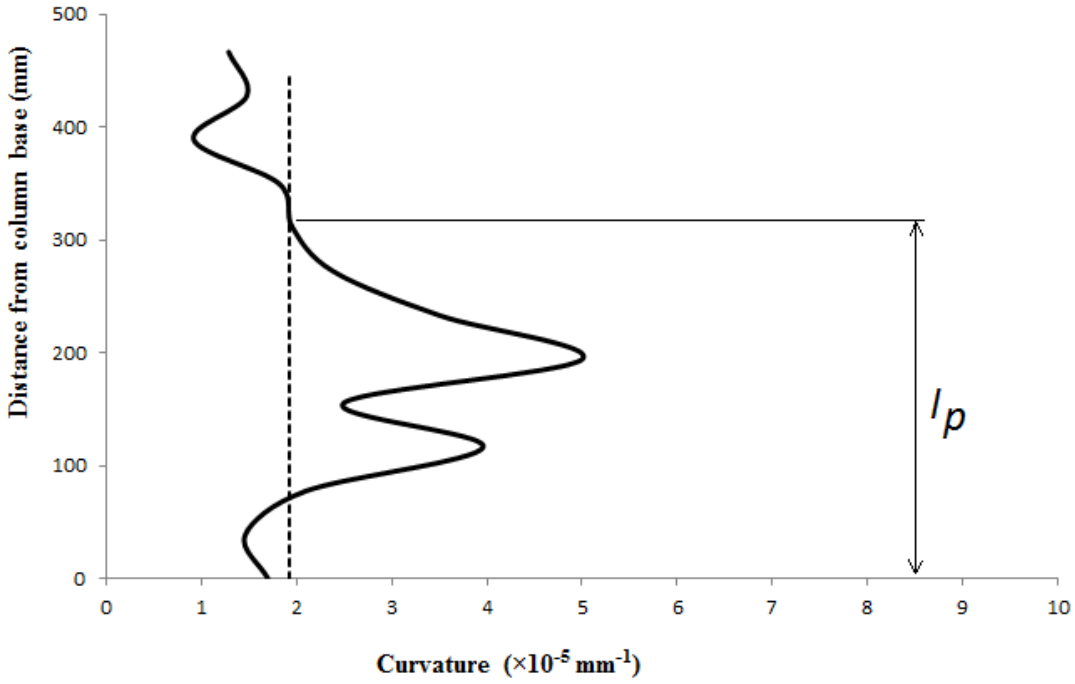

Figure 4.35. Curvature profile of Ph-6

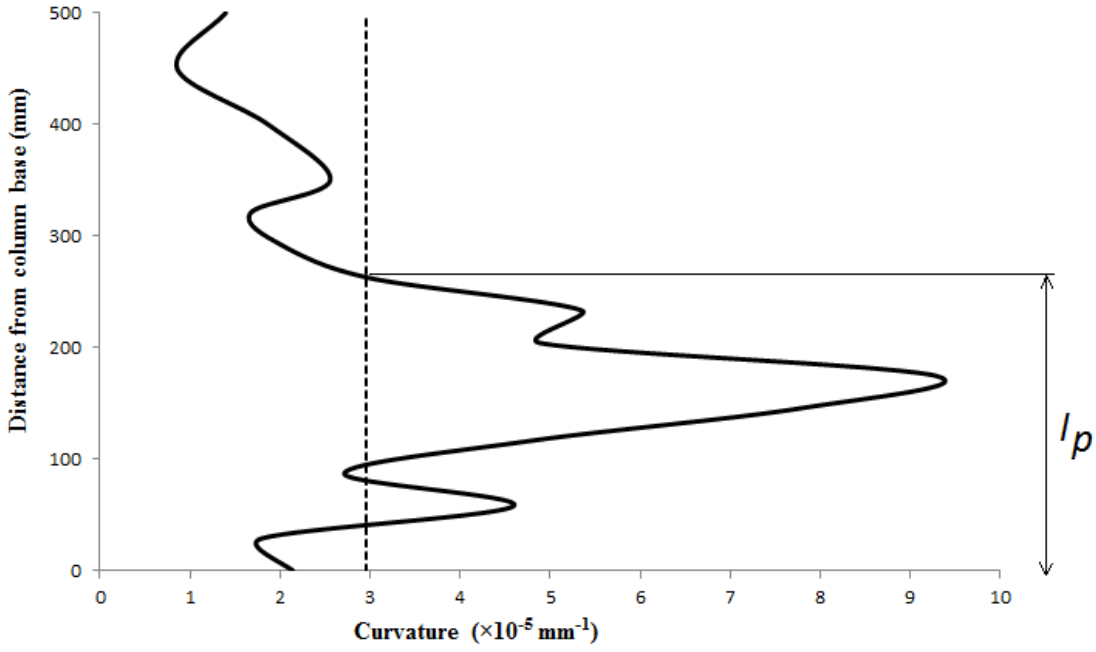

Figure 4.36. Curvature profile of Ph-7

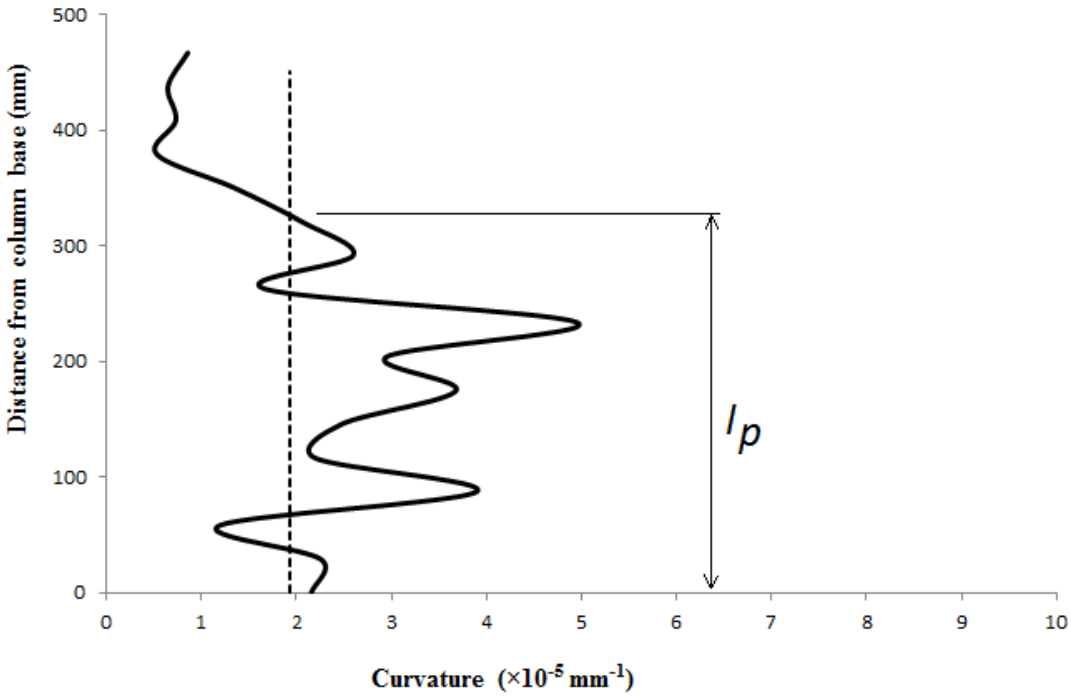

Figure 4.37. Curvature profile of Ph-8

Chapter 5

RESULTS AND DISCUSSIONS

5.1 General

In the present chapter, for the tested specimens and modelled columns, the obtained results are presented and discussed. Specifically, their hysteretic load-drift curves, load-drift envelopes, the interaction of moment-axial load, moment-curvature relationship, stiffness degradation, FE results, stress distribution and plastic hinge properties are presented.

5.2 Effect of pipe presence in columns

The difference between the column with solid section and the column with pipe is shown in figure 3.9 where the hysteretic force-drift responses of the columns C-1 and C-8, which were tested under high level of axial load, are depicted. The load–displacement data for the columns with pipe are presented by setting the exit pipe in compression in negative cycles and in tension in positive cycles. The presence of pipe in the specimen C-1 caused more than 32% decrease in lateral load strength of column in negative cycles, this remarkable strength loss can be attributed to the fact that under high level of axial load, both columns are in their compression failure range and the behavior is governed by a brittle failure mode. i.e., in compression failure range the lost area in the location of pipe exit causes huge reduction in moment capacity of the section. Also, comparing the rate of strength loss at 2% drift in specimens C-1 and C-8 reveals that, the column with pipe loses 56% of its strength compared with 21% for column with solid cross section. This comparison shows the destructive presence of

pipe, especially at the location of exit, causing disturbance of force flow in compression zone. In addition, considering the force-displacement response of column C-1 alone, reveals the asymmetrical behavior of columns with pipe. The results yielded 22% difference in strength between positive and negative cycles.

In fact, when the exit is in compression in regions around the opening, compression force is developed at sides of the hole and tension force is developed at the bottom and top of the hole. This great disturbance in force flow caused the specimen C-1 to develop some cracks at the top and bottom of the opening even at early stages of loading and under low drifts. Also, the compression force at sides caused crushing at both sides of the exit; this can be considered as another reason for the observed strength loss of specimen C-1. Figure 5.4 portrays the state of pipe exit in column C-1 after the test.

5.3 Effect of transverse reinforcement ratio on response of columns

Figure 3.10 shows the cyclic response of specimens C-2 and C-6. It can be stated that providing more confinement in specimen C-6 via decreasing the spacing of ties and also placing two ties exactly before and after the exit, slightly enhanced the overall behavior of specimen C-6 under low axial load levels. Specimen C-6 experienced 5% increase in its strength compared with C-2. Also, the strength loss at 2% drift was 24% for C-6 and 32% for C-2. This relatively minor difference can be explained by the fact that under low levels of axial load both columns are in tension failure range so confining the pipe exit does not have any significant effect on the behavior of the column. However, as is shown in Figure 3.11 where specimens C-1 and C-7 are compared, providing extra confinement for specimen C-7, when subjected to large axial load, especially in negative cycles, dramatically changed the behavior of the

specimen compared with specimen C-1. The lateral strength of specimen C-7 was found to be increased by 24% due to smaller spacing of ties compared with C-1 and its strength loss at 2% drift was found to be 39% compared with 56% for specimen C-1.

This huge difference is credited to the extra confinement provided to concrete, especially in the exit regions. It is well known that the lateral confining force applied by closed ties enhances the compressive strength of concrete in core regions, especially under high levels of axial load when the compressive strength of concrete governs the overall response of column. The response of specimen C-6 was obviously improved with a remarkable increase in both strength and ductility. Furthermore, the tension cracks around the exit which was observed in specimen C-1 was not seen in column C-7. Figure 5.4 and figure 4.5 show the state of specimens C-1 and C-7 after the test.

5.4 Effect of the location of pipe exit on response of columns

Figure 3.12 presents the hysteresis curve of specimens C-1 versus C-4. It can be concluded that specimen C-4 behaved slightly better than specimen C-1. This difference is not distinguishable when the exit is in tension but when the exit is in compression, at 2% drift the sample with 200 mm distance of exit from foundation behaved superior than to the one with 100 mm distance, with 32% increase in its strength. Two reasons can be ascribed to this phenomenon: first, the magnitude of moment is smaller at the location of pipe exit for specimen C-4; second, the location of exit in sample C-1 is in the region which is known as plastic hinge formation region by many researchers such as Priestley et al., 1987, Sheikh et al., 1993, Panagiotakos et al., 2001 and Bae et al., 2008.

5.5 Effect of axial load on response of columns

Figure 3.13 exhibits the responses of specimens C-1 and C-2 which have the same specifications and the only difference between them is the level of axial load they were subjected to. The figure reveals that the deterioration due to the pipe is considerably more when higher level of axial load is applied. In particular, it was noticed that in negative cycles when the level of axial load was higher, the lateral strength of specimen decreased by 24%. Also at 2% drift, 38% strength loss was recorded for sample C-2 versus more than 50% for C-1. This notable difference can be interpreted by the fact that by increasing the axial load level the mode of failure is altered hence sample C-1 underwent extensive damage compared to C-2.

5.6 Effect of the exit on the ductility of member

Under the assumption that a column is considered failed if its capacity drops 20% below its peak resistance or strength as proposed by Park and Ang 1987, Figure 5.1 and figure 5.2 are plotted as the backbone curves or envelopes of the hysteretic responses of the specimens indicated in each figure. The two figures show the relevant envelopes for the specimens subjected to high axial load and low axial load, respectively. It can be observed that all the specimens under high axial load suffered from premature failure to some extent but this is more evident for members with pipe. Also by comparing the positive and negative load cycles portions of the responses, the high asymmetrical behavior of all the columns with pipe is notable.

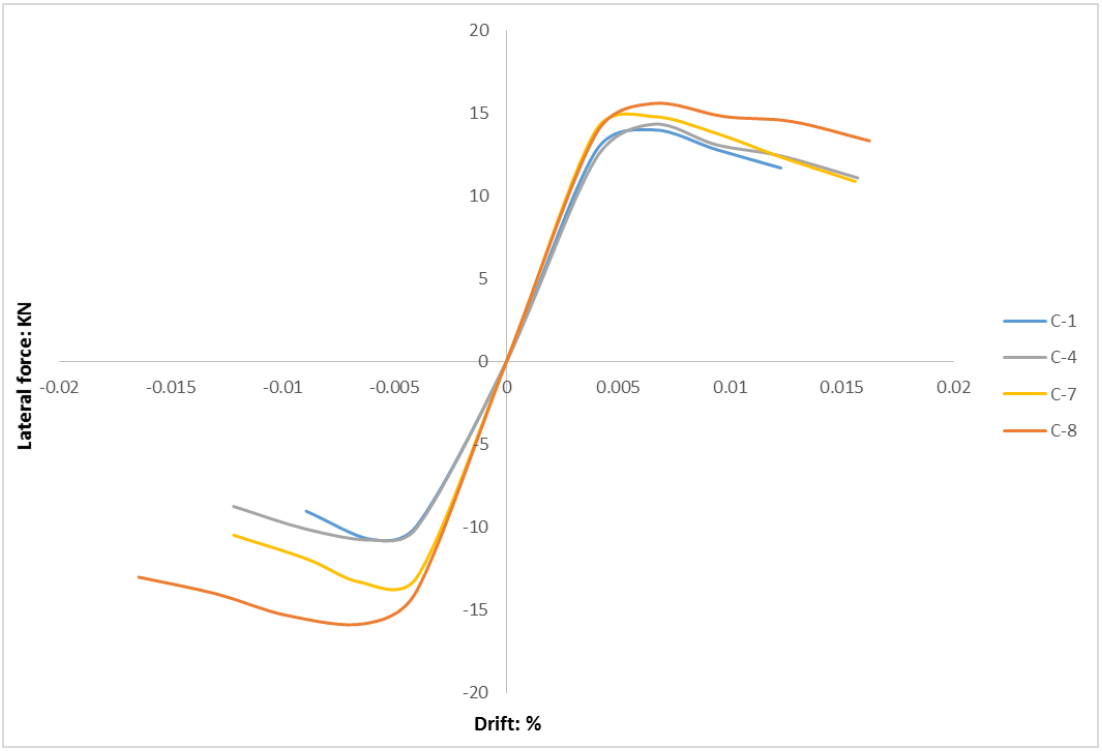

Figure 5.1. Envelopes of specimens subjected to high axial load

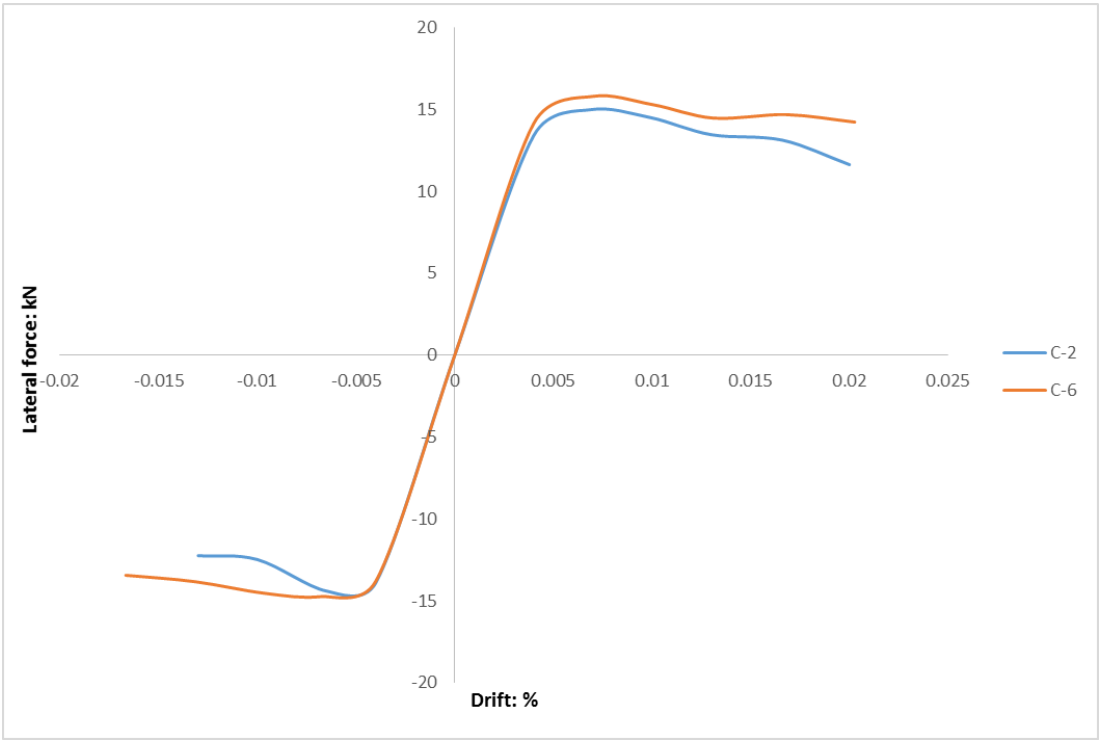

Figure 5.2. Envelopes of specimens subjected to low axial load

In order to compare the ductility of members parametrically, displacement ductility factor was computed for specimens in negative cycles from the following equation:

$$\mu = \frac{\Delta_{20\%} - \Delta_y}{\Delta_y} \quad (5.1)$$

Where $\Delta_{20\%}$ is the displacement corresponding to 20% strength loss and Δ_y is the displacement corresponding to yield state obtained based on the procedure provided in Annex B.3 of EC8-1 (Eurocode 2005) which assumes elastic-perfectly plastic load displacement relationship. Hence, by fitting a bilinear curve to the envelopes plotted in figure 5.1 and figure 5.2, the drift corresponding to yield was computed.

The calculated factors are tabulated in Table 5.1. By comparing ductility factor in negative cycles of control specimen (C-8) with specimens C-1 and C-4, it is revealed that the presence of the service pipes reduced the ductility factor by 57% and 39%, respectively. However, to some degree, this huge reduction could be compensated by providing extra confinement as in specimens C-6 and C-7. Under low level of axial load, reducing the spacing of ties increased the ductility factor by 35% in specimen C-6 and under high level of axial load the value increased by 56%. This meaningful difference highlights the role of confinement in columns, especially when they are subjected to high levels of axial load. The other noteworthy point is that in negative cycles, as it can be seen in Table 5.1, in the elements with the same specifications, the value of ductility factor decreases when the axial load increases.

In general, it can be stated that although the confined elements with pipe behaved inferior to the control specimen, it still showed a much better response in term of ductility in comparison with unconfined specimens.

Table 5.1. Ductility factor of tested columns in the negative load cycles

Specimen	Ductility factor , μ
C-1	1.95
C-2	2.51
C-4	2.69
C-6	3.39
C-7	3.05
C-8	4.49

5.7 Stiffness degradation

To depict the extent of stiffness degradation due to the pipe presence, Figure 5.3 is constructed by calculating the secant stiffness of the column in negative cycles is plotted as function of column drift for the section where the pipe exits the column. These curves are presenting approximate yet valuable data for evaluating the stiffness degradation of columns. As is evident, initially the stiffness of specimen C-7 is larger than the other specimens with 2 kN/mm at 0.4% drift and at final cycle the stiffness dropped to 13% of its initial value. This rather high initial stiffness is owed to the confinement provided in the particular specimen, especially in the exit region, which controlled premature cracks and stiffness degradation. Specimens C-1 and C-4 had almost the same initial stiffness, however, at final stage the values dropped to 9.1% and 12% respectively. This slight improvement in sample C-4 comes from the larger distance of pipe exit from the support face compared to that of C-1.

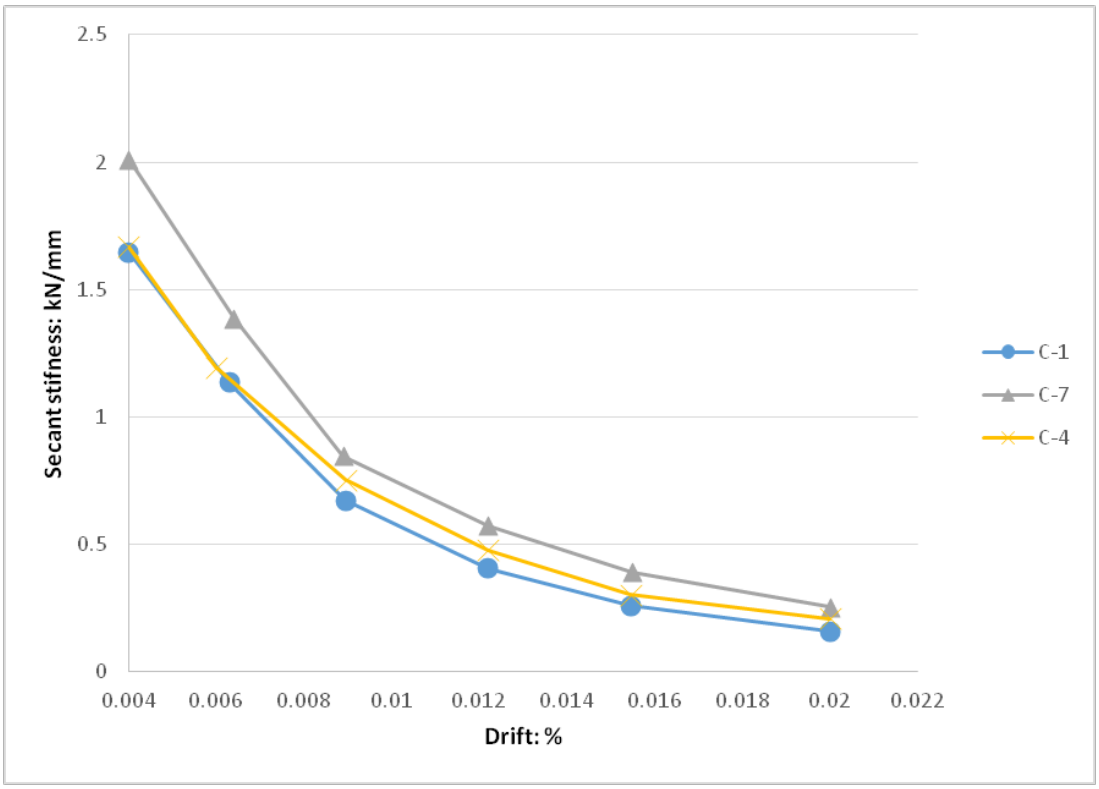

Figure 5.3. Secant stiffnesses of specimens C-1, C-4 and C-7

Figure 5.4. State of specimen C-1 after the test

Figure 5.5. State of specimen C-7 after the test

5.8 Effect of pipe on the value of balanced axial load

Firstly, by observing the value of balanced axial load (N_b) given in Table 4.9, it was determined that the presence of pipe decreased the value of N_b for the columns with 200 × 200 and 300 × 300 cross-sections by 26% and 17%, respectively. This reduction in the value of balanced axial load decreases the tension control region in the interaction diagram and the angle $e_{b=} \ tan^{-1}(P/M)$ is becoming smaller as shown in figure 4.22.

It is also notable that the performances of S-1 and S-2 are quite similar when they are subjected to lower axial loads, namely tension control range, however, when the column is subjected to higher levels of axial load, compression control range, the column S-2 behaves superior to S-1. This difference can be attributed to the missing area of concrete caused by penetration of pipe through the element, (See figure 4.21). The same pattern was observed for S-3 and S-4 as shown in figure 4.23 with smaller rate of reduction in the value of N_b .

It is worth noting that Euro Code 8 (Eurocode 2005) Clause 5.5.3.2.1 specifies that the normalized axial load should not exceed the ratio 0.55. Similarly the Turkish Earthquake Code 2007 (TEC 2007) defines this limit as 0.5. As it is shown in figure 4.22, owing to the presence of the pipe in the current test columns, the value of balance axial load capacity drops remarkably and due to this reduction the column may not be able to satisfy the codes requirement.

5.9 Effect of pipe on the moment-curvature relationship

As it is demonstrated in figure 4.24, whether the pipe exit is located on the compression or tension side of the cross-section has very little effect on the column moment capacity, but there is a huge difference in the ductility of columns, depending on the exit location relative to the direction of the applied lateral load. In both directions, the curvature at yield point was the same but the ultimate curvature of the case with exit on the compression side decreased drastically. By calculating the ductility ratio, which is the curvature at the ultimate stage divided by curvature at the yield stage, as shown in Equation 5.2, the ductility ratio for the cases with exit on the compression and tension sides of the column cross-section were computed as 5.25 and 7.09, respectively. This significant difference in ductility ratios supports the initial statement that under seismic excitation, columns with embed pipes, exhibit different amount ratios in the two directions.

$$Ductility\ ratio = \frac{\emptyset u}{\emptyset y} \qquad (5.2)$$

In which $Ø_u$ is the curvature at ultimate stage and $Ø_y$ is the curvature at yield stage.

Figure 4.25 and figure 4.26 show the moment curvature curves of S-1 and S-2 under two different levels of axial load, one below balanced value and one above balanced value. Figure 4.25 shows the values of moment and curvature before and at yield stage for both columns almost coincide which indicates that in elastic stage under low level of axial load the presence of pipe does not have any negative effect on the column behavior, this phenomenon was also shown by the interaction diagram of these two columns (see figure 4.22).

However at post yield stage and specifically ultimate point, the solid section S-2 behaves superior to S-1, the values in table 5.2 show ductility ratios of two sections. It can be seen that under 100 kN axial load the ductility ratio of S-1 compared with S-2 was reduced dramatically which is credited to the existence of the pipe. Based on figure 4.26, it can be observed that at both pre and post yield stages S-2 behave much better than S-1. It indicates that if the column is subjected to an axial load higher than balanced axial load value, the presence of the pipe reduces both the column ductility and resistance remarkably.

Table 5.2. Ductility factor of S-1 and S-2

Section	Ductility Ratio 100 kN	Ductility Ratio 300 kN
S-1	5.2	2.7
S-2	7.22	3.4

The same sort of behavior was observed for sections S-3 and S-4, since the magnitude of balanced axial load was much higher in these two sections, they were subjected to 300 and 600 kN axial load and based on their moment-curvature relations the ductility ratios were obtained are shown in table 5.3.

Table 5.3. Ductility factor of S-3 and S-4

Section	Ductility Ratio 300 kN	Ductility Ratio 600 kN
S-3	4.54	2.95
S-4	5.4	3.59

5.10 Effect of the exit on stress distribution

Stress analysis revealed high localized compressive stresses around the exit imposed by the discontinuity of the section. Due to this stress concentration, the concrete around the pipe exit experiences high compressive stresses even at early stages of loading.

These stresses caused premature crushing of concrete at the edges of the exit as observed during the testing of specimen C-1 (see figure 5.4). By calculating the maximum stress, which occurs at the periphery of the exit, (Figure 5.6) and dividing it by the average stress in elements at exit level, the theoretical stress concentration factor, k_t was calculated for four different sizes of sections and the results are presented in Figure 4.18. This factor is independent of the material properties and just depends on the geometry of the section and the hole. It can be seen perceived that with increasing the ratio of *r/(b-2r), r* being the hole or pipe outer radius and b the column width, the stress concentration decreases. Knowing k_t for a section is useful because it is indicative of potential stress amplification in the element.

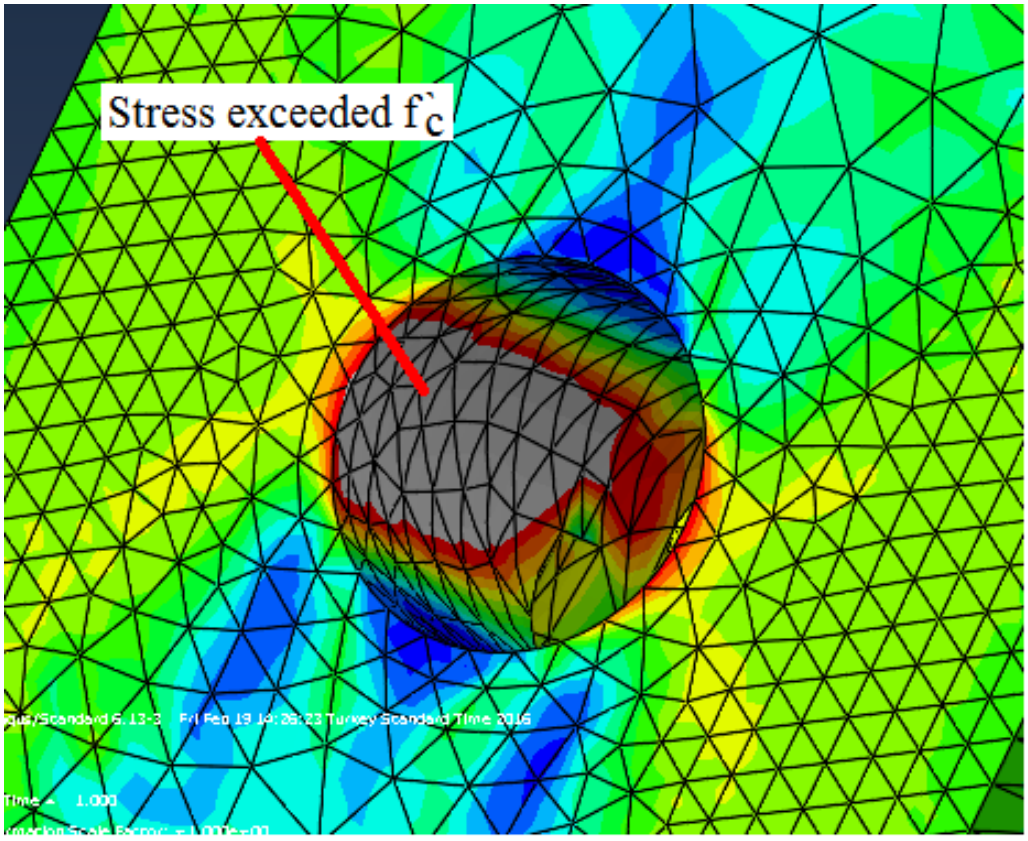

Figure 5.6. Stress concentration around the hole

5.11 Effect pipe on plastic hinge formation

Both experiment and numerical studies have proven that the presence of pipe in the column changes the length and location of plastic hinge significantly. From the experiment recall that four LVDTs were employed in the test, with one being mounted on the footing and the other three, one on the top level of column and two close to the support. All presented force displacement curves were plotted based on the displacement recorded by the top LVDT since the global behavior of the column was the matter of interest. However, with respect to local behavior, the data from the other LVDTs would be also important. Having the lateral displacement of the column and knowing that the displacement at the support is zero, chord rotation for three segments of the column can be obtained. This procedure is demonstrated in figure 5.7. For specimens C-1, C-2 and C-3 the three LVDTs were mounted at 100, 200 and 1200 mm distance from the footing. For specimen C-4 they were installed at 150, 300 and 1200 mm elevation from the footing level. Given that the distance between the LVDTs is known, by obtaining the data from each LVDT for each segment the rotation can be easily computed.

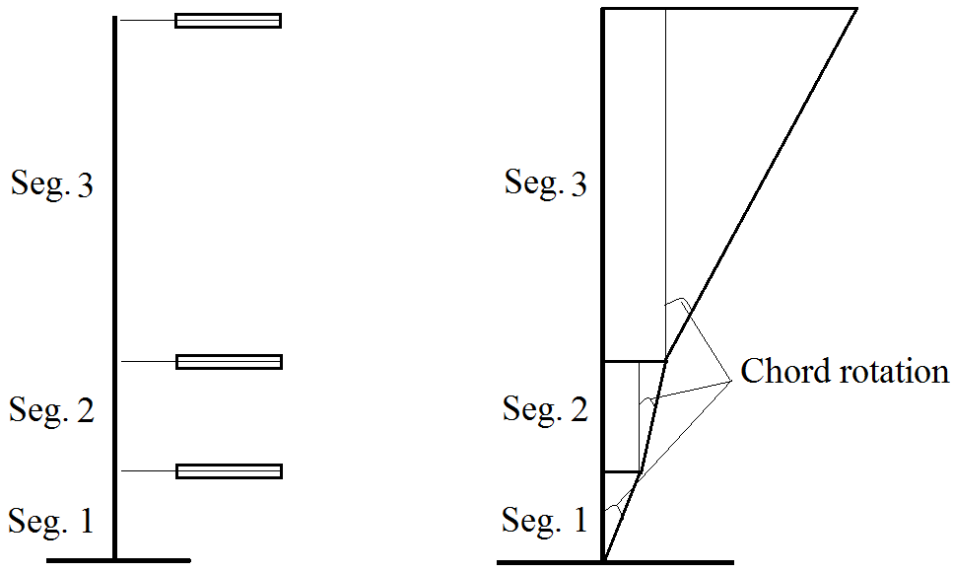

Figure 5.7. Dividing the column to three segments for finding chord rotation

Table 5.4 shows the obtained values of chord rotation for specimens C-1, C-2, C-3 and C-4. The meaningful difference between the values of rotation for segment 1 and 2 in C-1 and C-2 indicates that considering the rate of growth in rotation of the second segment, it can be concluded that in specimen C-1 the plastic hinge occurred in segment 2 since it increased significantly, however observations from the test and the obtained rotations for C-2 revealed that with increasing the level of axial load the plastic hinge location shifted upward. The excessive rate of increase in third segments rotation compared with the other two segments indicates that most probably the plastic rotation occurred in segment three. Considering C-3, it cannot be stated that the hinge is formed in second or third segment for sure since there was not a huge growth in rotations, however, considering C-4, the drastic increase in the value of rotation in third segment implies that the concentrated plasticity occurred at a level higher than 300 mm from the support. Comparing the obtained values from the experiment with the existing equations suggested by other researchers, shows that the irregularity of section changes the length of plastic hinge radically, but due to the limited number of LVDTs the length cannot be accurately evaluated. For this reason, and taking into consideration that the length of plastic hinge provides valuable information about the nonlinear response and energy dissipation capacity of structures, the finite element analysis results for some columns with holes are exploited to find the plastic hinge length.

Table 5.4. Chord rotations obtained in experiment

Specimen	**Rotation in Seg.1**	**Rotation in Seg.2**	**Rotation in Seg.3**
C-1	0.0080	0.0160	0.0212
C-2	0.0080	0.0100	0.0217
C-3	0.0078	0.0120	0.0215
C-4	0.0073	0.0080	0.0232

Table 5.5 presents the l_p of the simulated columns obtained from various researcher's proposed equations versus the ones obtained using the current finite element analysis results.

Table 5.5. Length of plastic hinge obtained by different proposed equations vs. obtained value

Column	Park et al.	Sheikh&khoury	Paulay& Priestley	Mander	Bae&Bayrak	Obtained value
Ph-1	0.4 *h*	1.0 *h*	1.19 *h*	1.0 *h*	0.25 *h*	0.7 *h*
Ph-2	0.4 *h*	1.0 *h*	1.19 *h*	1.0 *h*	0.92 *h*	1.05 *h*
Ph-3	0.4 *h*	1.0 *h*	1.19 *h*	1.0 *h*	0.25 *h*	0.9 *h*
Ph-4	0.4 *h*	1.0 *h*	1.19 *h*	1.0 *h*	0.92 *h*	1.17 *h*
Ph-5	0.4 *h*	1.0 *h*	1.19 *h*	1.0 *h*	0.25 *h*	1.2 *h*
Ph-6	0.4 *h*	1.0 *h*	1.19 *h*	1.0 *h*	0.92 *h*	1.57 *h*
Ph-7	0.4 *h*	1.0 *h*	1.19 *h*	1.0 *h*	0.25 *h*	1.3 *h*
Ph-8	0.4 *h*	1.0 *h*	1.19 *h*	1.0 *h*	0.92 *h*	1.63 *h*

Based on the presented values in table 5.5, evidently, the existing equations for computing l_p cannot be utilized for columns with embedded pipe since they are intended for columns without irregularity in their cross sections. It can be seen that some of the equations are overestimating the plastic hinge length while most of them are providing values which are far below the obtained values from the finite element model and observations in experiment. It is also notable that even for Pauley and Priestley`s proposed equation, which is known to yield conservative results, in the case

of specimens Ph-5, Ph-6, Ph-7 and Ph-8 the obtained values for plastic hinge length are larger than the computed ones by FE.

This, in some cases, huge difference can be attributed to the exit presence which intensifies the stress in extreme fibers of concrete when the exit is located on the compression side of the section and consequently localized high curvature values occur in these regions.

Furthermore, it is noteworthy to note that comparing the results from the finite element model with test results shows good agreement between them. For instance, considering specimen C-4 with its corresponding FE model, Ph-6, shows that based on Table 5.4 the plastic hinge happened in the third segment of the column which is more than 300 mm distance from the footing, this value agrees with the computed value for Ph-6 where the l_p is found to be 320 mm. The same trend is apparent for models C-1 and C-2 with their corresponding FE models Ph-1 and Ph-2 where in both cases the FE result accurately reflect the plastic hinge length of the column. Figure 5.8 depicts after the test the damaged state of column C-9, the control specimen with solid section.

Figure 5.8. State of column C-9 after the test

It can be seen that the localized damage occurred in the first 50 mm of the column from the footing which is the exact value proposed by Bae and Bayrak (0.25 *h*), this indicates that in the case of columns with solid section (without embedded pipe) their equation is capable of predicting l_p. However, from the state of specimen C-4 and its corresponding FE analyzed counterpart, Ph-6, as demonstrated in figure 5.9, the length of plastic hinge increased significantly due to section irregularity.

This indisputable differences in the length of plastic hinge for elements with embedded pipe demands special care and precautions such as providing extra confinement in the critical regions like the suggestion made by Mander 1983 which says due to the spread plastic curvature, it is better to provide detailed confinement for three equivalent plastic hinge length (referring to his proposed equation for l_p as presented in Equation 2.10).

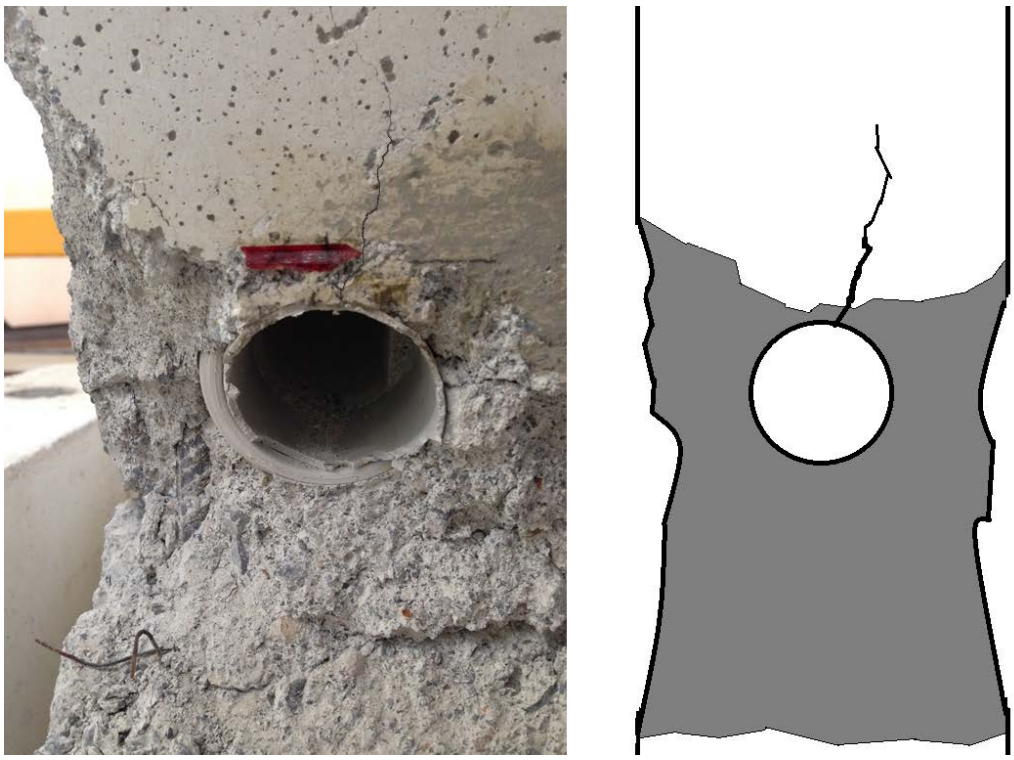

Figure 5.9. State of column C-4 after test

At the end of this discussion, it is worth mentioning that as stated before, in specimen C-5 the exit was embedded at the side of the column, perpendicular to the direction of the exerted lateral load, unlike other specimens in which the exit axis was parallel to the lateral force. The aim of the latter orientation of the exit was to see if any twisting of the column may occur due to lack of symmetry of the column cross section at the pipe exit level. Since the friction between axial jack plate and top surface of the column could prevent possible twist, the specimen was tested without the presence of any axial load and two LVDTs were placed at top corners of the column to record the displacement of each corner. Contrary to expectations, excluding the initial stages of loading, test results showed no noticeable twist in the element, the same thing was observed in FE model of specimen C-5.

The latter behavior can be explained by the fact that although at the location of the exit, the column has a channel-like cross section and the shear center of section at that location does not coincide with centroid, this does not affect the global behavior of column since the cross section is symmetrical at other parts of the element. The other reason can be that when the drift increases, the effective depth of compression zone decreases and except at small values of drift, the shape of compression block will be rectangular; consequently, the presence of pipe exit in the tension zone does not affect the behavior of the member.

Chapter 6

CONCLUSION

The seismic responses of RC columns with an embedded PVC pipe subjected to simultaneous actions of axial and lateral loading were experimentally and numerically investigated. The experimental study examined the effect of some key parameters on the columns' strength, stiffness, energy absorption and plastic deformation. Also a finite element study was conducted to examine the stress state, load-displacement response and curvature distribution of the test columns. The results from this study support the following conclusions:

(a) The presence of a pipe rendered the column cross-section at the level of the pipe exit asymmetric, and this lack of symmetry was reflected in the column's lateral load–displacement response under reversed cyclic loading.

(b) The level of applied axial load was found to be the key parameter insofar as the reduction in strength and ductility caused by the embedded pipe was concerned. Under an axial load greater than the column balanced axial load, the presence of a pipe reduced the column's ultimate moment capacity by 32% and its moment capacity at 2% drift by 61%.

(c) The calculated ductility factor of the column with an embedded pipe when subjected to a high axial load dropped by 57% compared with that of a companion column without a pipe.

(d) The provision of more confining steel, especially in the pipe exit region, enhanced the behavior of the column: by decreasing the spacing of ties from

200 mm to 80 mm, the ultimate lateral load, secant stiffness at the final stage (2% drift) and the ductility factor increased by 24%, 62% and 56%, respectively.

(e) The location of the pipe also proved to be a crucial parameter insofar as column strength and ductility are concerned. By increasing the distance between the pipe exit and the top of the foundation from 100 mm to 200 mm, the lateral load or ultimate moment resistance of the column in the final cycle before failure increased by 32% and its stiffness increased by 34% and the length of plastic hinge increased by 70%.

(f) The value of balanced axial load is reduced due to the presence of drain pipes. This reduction is shown to be more than 25% of the balanced axial load for a companion column without a pipe.

(g) Considering the interaction diagrams, it is notable that the pure axial load of columns with pipe are also affected and reduced. Also the value of balanced axial load is reduced by the presence of the pipe, a reduction that might change the mode of column failure from ductile to brittle.

(h) It is shown that the length of plastic hinge changes remarkably due to the presence of the pipe. Hence, most of the existing equations for the estimation of plastic hinge length underestimate the value of l_p such that in some equations the estimated value was less than one fourth of the obtained values for the tested columns.

With due regard to the limited scope of the present study, the following tentative design recommendations are made to mitigate the negative effects of an embedded pipe on the seismic response of columns:

a) The bottom of the pipe exit should be located from the end of the column a distance not less than the smaller side dimension of the column.

b) Confining reinforcement in the form of closed ties should be provided immediately above and below the pipe exit, beginning at the pipe surface, not less than the smaller side dimension of the column or three times the pipe outside diameter. The spacing of this reinforcement should conform to the requirements of ACI 318-14 (ACI, 2014) or its more recent editions for seismically designed columns.

REFERENCES

ABAQUS, U. S. M., & Manuals, E. U. S. (2002). Version 6.3, Hibbitt, Karlsson & Sorensen. *Inc. Rhode Island*.

ACI Committee. (1963). Building code requirements for reinforced concrete (ACI 318-63). *American Concrete Institute.*

ACI-ASCE Committee 428. (1968). Progress report on code clauses for limit design. *In ACI J. Proc.* (Vol. 65, No. 9, pp. 713-715).

American Concrete Institute. (2004). *Building code requirements for structural concrete (ACI 318-05) and commentary (ACI 318R-05)*. American Concrete Inst.

ACI (American Concrete Institute). (2014). Building code requirements for reinforced concrete. *ACI 318-14*.

Ashour, A. F., & Rishi, G. (2000). Tests of reinforced concrete continuous deep beams with web openings. *Structural Journal*, *97(3)*, 418-426.

Bae, S. (2005). *Seismic performance of full-scale reinforced concrete columns* (Doctoral dissertation).

Bae, S., & Bayrak, O. (2008). Plastic hinge length of reinforced concrete columns. *ACI Structural Journal*, *105*(3), 290.

Baker, A. L. L. (1956). *The ultimate load theory applied to the design of reinforced & prestressed concrete frames*. Concrete Publ. Lmd.

Bakhteri, J., & Iskandar, S. A. (2005). Experimental Study of Reinforced Concrete Columns Concealing Rain Water Pipe. *Journal of Civil Engineering*, *43*, 13-26.

Balan, T. A., Spacone, E., & Kwon, M. (2001). A 3D hypoplastic model for cyclic analysis of concrete structures. *Engineering Structures*, *23*(4), 333-342.

Bayrak, O., & Sheikh, S. A. (1997). High-strength concrete columns under simulated earthquake loading. *Structural Journal*, *94*(6), 708-722.

Bourdette, B., Ringot, E., & Ollivier, J. P. (1995). Modelling of the transition zone porosity. *Cement and concrete research*, *25*(4), 741-751.

Code, P. (2005). Eurocode 8: Design of structures for earthquake resistance-part 1: general rules, seismic actions and rules for buildings. Brussels: *European Committee for Standardization.*

Code, T. E. (2007). Specification for structures to be built in disaster areas. *Ministry of Public Works and Settlement Government of Republic of Turkey*.

Darwin, D., & Pecknold, D. A. (1977). Analysis of cyclic loading of plane RC structures. *Computers & Structures*, *7*(1), 137-147.

FEMA, F. (2007). 461-Interim protocols for determining seismic performance characteristics of structural and nonstructural components through laboratory testing, *Federal Emergency Management Agency* (FEMA), Document No. *Redwood City, CA*.

Hsieh, S. S., Ting, E. C., & Chen, W. F. (1982). A plastic-fracture model for concrete. *International Journal of Solids and Structures*, *18*(3), 181-197.

Hu, H. T., Lin, F. M., Liu, H. T., Huang, Y. F., & Pan, T. C. (2010). Constitutive modeling of reinforced concrete and prestressed concrete structures strengthened by fiber-reinforced plastics. *Composite Structures*, *92*(7), 1640-1650.

Jankowiak, T., & Lodygowski, T. (2005). Identification of parameters of concrete damage plasticity constitutive model. *Foundations of civil and environmental engineering*, *6*(1), 53-69

Kotsovos, M. D., & Newman, J. B. (1977, September). Behavior of concrete under multiaxial stress. In *Journal Proceedings* (Vol. 74, No. 9, pp. 443-446).

Kupfer, H., Hilsdorf, H. K., & Rusch, H. (1969, August). Behavior of concrete under biaxial stresses. In *Journal Proceedings* (Vol. 66, No. 8, pp. 656-666).

Kwak, H. G., & Filippou, F. C. (1997). Nonlinear FE analysis of RC structures under monotonic loads. *Computers & Structures*, *65*(1), 1-16.

Lee, J. J., & Fenves, G. L. (1998). Plastic-damage model for cyclic loading of concrete structures. *Journal of engineering mechanics*, *124*(8).

Li, B., Pan, Z., & Zhao, Y. (2015). Seismic behaviour of lightly reinforced concrete structural walls with openings.

Lotfy, E. M. (2013). Nonlinear analysis of reinforced concrete columns with holes. *International Journal of Civil and Structural Engineering*, *3*(3), 655.

Lubliner, J., Oliver, J., Oller, S., & Onate, E. (1989). A plastic-damage model for concrete. *International Journal of solids and structures*, *25*(3), 299-326.

Mander, J. B. (1983). Seismic design of bridge piers.

Mansur, M. A., Tan, K. H., & Lee, S. L. (1984). Collapse loads of r/c beams with large openings. *Journal of Structural Engineering*, *110*(11), 2602-2618.

Mansur, M. A., & Tan, K. H. (1999). *Concrete beams with openings: Analysis and design* (Vol. 20). CRC Press.

Mohamed, A. R., Shoukry, M. S., & Saeed, J. M. (2014). Prediction of the behavior of reinforced concrete deep beams with web openings using the finite element method. *Alexandria Engineering Journal*, *53*(2), 329-339.

Nataj, A. B., Şensoy, S., & Razaqpur, G. (2018). Seismic behaviour and strength of reinforced concrete columns with embedded drain pipe. *Magazine of Concrete Research*, 1-10.

Ngo, D., & Scordelis, A. C. (1967, March). Finite element analysis of reinforced concrete beams. In *Journal Proceedings* (Vol. 64, No. 3, pp. 152-163).

Ortiz, M. (1985). A constitutive theory for the inelastic behavior of concrete. *Mechanics of materials*, *4*(1), 67-93.

Panagiotakos, T. B., & Fardis, M. N. (2001). Deformations of reinforced concrete members at yielding and ultimate. *Structural Journal*, *98*(2), 135-148.

Panoskaltsis, V. P., Lubliner, J., & Monteiro, P. J. M. (1994). Rate dependent plasticity and damage for concrete. In *Cement Manufacture and Use* (pp. 27-40). ASCE.

Park, Y. J., Ang, A. H., & Wen, Y. K. (1987). Damage-limiting aseismic design of buildings. *Earthquake spectra*, *3*(1), 1-26.

Petersson, P. E. (1981). *Crack growth and development of fracture zones in plain concrete and similar materials* (Doctoral dissertation, Division, Inst.).

Priestley, M. J. N., & Park, R. (1987). Strength and ductility of concrete bridge columns under seismic loading. *Structural Journal*, *84*(1), 61-76.

Priestley, M. J. N., Potangaroa, R. T., & Park, R. (1981). Ductility of spirally-confined concrete columns. *Journal of the Structural Division*, *107*(1), 181-202.

Qian, K., Li, B., & Liu, Y. (2016). Experimental and analytical study on load paths of RC squat walls with openings. *Magazine of Concrete Research*, *69*(1), 1-23.

Sakai, K., & Sheikh, S. A. (1989). What do we know about confinement in reinforced concrete columns. *ACI Structural journal*, *86*(2), 192-207.

Sankarasubramanian, G., & Rajasekaran, S. (1996). Constitutive modeling of concrete using a new failure criterion. *Computers & structures*, *58*(5), 1003-1014.

Sheikh, S. A., & Khoury, S. S. (1993). Confined concrete columns with stubs. *ACI Structural Journal*, *90*, 414-414.

Simpson, D. (2003). The provision of holes in reinforced concrete beams. *Concrete*, *37*(3), 24-25.

Standard, A. S. T. M. (2015). C39/C39M-15a, 2015. *Standard Test Method for Compressive Strength of Cylindrical Concrete Specimens*.

Systèmes, D. (2009). Abaqus 6.9 Documentation, Dassault Systemes Simulia Corp, *Providence*, RI, USA.

Tan, K. H., & Mansur, M. A. (1996). Design procedure for reinforced concrete beams with large web openings. *Structural Journal*, *93*(4), 404-411.

Tanaka, H. (1990). Effect of lateral confining reinforcement on the ductile behaviour of reinforced concrete columns.

Tayel, M. A., Soliman, M. H., & Ibrahim, K. A. (2004). Experimental behavior of flat slabs with openings under the effect of concentrated loads. *Alexandria engineering journal*, *43*(2), 203-214.

Turkish Standards Institute. (2000). Requirements for design and construction of reinforced concrete structures. TS500-2000.

Vecchio, F. J. (1992). Finite element modeling of concrete expansion and confinement. *Journal of Structural Engineering*, *118*(9), 2390-2406.

Wang, J., SAKASHITA, M., Kono, S., Tanaka, H., & Warashina, M. (2008). A macro model for reinforced concrete structural walls having various opening ratios. In *The 14th World Conference on Earthquake Engineering, Beijing, China.*